UNIVERSITY OF THE WITWATERSRAND, JOHANNESBURG

FACULTY OF HEALTH SCIENCES

The effect of copper-imidazo[1,2-*a*]pyridine complexes on HT-29 and DLD-1 colorectal cancer cells

Nadia Gangat

A dissertation submitted to the Faculty of Health Sciences, University of the Witwatersrand, Johannesburg, in fulfilment of the requirements of the degree of Master of Science in Medicine

Johannesburg, 2018

Declaration

I, Nadia Gangat, declare that this Dissertation is my own, unaided work. It is being submitted for the Degree of Master of Science in Medicine at the University of the Witwatersrand, Johannesburg. It has not been submitted before for any degree or examination at any other University.

……

Nadia Gangat

On this……day of……2018

Dedication

I dedicate this dissertation to my parents,
Shiraaz and Nafisa to whom I owe the world,
my fiancé Yahyaa, for your infinite love and endless faith in me
and my grandmom who redefined strength, fighting this cancer.

Abstract

Colorectal cancer (CRC) is the third leading cause of cancer-related deaths. In Sub-Saharan Africa CRC is associated with late-stage diagnosis, poor prognosis and limited chemotherapeutic efficacy. Current chemotherapy for the treatment of metastatic CRC is associated with severe adverse drug reactions and therapeutic failure. This study investigates the *in vitro* effects of a total of 25 test compounds belonging to three different classes; nucleoside analogues, novel epidermal growth factor receptor kinase inhibitors and copper-imidazo[1,2-*a*]pyridines compared to positive controls camptothecin and staurosporine against two colorectal cancer cell lines.

The HT-29 and DLD-1 colorectal cancer cell lines were maintained in culture and the cytotoxic potential of the compounds was determined by the MTT assay. Fluorescent stains were used to evaluate morphological changes. The potential of the active compounds to induce apoptosis was evaluated by the annexin-V binding assay, a fluorometric caspase-3/7 assay, mitochondrial membrane depolarization and a caspase-9 activity assay. In HT-29 cells, an apoptotic proteome array was used to measure expression of other apoptotic proteins.

Four copper-imidazo[1,2-*a*]pyridines; JD46, JD47, JD49 and JD88 were found to be the most active, with IC_{50} values in HT-29 cells ranging between 0.8 and 8.5 μM and in DLD-1 cells between 9.0 and 12.0 μM. Morphological evaluation showed membrane blebbing and fragmented nuclei. Both cell lines showed increased binding of annexin-V to the cell surface, and an increase of caspase-3/7 activity. The active compounds caused a loss of mitochondrial membrane potential as well as an increase in caspase-9 activity. This indicates that the copper-imidazo[1,2-*a*]pyridines induced apoptotic cell death via the intrinsic apoptotic pathway. Compared to the DLD-1 cells, HT-29 cells displayed increased sensitivity to the copper-imidazo[1,2-*a*]pyridines. HT-29 was most sensitive to three of the copper-imidazo[1,2-*a*]pyridines; JD46, JD47 and JD88.

In HT-29 cells an apoptotic proteome array shows that JD46, JD47 and JD88 decreased the presence of phosphorylated p53. The expression of the HSP32 was enhanced, while catalase was inhibited suggesting the accumulation of reactive oxygen species. Moreover, JD46, JD47 and JD88 caused a decrease in expression of several inhibitors of apoptosis proteins (IAPs) as well as the antiapoptotic proteins, Bcl-2 and Bcl-x. An increase in expression of TRAIL death receptor proteins indicates the involvement of the extrinsic apoptotic pathway. Additionally, the decrease in IAPs and tumor necrosis factor receptor expression suggested that TNFR1 induction of the anti-apoptotic NFκB transcription factor may have been inhibited, enabling the pro-apoptotic status of HT-29 cells when treated with copper-imidazo[1,2-*a*]pyridines.

In summary, the copper-imidazo[1,2-*a*]pyridines were effective inducers of apoptotic cell death through activation of the intrinsic pathway and warrants further investigation.

Acknowledgments

In the name of God, The Most Gracious, The Most Merciful.

I would like to acknowledge the following people for the fundamental role they played in my life during completion of this dissertation:

- My supervisor, Dr. Leonie Harmse, words cannot express how grateful I am to you for your continuous, patience, understanding, advice and motivation. Thank you for all your help ensuring my success. Without you, this dissertation would not have been possible.

- Professor Charles de Koning, from the WITS School of Chemistry, thank you for your continuous financial support throughout this study.

- Dr. Jean Dam, from the WITS School of Chemistry, thank you for developing the compounds used in this study.

- The National Research Foundation, Blue Skies Grant for their financial support during this study.

- My friends, Saajida, Zeenat, Raeesa and Shaahid, thank you for your love, laughter, encouragement and late night trips to the lab and most importantly, thank you for keeping me sane.

- My family, particularly, my cousins, thank you for all your love and for willingly accepting me despite all the crazy, inexplicable emotions during my write-up.

- My fiancé, Yahyaa, your endless love and your unwavering faith in me is all I could ever ask for and all I ever need. You are my biggest source of strength. Thank you for always believing in me. This is for us.

- Most importantly, my parents, Shiraaz and Nafisa, without you, completion of this dissertation would have been a distant dream.

- Thank you, mom, for always encouraging me to be the best version of myself, for always reminding me that no goal is unattainable, for always believing in me and for always inspiring me. Thank you for your immeasurable love and support.

- Dad, thank you for giving me an education from the best institutions in the world. Thank you for your unwavering love and most importantly for always inspiring my success.

Research Outputs

Conference Proceedings

Gangat, N., Dam, J., de Koning, C., and Harmse, L. (2016). Imidazo[1,2-*a*]pyridines and nucleoside analogues causes apoptosis of colorectal cancer cell lines. Poster presentation at the WITS Faculty of Health Sciences Research Day & Postgraduate Expo, 2016, 1st September.

Gangat, N., Dam, J., de Koning, C., and Harmse, L. (2016). Imidazo[1,2-*a*]pyridines and nucleoside analogues causes apoptosis of colorectal cancer cell lines. Poster presentation at the All Africa Congress on Pharmacy and Pharmacology, 2016, 5th – 8th October.

Gangat, N., Dam, J., de Koning, C., and Harmse, L. (2017). Imidazo[1,2-*a*]pyridines and nucleoside analogues cause apoptosis of colorectal cancer cell lines. Poster presentation at the Cancer Research Symposium, WITS University, 2017, 9 February.

Young Scientist Award in Basic Pharmacology – Best poster presentation: Awarded 2nd prize. 7th October 2016 at the All Africa Congress on Pharmacy and Pharmacology.

Publications

Dam, J., Ismail, Z., Kurebwa, T., Gangat, N., Harmse, L., Marques, H., Lemmerer, A., Bode, M.L. and de Koning, C. (2017). Synthesis of copper and zinc 2-(pyridin-2-yl)imidazo[1,2-a]pyridine complexes and their potential anticancer activity. *European Journal of Medicinal Chemistry, 126*, 353-368. Doi: http://dx.doi.org/10.1016/j.ejmech.2016.10.041

Table of Contents

Declaration ii

Dedication iii

Abstract iv

Acknowledgments vi

Research Outputs viii

Table of Contents ix

List of Figures xvi

List of Tables xix

Abbreviations, Acronyms and Symbols xxi

Chapter I. Introduction 1

1.1 Cancer 1

1.2 Cancer statistics 1
1.3 Cancer classification 1
1.4 Hallmarks of cancer 2
1.5 The molecular basis of cancer 2
1.5.1 p53 tumor suppressor genes 3
1.5.2 Oncogenes 4

1.6 Management of cancer 4

2.1 Colorectal cancer 4

2.2 Colorectal cancer incidence in South Africa 5
2.3 Causative risk factors associated with colorectal cancer 5

2.3.1 Genetic risk factors 6

2.3.1.1 Lynch syndrome 6
2.3.1.2 Familial adenomatous polyposis (FAP) 7

2.4 Colorectal cancer symptoms 7
2.5 Pathology and staging 7

2.5.1 Tumorigenesis pathways in CRC 8

2.5.1.1. Chromosomal instability pathway (CIN) 9

2.5.1.1.1 *APC* and ß-catenin 9
2.5.1.1.2 p53 9
2.5.1.1.3 *KRAS* 10

2.5.1.2 Microsatellite instability pathway (MSI) 10
2.5.1.3 CpG island methylator phenotype (CIMP) pathway 11

2.6 Treatment of colorectal cancer 11

2.6.1 Chemotherapeutic drugs used in the treatment of metastatic CRC 12

2.6.1.1 FOLFOX and FOLFIRI 12

2.6.2 Targeted therapies in colorectal cancer 13

2.6.2.1 Bevacizumab 13
2.6.2.2 Cetuximab 13

3.1 Apoptosis and cancer 14

3.2 The apoptotic pathways 15

3.2.1 The extrinsic (death receptor) pathway 15
3.2.2 The intrinsic (mitochondrial) pathway 15
3.2.3 Convergence between the extrinsic and intrinsic pathway 17
3.2.4 Caspases 17
3.2.5 The execution phase of apoptosis 17

4.1 Apoptotic pathways and colorectal cancer 18

4.2 The extrinsic pathway in colorectal cancer 18

4.2.1 The TRAIL ligand and its receptors 18
4.2.2 c-FLIP 19
4.2.3 The Fas receptor and FasL 19

4.3 The intrinsic pathway in colorectal cancer 19

4.3.1 Bcl-2 family proteins 19
4.3.2 p53 and apoptosis 20

4.4 Inhibitors of apoptosis proteins (IAPs) 21
4.5 Heat shock proteins (HSPs) 22

5. Phenotypic and targeted based novel compounds for cancer 23

5.1 Novel nucleoside analogues 23
5.2 Small molecule epidermal growth factor receptor kinase inhibitors (EKIs) 23
5.3 Copper-imidazo[1,2-a]pyridines 23

6.1 Colorectal cancer cell lines 24
6.2 The HT-29 cell line 24

6.3 The DLD-1 cell line 24

7. Aims and objectives of this study 24

Chapter II. Materials and Methodology 26

2.1 Cell culture 26

2.1.1 Cell culture reagents 26
2.1.2 Cell maintenance and sub-culture 27
2.1.3 Determination of cell numbers and cell viability before use in experiments 27
2.1.4 Cryopreservation 28

2.2 Test compounds 28

2.3 The 3-[4,5-dithylthiazol-2-yl]-2,5 diphenyl tetrazolium bromide (MTT) cell viability assay 29

2.4 Cell morphology 30

2.4.1 Preparation of cells for morphology studies 30
2.4.2 Phase contrast images 30
2.4.3 Vital dye staining using a combination of Acridine Orange/Ethidium Bromide/Hoechst (AO-EtBr-HO) 31

2.4.3.1 Staining procedure 32

2.5 Evaluation of apoptosis 33

2.5.1 Annexin-V 33
2.5.2 Measurement of caspase-3/7 activity 34
2.5.3 Protein estimation 36
2.5.4 Mitochondrial membrane potential assay 36
2.5.5 Caspase-9 detection 37

2.6 Expression of apoptosis-related proteins using a proteome array 38

Chapter III. Results 43

3.1 Screening of test compounds on HT-29 and DLD-1 cell lines 43

3.1.1 IC_{50} values of the nucleoside analogues on DLD-1 and HT-29 cells 45
3.1.2 IC_{50} values of the copper-imidazo[1,2-*a*]pyridines on DLD-1 and HT-29 cells 46
3.1.3 Selection of compounds for further investigation 48

3.2 Copper-imidazo[1,2-*a*]pyridines induced changes to the cell morphology of HT-29 and DLD-1 cells 50

3.2.1 Phase contrast microscopy evaluation of copper-imidazo[1,2-*a*]pyridines induced morphological changes in HT-29 cells 50
3.2.2 Phase contrast microscopy evaluation of copper imidazo[1,2-*a*]pyridines induced morphological changes in DLD-1 cells 52
3.2.3 Preliminary investigation of the mechanism of cell death with vital dyes 55

3.2.3.1 The effect of copper-imidazo[1,2-*a*]pyridines on the mechanism of cell death in HT-29 cells 56
3.2.3.2 The effect of copper-imidazo[1,2-*a*]pyridines on the mechanism of cell death in DLD-1 cells 58

3.3 The exposure of phosphatidylserine on the surface of HT-29 and DLD-1 cells after treatment with copper-imidazo[1,2-*a*]pyridines 60

3.3.1 The effect of copper-imidazo[1,2-*a*]pyridines on annexin-V binding in HT-29 cells 60
3.3.2 The effect of copper-imidazo[1,2-*a*]pyridines on annexin-V binding in DLD-1 cells 63

3.4 Activation of caspase-3/7 in HT-29 and DLD-1 cells by copper imidazo[1,2*a*]pyridines 66

3.4.1 Induction of caspase-3/7 activity by copper-imidazo[1,2-*a*]pyridines in HT-29 cells 67
3.4.2 Induction of caspase-3/7 activity by copper-imidazo[1,2-*a*]pyridines in DLD-1 cells 68

3.5 The effect of copper-imidazo[1,2-*a*]pyridines on the mitochondrial membrane potential of HT-29 and DLD-1 cells 69

3.5.1 The effects of copper-imidazo[1,2-*a*]pyridines on the mitochondrial membrane potential of HT-29 cells 70
3.5.2 The effects of copper-imidazo[1,2-*a*]pyridines on the mitochondrial membrane potential of DLD-1 cells 72

3.6 The determination of the induction of caspase-9 activity in HT-29 and DLD-1 cells 75

3.6.1 Induction of caspase-9 activity by copper-imidazo[1,2-*a*]pyridines in HT-29 cells 75

3.6.2 Induction of caspase-9 activity by copper-imidazo[1,2-*a*]pyridines in DLD-1 cells 78

3.7 The effect of copper-imidazo[1,2-*a*]pyridines on the apoptotic protein profile of HT-29 cells 80

3.7.1 Copper-imidazo[1,2-*a*]pyridines decrease the levels of apoptotic inhibitory proteins 81
3.7.2 Copper-imidazo[1,2-*a*]pyridines decreases the levels of TNFR1 84
3.7.3 Copper-imidazo[1,2-*a*]pyridines increases the levels of HO-1/HMOX-1/HSP32 84
3.7.4 Copper-imidazo[1,2-*a*]pyridines decreases the levels of p53 in HT-29 cells 85
3.7.5 Changes in other apoptotic proteins 86

3.7.5.1 The Bcl-2 family 86
3.7.5.2 Pro-caspase-3 and cleaved caspase-3 86
3.7.5.3 Cytochrome c 86
3.7.5.4 Catalase 87
3.7.5.5 Claspin 87
3.7.5.6 Clusterin 87
3.7.5.7 HIF-1α 87
3.7.5.8 HtrA2/Omi and Smac/Diablo 88

Chapter IV. Discussion 89

4.1 The cytotoxicity of nucleoside analogues, EKI inhibitors and copper-imidazo[1,2-*a*] pyridines on HT-29 and DLD-1 cells 89

4.1.1 Structure activity relationships of copper-imidazo[1,2-*a*]pyridines 92

4.2 The morphology of copper-imidazo[1,2-*a*]pyridines on HT-29 and DLD-1 cells 93

4.3 Annexin-V binding to phosphatidylserine and induction of caspase-3/7 activity indicate that copper-imidazo[1,2-*a*]pyridines cause apoptosis 94

4.4 Copper-imidazo[1,2-a]pyridines cause a loss of mitochondrial membrane potential and increase the activity of caspase-9 in HT-29 and DLD-1 cells 96

4.5 The apoptotic protein profile of test compounds on HT-29 cells 98

4.5.1 Copper-imidazo[1,2-*a*]pyridines decrease the expression of cIAP-1 and cIAP-2 and increases the expression of TRAIL R1/DR4 and TRAIL R2/DR5 in HT-29 cells 98

4.5.1.1 Copper-imidazo[1,2-*a*]pyridines decreases the expression of inhibitors of apoptosis proteins in HT-29 cells 99
4.5.1.2 Copper-imidazo[1,2-*a*]pyridines increases the expression of TRAIL R1/DR4 and TRAIL R2/DR5 in HT-29 cells 99

4.5.2 Copper-imidazo[1,2-*a*]pyridines decreases TNFR1 in HT-29 cells 100

4.5.3 Copper-imidazo[1,2-*a*]pyridines decreases Bcl-2 and Bcl-x expression in HT-29 cells 101

4.5.4 Copper-imidazo[1,2-*a*]pyridines decreases the expression of HtrA2/Omi in HT-29 cells 101

4.5.5 Copper-imidazo[1,2-*a*]pyridines increases HO-1/HMOX/HSP32 expression 102

4.5.6 Copper-imidazo[1,2-*a*]pyridines decreases expression catalase expression 103

4.5.7 Copper-imidazo[1,2-*a*]pyridines decreases expression levels of phosphorylated p53 103

4.5.8 JD88 increases pro-caspase-3 expression 105

4.5.9 Copper-imidazo[1,2-*a*]pyridines decreases expression levels of cytochrome c 105

4.6 Future investigations 106

Chapter V. Conclusion 108

5.1 Copper-imidazo[1,2-*a*]pyridines is cytotoxic towards HT-29 and DLD-1 cell lines 108

5.2 Copper-imidazo[1,2-*a*]pyridines cause cell death by apoptosis 109

5.3 Copper-imidazo[1,2-*a*]pyridines activates the intrinsic apoptotic pathway 109

5.4 Apoptosis array proteome profiling in HT-29 cells 110

5.5 In summary 110

References 111

Appendix 131

Appendix A Structures of the 'non-active' test compounds 131

Appendix B MTT calibration curves 134

Appendix C	Dose response curves	135
Appendix D	Standard curves	137
Appendix E	Caspase-3/7 calculations for specific activity	139
Appendix F	Apoptotic protein profile	141
Appendix G	Human ethics clearance certificate	143
Appendix H	Approval for change of title	144

List of Figures

Chapter I. Introduction

Figure 1.1	Molecular cancer genesis	3
Figure 1.2	Development from normal colonic mucosa to tumor	8
Figure 1.3	A schematic diagram of the two major pathways of apoptosis	16

Chapter II. Materials and Methodology

Figure 2.1	Fluorescent micrographs showing normal and apoptotic nuclei and necrotic cells as stained by the vital dyes, HO, AO and EtBr	32
Figure 2.2 (A)	Flow diagram of day one of the human apoptosis array method	41
Figure 2.2 (B)	Flow diagram of day two of the human apoptosis array method	42

Chapter III. Results

Figure 3.1	The effect of test compounds on the cell viability of HT-29 cells	43
Figure 3.2	The effect of test compounds on the cell viability of DLD-1 cells	44
Figure 3.3	IC_{50} values of nucleoside analogues and the positive controls, camptothecin and staurosporine in HT-29 and DLD-1 cells	45
Figure 3.4	IC_{50} values of copper-imidazo[1,2-*a*]pyridines and the positive controls, camptothecin and staurosporine in HT-29 and DLD-1 cells	47
Figure 3.5 (A)	Photomicrographs of HT-29 cells showing morphological changes after treatment with copper-imidazo[1,2-*a*]pyridines	51
Figure 3.5 (B)	Photomicrographs of HT-29 cells showing morphological changes after treatment with camptothecin and staurosporine	52
Figure 3.6 (A)	Photomicrographs of DLD-1 cells showing morphological changes after treatment with 1 copper-imidazo[1,2-*a*]pyridines	54
Figure 3.6 (B)	Photomicrographs of DLD-1 cells showing morphological changes after treatment with camptothecin and staurosporine	55
Figure 3.7	Fluorescent micrographs of HT-29 cells after treatment with copper-imidazo[1,2-*a*]pyridines and staurosporine	57

Figure 3.8	Fluorescent micrographs of DLD-1 cells after treatment with copper-imidazo[1,2-*a*]pyridines and staurosporine	59
Figure 3.9	Annexin-V/PI stained HT-29 cells following exposure to active copper-imidazo[1,2-*a*]pyridines	62
Figure 3.10	Average percentage of HT-29 cells positive for annexin and PI after a 12 hour exposure to copper-imidazo[1,2-*a*]pyridines	63
Figure 3.11	Annexin-V/PI stained DLD-1 cells following exposure to active copper-imidazo[1,2-*a*]pyridines	65
Figure 3.12	Average percentage of DLD-1 cells positive for annexin-V and PI after a 16 hour exposure to copper-imidazo[1,2-*a*]pyridines	66
Figure 3.13	Fold increase in caspase-3/7 activity in HT-29 cells after a 20 hour exposure to copper-imidazo[1,2-*a*]pyridines	67
Figure 3.14	Fold increase in caspase-3/7 activity in DLD-1 cells after a 20 hour exposure to copper-imidazo[1,2-*a*]pyridines	68
Figure 3.15	Copper-imidazo[1,2-*a*]pyridines cause disruption of the mitochondrial membrane potential in HT-29 cells	71
Figure 3.16	Percentage of HT-29 cells showing JC-1-aggregates and JC-1-monomers after treatment with copper-imidazo[1,2-*a*]pyridines and staurosporine	72
Figure 3.17	Copper-imidazo[1,2-*a*]pyridines cause disruption of the mitochondrial membrane potential in DLD-1 cells	73
Figure 3.18	Percentage of DLD-1 cells showing JC-1-monomers and JC-1-aggregates after treatment with copper-imidazo[1,2-*a*]pyridines and staurosporine	74
Figure 3.19	Copper-imidazo[1,2-*a*]pyridines stimulate caspase-9 activity in HT-29 cells	77
Figure 3.20	JD46 stimulates caspase-9 activity in DLD-1 cells	79
Figure 3.21	Percentage of caspase-9 apoptotic cells in HT-29 and DLD-1 cells treated with copper-imidazo[1,2-*a*]pyridines and staurosporine	80
Figure 3.22	Chemiluminescent signals of apoptosis-related proteins captured on nitrocellulose membranes	81
Figure 3.23	Expression of apoptosis-related proteins in HT-29 cells which showed a greater than 20 % change when treated with copper-imidazo[1,2*a*] pyridines	83

Figure 3.24 Copper-imidazo[1,2-*a*]pyridines increased HO-1/HMOX1/HSP-32 expression in HT-29 cells 84

Figure 3.25 Copper-imidazo[1,2-*a*]pyridines decreased phosphorylated p53 expression in HT-29 cells 85

Chapter IV. Discussion

Figure 4.1 Substituent additions to C5 and C4 of the imidazo[1,2-*a*]pyridine ring of copper-imidazo[1,2-*a*]pyridine test compounds impacts their potency 93

List of Tables

Chapter I. Introduction

Table 1.1	Colorectal Cancer incidence in 2012 and 2013 in South Africa per ethnicity and gender	5

Chapter II. Materials and Methodology

Table 2.1	Reagents requiring preparation prior to usage	40

Chapter III. Results

Table 3.1	Chemical structures of active copper-imidazo[1,2-*a*]pyridines	49
Table 3.2	Average percentage of HT-29 cells showing annexin-V- and PI	61
Table 3.3	Average percentage of DLD-1 cells showing annexin-V- and PI activity	64
Table 3.4	Comparison of caspase-3/7 activity in HT-29 and DLD-1 cells	69
Table 3.5	Expression levels of proteins displaying a greater than 20 % change in HT-29 cells	82

Chapter IV. Discussion

Table 4.1 (A)	IC_{50} values of nucleoside analogues in HT-29 and DLD-1 cell lines	90
Table 4.1 (B)	IC_{50} values of copper-imidazo[1,2-*a*]pyridines in HT-29 and DLD-1 cell lines	90
Table 4.2	Mutations in key cancer genes in the HT-29 and DLD-1 colorectal cancer cell lines	92
Table 4.3	The percentage expression of inhibitors of apoptosis proteins and death receptor proteins in HT-29 cells	99
Table 4.4	The percentage expression of TNFR1 in HT-29 cells	100
Table 4.5	The percentage expression of Bcl-2, Bcl-x and Bad in HT-29 cells	101
Table 4.6	The percentage expression of HtrA2/Omi in HT-29 cells	102
Table 4.7	The percentage expression of HSP32 in HT-29 cells	103
Table 4.8	The percentage expression of catalase in HT-29 cells	103

Table 4.9	The percentage expression of phosphorylated p53 at serine sites 15, 46 and 392 in HT-29 cells	105
Table 4.10	The percentage expression of pro-caspase-3 and cytochrome c in HT-29 cells	105
Table 4.11	The percentage expression of cytochrome c in HT-29 cells	106

Abbreviations, Acronyms and Symbols

ACRV2	-	Activin type 2 receptor
AFC	-	7-amino-4-trifluoromethylcoumarin
AIDS	-	Acquired immune deficiency syndrome
AIF	-	Apoptosis inducing factor
AO	-	Acridine orange
APC	-	Adenomatous polyposis coli
Apaf-1	-	Apoptotic protease-activating factor 1
ATM	-	Ataxia-telangiectasia mutated
ATP	-	Adenosine triphosphate
BAX	-	Bcl-2-associated X protein
Bcl-2	-	B-cell lymphoma-2
BSA	-	Bovine serum albumin
CAD	-	Caspase-activated deoxyribonuclease
CDK	-	Cyclin-dependent kinases
ChK	-	Checkpoint kinase
cm^2	-	Centimeter squared
CO_2	-	Carbon dioxide
CpG	-	Cytosine preceding guanine
c-FLIP	-	Cellular flice-like inhibitory protein
CIMP	-	CpG island methylator phenotype
CIN	-	Chromosomal instability pathway
CRC	-	Colorectal cancer
DIABLO	-	Direct IAP binding protein with low PI
DMEM	-	Dulbecco's Modified Eagle's Medium
DD	-	Death domain
DdH_2O	-	Double distilled water
DISC	-	Death-inducing signaling complex
DNA	-	Deoxyribonucleic acid
dTMP	-	Deoxythymidine monophosphate
DTT	-	Dithiothreitol
DUMP	-	Deoxyuridine monophosphate

DYRK2	-	Dual-specificity tyrosine-phosphorylation-regulated kinase 2
EtBr	-	Ethidium bromide
EDTA	-	Ethylene diamine tetra-acetic acid
EGFR	-	Epidermal growth factor receptor
ER	-	Endoplasmic reticulum
FADD	-	Fas-associated death domain
FAP	-	Familial adenomatous polyposis
fdUMP	-	Fluorodeoxyuridine monophosphate
FdUTP	-	Fluorodeoxyuridine triphosphate
FUTP	-	Fluorouridine triphosphate
FOBT	-	Fecal occult blood test
FOLFIRI	-	5-Fluorouracil/leucovorin and irinotecan
FOLFOX	-	5-Fluorouracil/leucovorin and oxaliplatin
FOLFOXIRI	-	5-Fluorouracil/leucovorin, oxaliplatin and irinotecan
FBS	-	Fetal bovine serum
G_0	-	Quiescence
G_1	-	First growth phase of the cell cycle
G_2	-	Second growth phase of the cell cycle
hCTR1	-	Human orthologue transporter
HIF-1α	-	Hypoxia inducible factor
HIPK2	-	Homeodomain interacting protein kinase 2
HRP	-	Horse radish peroxidase
HNPCC	-	Hereditary nonpolyposis colorectal cancer
HO	-	Hoechst 33342
HRP	-	Horse radish peroxidase
HSP	-	Heat shock protein
HtrA2	-	Heat temperature requirement protein
IARC	-	International Agency for Research on Cancer
IAP	-	Inhibitors of apoptosis protein
ICAD	-	Inhibitor of the caspase-activated deoxyribonuclease
IC_{50}	-	Half maximal inhibitory concentration

JC-1	-	5',6,6'-tetrachloro-1,1',3,3'-tetraethylbenzimidazolylcarbocyanine iodine
KCl	-	Potassium chloride
KH_2PO_4	-	Potassium dihydrogen phosphate
KRAS	-	Kirsten rat sarcoma viral oncogene homolog
LOH	-	Loss of heterozygosity
M	-	Mitosis
mCRC	-	Metastatic colorectal cancer
MDM2	-	Murine double minutes 2
Min	-	Minutes
ml	-	Milliliter
mM	-	Millimolar
MMR	-	Mismatch repair
MOMP	-	Mitochondrial outer membrane permeabilization to
ms	-	Milliseconds
MSI	-	Microsatellite instability pathway
MSS	-	Microsatellite stable
mtDNA	-	Mitochondrial DNA
MTT	-	3-(4,5-dimethylthiazol-2-yl)-2,5-diphenyl tetrazolium bromide
NaCl	-	Sodium chloride
$NaHPO_4$	-	Disodium hydrogen phosphate
NCID	-	National Cancer Institute for Communicable Diseases
NCR	-	National cancer registry
NFκB	-	Nuclear factor kappa-light-chain-enhancer of activated B cells
nM	-	Nanomolar
PBS	-	Phosphate buffered saline
PI	-	Propidium iodide
PS	-	Phosphatidylserine
RNAi	-	RNA interference
ROS	-	Reactive oxygen species
rpm	-	Rotations per minute

RPMI	-	Rosewell park memorial institute
S	-	Synthetic phase of the cell cycle
Scid	-	Severe combined immunodeficiency
siRNA	-	Small interfering RNA
Smac	-	Second mitochondria-derived activator of caspase
SSA	-	Sessile serrated adenomas
TB	-	Tuberculosis
tBid	-	Truncated bid
TGFßRII	-	Transforming growth factor ß receptor II
TKI	-	Tyrosine kinase inhibitor
TNM	-	Tumor, node, metastasis
TNF	-	Tumor necrosis factor
TNFR1	-	Tumor necrosis factor receptor 1
TRADD	-	TNFR-1 associated death domain
TRAIL	-	(TNF)-related apoptosis-inducing ligand
TS	-	Thymidylate synthase
VEGF	-	Vascular endothelial growth factor
v/v	-	Volume per volume
WHO	-	World Health Organization
w/v	-	Weight per volume
XIAP	-	X-linked inhibitor of apoptosis
5-FU	-	5-fluorouracil
µl	-	Microliter
µM	-	Micromolar
°C	-	Degrees Celsius
%	-	Percent
$\Delta\psi m$	-	Mitochondrial membrane potential

Chapter I. Introduction

1.1 Cancer

Cancer is a pathological disorder characterized by the uncontrolled division and proliferation of abnormal cells that have the ability to invade surrounding tissues and metastasize (Duff and Markham, 2012). Cancer cells also stimulate angiogenesis and manage to evade programmed cell death (Jacob *et al*., 2015). Cancer is a progressively developing disease that results from somatic mutations in the genetic structure of a cell (Alberts *et al*., 2002). Globally, the most common types of cancer-related mortality include lung, breast, colorectal, prostate, stomach and liver cancer (Ferlay *et al*., 2015).

1.2 Cancer statistics

Cancer is among the leading causes of morbidity and mortality worldwide. Based on the GLOBOCAN 2012 estimates, approximately 14.1 million new cancer cases and 8.2 million cancer-related deaths occurred in that year alone. The global cancer burden is expected to escalate to approximately 20 million new cases every year, by the year 2025 (Ferlay *et al.,* 2015).

Globally, cancer causes more deaths than acquired immune deficiency syndrome (AIDS), tuberculosis (TB) and malaria combined. However, in Sub-Saharan Africa, AIDS, TB and malaria are responsible for seven times more deaths than cancer. Despite the fact that infectious diseases continue to plague sub-Saharan Africa, non-communicable diseases are increasing in incidence. The overall disease burden associated with cancer is rising and is estimated to have more than an 85 % increase in incidence by 2030, due to demographic changes (Morhason-Bello *et al.,* 2013). In this region, approximately 5 % of patients receive chemotherapy and as a result, cancer survival is very low (Vento, 2013).

1.3 Cancer classification

Cancer can be diagnosed in two ways; by histological examination or by their site or origin (e.g. breast, colon, prostate). Histologically, cancers are classified into four key categories:

carcinomas, sarcomas, leukemias and lymphomas (Clark and Longo, 2014). The most common are carcinomas which are derived from epithelial tissues that line the body's internal organs. They can be further classified based on their histologic appearance. Cells that have a glandular appearance are known as adenocarcinomas and those originating from the squamous epithelium are known as squamous cell carcinomas. Sarcomas are derived from mesenchymal tissue and include muscle, bone and connective tissue (Sabel, 2014). Cancers derived from the hemotopoeitic tissue are leukemias and lymphomas (Clark and Longo, 2014).

1.4 Hallmarks of cancer

Tumors are defined as benign or malignant. Benign tumors have an unregulated growth, surrounded by a capsule and are unable to invade surrounding tissues (Sabel, 2014). Malignant tumors also present with an unregulated growth pattern but are able to break away from their site of origin and metastasize to distal sites within the host (Clark and Longo, 2014). Unlike normal cells, cancer cells become unresponsive to normal growth controls and are thus able to proliferate rapidly and replicate infinitely (Jacob *et al*., 2015). Tumors acquire new blood vessels by a process known as angiogenesis which supplies the tumor with oxygen and nutrients. Growth and division of normal cells are regulated by contact inhibition, a process which stops the cells dividing. Characteristically, cancer cells also manage to evade apoptosis, a form of programmed cell death (Jacob *et al.,* 2015).

1.5 The molecular basis of cancer

Environmental factors are notable contributors toward cancer. However, most cancers develop as a result of uncontrolled cell division. Cancers arise resulting from an accumulation of inherited and somatic mutations in proto-oncogenes and tumor suppressor genes (Turnpenny and Ellard, 2005) (Figure 1.1). The combined effect of the loss of activity of tumor suppressor genes and increased activity in oncogenes are the driving force of continuous cell proliferation. (Jacob *et al.,* 2015).

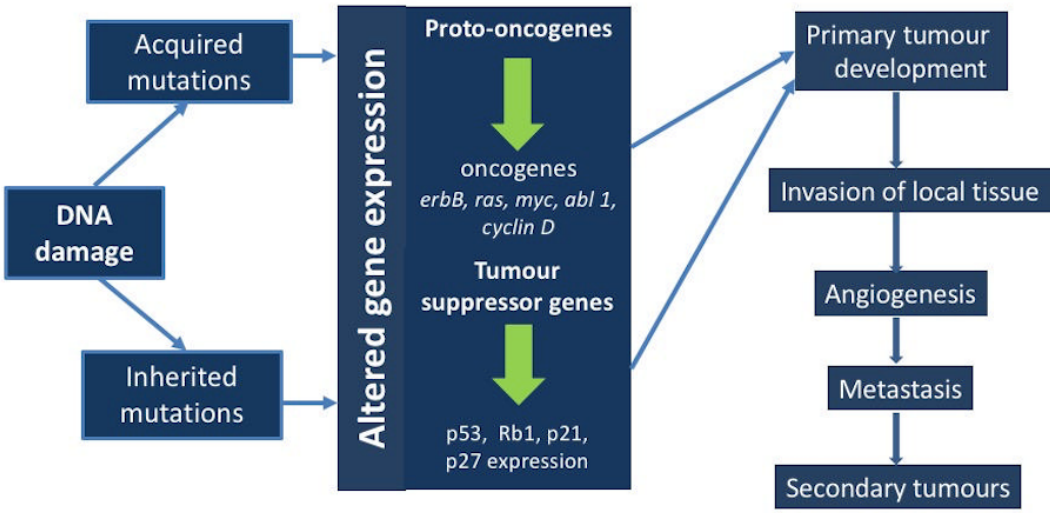


Figure 1.1 Molecular cancer genesis. Acquired and inherited mutations in proto-oncogenes and tumor suppressor genes result in the development of a primary tumor which is able to invade local tissues and metastasize, resulting in metastatic disease.

1.5.1 p53 tumor suppressor genes

Tumor suppressor genes produce protein products responsible for suppressing cellular division. When the gene undergoes mutation, it loses its inhibitory effects (Jacob *et al.,* 2015). The best described tumor suppressor gene is p53 (also known as TP53), encoding the p53 transcription factor, which plays a pivotal role in preventing tumor initiation and progression within the cell cycle (Chen, 2016; Yue *et al*., 2017). In normal cells, p53 is present at low levels (Yue *et al.,* 2017). It is activated and accumulates within the cell in response to intra- and extracellular stress signals such as DNA damage, oncogene activation, reactive oxygen species (ROS) and hypoxia. It then selectively regulates the transcription and expression of numerous target genes which are involved in DNA repair, apoptosis and senescence (cell growth arrest) to prevent tumor formation (Yue *et al.,* 2017; Liu *et al.,* 2015a). In response to DNA damage, p53 halts progression of the cell cycle until the damage is repaired. If the damage is not repaired, p53 initiates apoptosis through the mitochondrial (intrinsic) pathway (Zeestraten *et al*., 2013). Mutation of the p53 gene is present in more than half of all human cancers. (Yue *et al.,* 2017).

1.5.2 Oncogenes

Proto-oncogenes facilitate cellular proliferation and differentiation pathways. In addition, they regulate progression through the cell cycle and are essential for cellular growth. A mutated proto-oncogene is known as an oncogene which encodes proteins that accelerates the growth of cancer cells (Jacob *et al*., 2015). Oncogenes can be activated or overexpressed. Examples of oncogenes include i) growth factor receptors such as tyrosine kinases, c-*ERB*-B2 which encodes the epidermal growth factor receptor (EGFR), ii) nuclear transcription factor, c-*MYC* which stimulates cells to progress from the G_1 to the S phase of the cell cycle and iii) b-cell lymphoma-2 (*Bcl*-2), associated with apoptosis inhibition (Turnpenny and Ellard, 2005). Other oncogenes alter transcription or deregulates the cell cycle (Meric-Bernstam and Pollock, 2015; Jacob *et al.,* 2015). Oncogenes accelerate cell growth and prevent cell death leading to tumor development.

1.6 Management of cancer

Cancer treatment requires a multidisciplinary approach. Treatment is divided into three categories; surgery, systemic chemotherapy and radiation. Solid tumors require surgical excision, an approach which is taken whenever possible, whereas haematologic malignancies can be treated with chemotherapy and/or radiation. Drug therapy includes a wide range of drug classes such traditional cytostatic chemotherapy, targeted therapy, immunotherapy, biologic therapy and hormonal therapy. Treatment regimens depend on the goals of treatment and national guidelines. Radiation is used to shrink the tumor or to reduce the risk of local cancer recurrence. (Duff and Markham, 2012).

2.1 Colorectal Cancer

Colorectal cancer (CRC) is a malignant neoplasm originating in the colon, rectum or anal canal (Wells *et al*., 2017). More than 85 % of CRCs are adenocarcinomas that develop from malignant transformations of adenomatous polyps or serrated polyps (Papadakis and McPhee, 2017; Wells *et al*., 2017). The five-year survival rate for localized tumors is 90 % as opposed to 13 % with metastatic CRC (Wells *et al*., 2017).

2.2 Colorectal cancer incidence in South Africa

Globally, colorectal cancer is the second most commonly diagnosed cancer in women and the third in men with 1.4 million new cases diagnosed in 2012 according to GLOBOCAN (Ferlay *et al.,* 2015). Incidence rates vary within both genders and is higher in men than in women. The average age of diagnosis is 68 years for men and 72 years for women (Cohan and Varma, 2014). Approximately 55% of diagnosed cases are found in high income countries, with the lowest rates present in Sub-Saharan Africa (Rabeneck *et al.,* 2015). Colorectal cancer is the fifth most common cancer in men and women in South Africa (National Cancer Registry, 2012). Despite the low incidence rate of CRC in Sub-Saharan Africa, the mortality rate is substantially higher compared to developed countries. This is due to significant under-diagnosing and a high burden of late diagnosis (Katsidzira *et al.,* 2016).

In South Africa, CRC incidence is further subdivided into categories based on ethnicity and gender. According to the statistics provided by the National Institute for Communicable Diseases' (NICD), most recent National Cancer Registry (NCR), in the table below, the general trend in incidence has increased from 2013 to 2014. Statistics obtained from the NCR demonstrate that CRC is most common in the Asian population and least common in the Black population (Table 1.2).

Table 1.1: Colorectal Cancer incidence in 2013 and 2014 in South Africa per ethnicity and gender (National Institute for Communicable Diseases, National Cancer Registry, 2013 and 2014).

	Percentage of colorectal cancer relative to the total cancer population (%)							
Incidence (year)	**Asian**		**Black**		**White**		**Colored**	
	Men	**Women**	**Men**	**Women**	**Men**	**Women**	**Men**	**Women**
2013	13.63	7.41	4.81	2.73	5.15	5.07	5.61	5.76
2014	16.30	7.40	4.38	2.89	4.94	5.09	6.87	5.67

2.3 Causative risk factors associated with colorectal cancer

There are several risk factors associated with colorectal cancer including age, diet and familial history. Ninety percent of diagnosed CRC cases occur in people over the age of 50.

Inflammatory bowel disease, Crohn's disease and a history of adenomatous polyps increases the risk in the younger population (Cohan and Varma, 2014; Bullard Dunn and Rothenberger, 2015).

A diet high in saturated fats, processed and red meats and alcohol combined with a sedentary lifestyle increases the risk of the malignancy. Obesity and diabetes increase the risk of CRC mortality (Cohan and Varma, 2014; Bullard Dunn and Rothenberger, 2015). The development of colorectal carcinomas has been linked to a Western diet and lifestyle and since low and middle-income countries have been adopting this lifestyle, there is a notable increase in CRC incidence (Chan and Giovannucci, 2010). Other lifestyle factors aside from diets contributing to a higher CRC incidence include a lack of exercise, exposure to environmental toxins, cigarette smoking and alcohol consumption (Hang *et al*., 2015).

2.3.1 Genetic risk factors

Roughly 20 % of colorectal cancers occur in patients with a family history of CRC (Bullard Dunn and Rothenberger, 2015). The lifetime risk of developing CRC increases with an increasing number of first-degree relatives affected with the malignancy (Valle, 2017). Approximately 3-6 % of affected patients carry germline mutations, such as hereditary non-polypopsis colorectal cancer (HNPCC) also known as Lynch syndrome or familial adenomatous polyposis (FAP), genetically predisposing them to CRC (Valle, 2017). These conditions are inherited autosomal-dominant syndromes which pose a great risk towards the development of CRC (Jasperson *et al.,* 2010).

2.3.1.1 Lynch syndrome

Lynch syndrome is characterized by the presence of less than ten adenomatous polyps within the colons of patients, younger than 40 years of age (Bhattacharya and McHugh, 2017). Lynch syndrome is caused by germline mutations in one of four DNA mismatch repair (*MMR*) genes; *MSH2*, *MLH1*, *MSH6* and *PMS2*. *MMR* genes are essential components responsible for repairing incorrect base pairs of nucleosides during the DNA replication process. If mismatched bases aren't amended, the risk of CRC increases due to the propagation of gene mutations giving rise to the formation of nonfunctional proteins. Due to an inherited mutation, patients are born with one functional allele and one non-functional

allele of a gene. In the occurrence of an acquired mutation of the functional allele, the lifetime risk for developing CRC increases by 80% (Bhattacharya and McHugh, 2017).

2.3.1.2 Familial adenomatous polyposis (FAP)

FAP is accountable for 1 % of all CRC cases. It is characterized by the development of hundreds to thousands of adenomatous polyps in the colon which increases the risk for the formation of malignancies (De Marchis *et al.,* 2017). It is caused by a mutation of the adenomatous polyposis col (*APC*) gene, located on chromosome 5q21. *APC* is a tumor suppressor gene which has a vital role in cell-cell adhesions, cell cycle regulation and apoptosis. The condition has an early onset and by the age of 40, the lifetime risk of developing CRC is almost 100 % (De Marchis *et al.,* 2017).

2.4 Colorectal cancer symptoms

Colorectal cancer is a slow progressing disease with a ten-year latency period between the transformation of precancerous polyps to carcinomas (Carroll *et al.,* 2014). The tumor may be present for years before symptoms emerge. Symptoms vary and depend on the location of the lesion. Patients with tumors located on the right side of the colon (ascending) present with fatigue and weakness, characterized by iron deficiency anemia. Left sided tumors (descending colon) are depicted by fluctuations in bowel movements; from constipation to increased frequencies of blood streaked, loose stools, presenting with abdominal pain (Cornett and O. Dea, 2018). Common symptoms of rectal tumors are tenesmus (the feeling of wanting to defecate without having stools) (Rodriquez-Bigas *et al*., 2003) and recurrent hematochezia (passing fresh blood through the stools). Upon physical examinations, a mass can be palpated in the abdomen and combined with the finding of hepatomegaly suggests metastatic disease (Cornett and O. Dea, 2018).

2.5 Pathology and staging

Colorectal cancer is a heterogeneous group of diseases that develops from one organ (Roseweir *et al.,* 2017). More than 90 % of colorectal carcinomas arise from an adenocarcinoma. Adenocarcinomas are histologically graded into well, moderately or poorly differentiated based on their characteristic glandular formation (Fleming *et al.,* 2012).

Endoscopic biopsies in symptomatic patients are required for a CRC diagnosis, furthermore, the affirmative diagnosis of colorectal adenocarcinomas requires the invasion of the tumor through the muscularis mucosa into the submucosa (Mohamed and Schofield, 2014). The most common sites of metastasis include the liver, thorax and peritoneum (Riihimaki *et al.*, 2016).

CRC is classified according to the tumor, node, metastases (TNM) staging system which stipulates dependable guidelines for prognosis and treatment. The TNM system defines the anatomic extent of the cancer and is based on the growth of the primary tumor (T), the presence or absence of lymph node metastases (N) and distant metastases (M) (Duff and Markham, 2012). It is essential to retrieve a minimal of 12 nodes to assess lymph node metastases accurately.

2.5.1 Tumorigenesis pathways in CRC

In 1990, Fearon and Vogelstein established the adenoma-carcinoma sequence suggesting a sequential development from normal colonic mucosa, benign adenomas to invasive adenocarcinomas (Figure 1.2) through the accumulation of mutations of tumor suppressor genes and oncogenes (Pino and Chung, 2010). Genetic and epigenetic modifications are responsible for either initiating tumor formation from healthy tissue or driving the progression towards malignancy (Colussi *et al.,* 2013). Genomic instability causes molecular changes that enables CRC tumor formation through three distinct pathways: the chromosomal instability (CIN), the microsatellite instability (MSI) and the CpG (cytosine preceding guanine) island methylator phenotype (CIMP) pathways. Tumors can exhibit characteristics of one or more pathways resulting in different pathologic features amongst neoplasms (Rodriguez-Salas *et al.,* 2017).

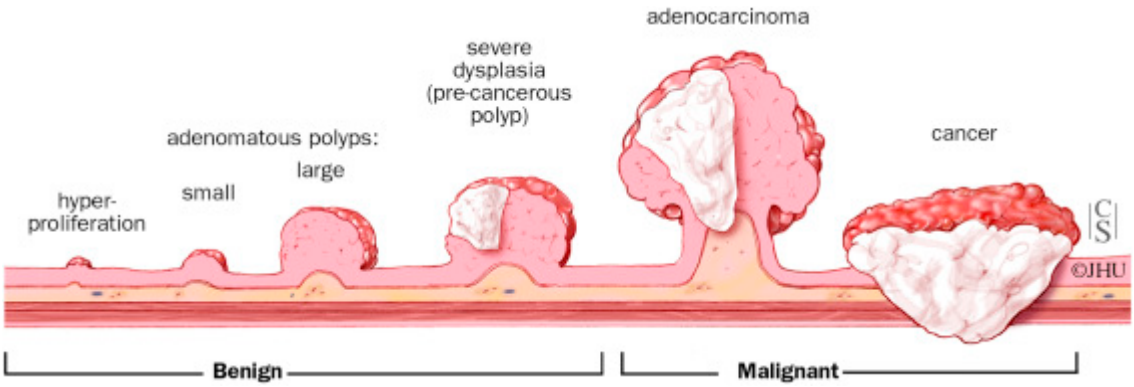


Figure 1.2 Development from normal colonic mucosa to tumor (Choi *et al.,* 2017).

2.5.1.1 Chromosomal instability pathway (CIN)

Chromosomal instability (CIN) is the most common pathway with a poor prognosis, which comprises 80-85 % CRC cases. (Singh *et al.,* 2017). CIN results in extensive loss of heterozygosity (LOH), chromosomal abnormalities and an imbalance in chromosome number (aneuploidy) (Pino and Chung, 2010). This dysregulation includes hypomethylation, leading to oncogene activation and chromosomal instability. CIN tumors are associated with the accumulation of mutations in the tumor suppressor genes; *APC*, ß-catenin and p53 and the proto-oncogenes; *KRAS* (Kirsten rat sarcoma viral oncogene homolog), and *EGFR* (epidermal growth factor receptor) (Pino and Chung, 2010).

2.5.1.1.1 *APC* and ß-catenin

APC is a multifunctional protein that regulates adhesion, cell-cycle control, migration and apoptosis (Pino and Chung, 2010). APC is a negative regulator of the Wnt signaling pathway and its mutation results in CIN in CRC (Novellasdemunt, Antas and Li, 2015). Activation of the Wnt signaling pathway results in the inability to degrade ß-catenin. ß-catenin increases in concentration within the cytoplasm and is translocated to the nucleus where it catalyzes the transcription of genes involved in tumor growth and invasion. APC mutations have been found in approximately 70 % of colorectal cancers (Pino and Chung, 2010; Rodriquez-Bigas *et al.,* 2003; Singh *et al.,* 2017).

2.5.1.1.2 p53

p53 mutation is found in 50-75 % of CRCs and LOH of p53 facilitates the progression from adenomas to carcinomas (Singh *et al.,* 2017). Mutations in p53 is a crucial step in CRC tumorigenesis allowing cells to forego their normal processes thereby promoting tumor progression and the inability to undergo apoptosis (Rodriguez-Salas *et al.,* 2017). Studies have shown that a combination of *KRAS* and wild type p53 in metastatic CRC express increased sensitivity to oxaliplatin (Singh *et al.,* 2017).

2.5.1.1.3 *KRAS*

Following genetic APC alterations in the CIN pathway, the progression from adenoma to carcinoma is accelerated by *KRAS*, a proto-oncogene involved in transduction and propagation of extracellular signals (Colussi *et al*., 2013). Mutations in *KRAS* permits continuous activation of the oncogene thereby interacting with downstream signaling molecules resulting in overstimulation of cellular proliferation and apoptosis suppression (Rodriguez-Bigas *et al.,* 2003; Knickelbein and Zhang, 2015). More than 40 % of *KRAS* mutations are present in codon 12 and 13 in patients with metastatic CRC (Tosi *et al.,* 2017). Codon 12 has a more oncogenic phenotype and predisposes tumor cells to local invasion and metastases, whereas codon 13 is involved in the transition of adenoma to carcinoma (Colussi *et al.,* 2013).

KRAS mutations are examined in metastatic CRC in order to direct therapy (Knickelbein and Zhang, 2015). EGFR is a receptor tyrosine kinase that is overexpressed in CRC (Williet *et al*., 2017). Mutant *KRAS* initiates intracellular defects that perpetuates EGFR signaling (Rodriguez-Salas *et al.,* 2017). EGFR antibodies, such as cetuximab are a class of monoclonal antibodies used in targeted therapy of CRC. They act by inhibiting extracellular ligand binding and promoting EGFR degradation. However, *KRAS* mutations renders CRC tumors resistant to anti-EGFR antibody treatment (Knickelbein and Zhang, 2015).

2.5.1.2 Microsatellite instability pathway (MSI)

The MSI pathway is characterized by the inactivation of DNA mismatch repair (MMR) genes and is responsible for approximately 15 % of CRCs. MMR dysfunction renders proteins unable to correct nucleoside mismatches at microsatellite sequences (repetitive DNA sequences) (Colussi *et al.,* 2013). The MMR system only functions when cells manage to evade intrinsic error checking carried out by DNA polymerase (Colussi *et al.,* 2013). MSI analysis illustrates five MSI detection markers; when two or more microsatellites show instability, it is classified as MSI-high, MSI-low when one marker shows instability and MSS (microsatellite stable) if instability isn't present (Ghanipour *et al.,* 2017). MSI-high tumors do not respond to 5-fluorouracil based chemotherapy but have a better prognosis than tumors that are CIN positive. MSI-high tumors also share similar characteristics to the CIMP pathway, described below in section 2.4.1.3 (Colussi *et al.,* 2013).

Genes that are frequently mutated in MSI tumors include *BRAF*, transforming growth factor ß II (TGFRßII), activin receptor type 2 (ACRV2), or Bcl-2 associated X protein (*BAX*) (Colussi *et al.,* 2013). *BRAF* mutation shows methylation and epigenetic silencing of the MLH1 gene, found in approximately 70-90 % of sporadic CRCs with MSI (Fleming *et al.,* 2012). The presence of *BRAF* mutations also play a significant role in MSI prognosis, MSI-high tumors with wild type *BRAF* have a better prognosis than *BRAF* mutated MSS tumors (Fleming *et al.,* 2012).

2.5.1.3 CpG island methylator phenotype (CIMP) pathway

CpG islands are short stretches of CpG rich regions in DNA and are associated with the promotor regions of genes. Methylation of these CpG regions cause transcription silencing (Mojarad *et al*., 2013). The CIMP pathway is characterized by aberrant hypermethylation of CpG sequences within the gene resulting in the inactivation of tumor suppressor genes (Colussi *et al.,* 2013; Fleming *et al.,* 2012). It occurs in 20-30 % of CRCs with clinical features similar to MSI tumors. CIMP is classified into CIMP-high and CIMP-low according to their degree of methylation. Both types have different phenotypes, with CIMP-low tumors presenting with significantly lower DNA methylation (Colussi *et al.,* 2013). Features associated with this pathway include a proximal colonic location, high-grade dysplasia, MMR deficient, and mutant *BRAF* and *KRAS* (Cohen *et al.,* 2016). Mutant *BRAF* is seen in CIMP-high CRCs and present with MSI features suggesting that they derive from the serrated pathway in sessile serrated adenomas (SSA). *KRAS* is found in CIMP-low tumors (Cohen *et al*., 2016).

2.6 Treatment of colorectal cancer

Management of CRC includes resection of the tumor and corresponding lymph vessels, followed by radiotherapy and chemotherapy (Brenner *et al.,* 2014). Surgery is the primary step of curative, localized CRC (Hatcher and Kumar, 2014). Surgical procedures for rectal cancer necessitates total mesorectal excision whereas resection of the tumor and corresponding lymph vessels is required in colon cancer (Brenner *et al.,* 2014).

2.6.1 Chemotherapeutic drugs used in the treatment of metastatic CRC

The primary goal of chemotherapy is to reduce local and systemic recurrence by inhibiting the proliferation of tumor cells in order to improve overall survival of the patient (Chu, 2017). Adjuvant chemotherapy aims to eradicate micrometastases and is administered after surgery in patients with node positive CRC (Hatcher and Kumar, 2014). Post-operative adjuvant combination chemotherapy with FOLFOX (5-FU/leucovorin and oxaliplatin) and FOLFIRI (5-FU/leucovorin and irinotecan) have been established as preferred treatment regimens however, FOLFOX remains the current first-line treatment in patients with metastatic colorectal cancer (mCRC) (Gustavsson *et al*., 2015). The combination therapies, FOLFOX (5-FU/leucovorin and oxaliplatin) and FOLFIRI (5-FU/leucovorin and irinotecan) are established as effective regimens for the treatment of mCRC with an overall survival period of two years (Gustavsson *et al*., 2015). Targeted therapy with monoclonal antibodies such as bevacizumab or cetuximab have been found to enhance the effects of cytotoxic therapy and is used as adjuvant chemotherapy in patient with mCRC (Marques *et al*., 2017).

2.6.1.1 FOLFOX and FOLFIRI

5-Fluorouracil (5-FU) is a pyrimidine antimetabolite that functions as a thymidylate synthase (TS) inhibitor. Intracellularly, 5-FU is converted into three active metabolites: fluorodeoxyuridine monophosphate (FdUMP), fluorodeoxyuridine triphosphate (FdUTP) and fluorouridine triphosphate (FUTP). Thymidylate synthase is an enzyme that catalyzes the synthesis of deoxythymidine monophosphate (dTMP) from dUMP, thereby producing the only source of thymidylate, vital for DNA synthesis and repair and is inhibited by the active metabolite of 5-FU, FdUMP. Leucovorin is a 5-formyl derivative of tetrahydrofolic acid that binds to the active site of thymidylate synthase and thereby facilitates the binding of 5-FU to the enzyme. It has no intrinsic cytostatic activity (Chabner *et al*., 2011; Wang *et al*., 2017). Exogenous folates such as leucovorin potentiates the effects of 5-FU and is given in combination with 5-FU (Gustavsson *et al*., 2015).

Oxaliplatin, is a platinum derivative that induces cross-linking between active platinum and specific base sequences (two adjacent guanine-adenine bases) to form DNA adducts that induces a higher degree of DNA synthesis inhibition than cisplatin (Comella *et al*., 2009). Irinotecan is a topoisomerase I inhibitor that causes DNA fragmentation and apoptosis.

Goldberg *et al* (2004) found that the efficacy of the FOLFOX regimen was significantly superior compared to that of FOLFIRI with regard to time to progression, response rate, toxicity and survival time. The FOLFOX regimen had lower rates of severe nausea, vomiting, diarrhea, febrile neutropenia and dehydration (Goldberg *et al.,* 2004). A relevant issue with the FOLFOX regimen, despite its efficacy, is the cost of treatment and toxicity. Neurotoxicity, specifically oxaliplatin-induced dose-dependent peripheral neuropathy occurred in 92.1 % of patients receiving treatment. Twelve percent of patients reported grade three neurotoxicity one year after treatment (Tsai *et al*., 2016).

Recent studies compare the use of FOLFOX and FOLFIRI with triplet therapy using 5-FU (plus leucovorin), oxaliplatin and irinotecan (FOLFOXIRI). A 25 % survival increase was noted in patients treated with FOLFOXIRI. However, patients experienced additional toxicity with an increased risk of neuropathy, non-febrile neutropenia and diarrhea (Marques *et al*., 2017).

2.6.2 Targeted therapies in colorectal cancer

Targeted therapy with monoclonal antibodies enhance the effects of cytotoxic regimens in patients with stage IV mCRC.

2.6.2.1 Bevacizumab

Bevacizumab is a recombinant humanized monoclonal antibody that functions as a vascular endothelial growth factor (VEGF) inhibitor, thus inhibiting angiogenesis (Jang *et al*., 2017). Patients treated with a combination of FOLFOX and bevacizumab had an increased overall survival, progression free survival and relative risk compared to patients treated with FOLFOX alone (Gustavsson *et al*., 2015). A meta-analysis with randomized controlled trials in first-line mCRC treatment was conducted by Jang *et al* (2017). The study confirmed the addition of bevacizumab to FOLFOX and FOLFIRI prolonged overall survival and progression free survival (Jang *et al*., 2017).

2.6.2.2 Cetuximab

Cetuximab is a monoclonal antibody directed against the endothelial growth factor receptor and is used in the treatment of mCRC. EGFR is a transmembrane glycoprotein that is required in signaling pathways affecting cell growth, proliferation and programmed cell death

(Wolpin and Mayer, 2008). EGFR is overexpressed in 80 % of CRC tumors and typically carry a poorer prognosis (Wolpin and Mayer, 2008). Noted adverse effects with cetuximab treatment include acneiform rash, hypomagnesemia and infusion reactions. An increase in progression-free survival (8.9 months vs. 8.0 months) was noted in patients receiving cetuximab with FOLFIRI treatment (Wolpin and Mayer, 2008).

3.1 Apoptosis and cancer

There are three major types of cell death based on their morphological appearance; apoptosis, authophagy and necrosis (Kroemer *et al*., 2009). Necrosis is a non-specific form of cell death, morphologically characterized by swelling of organelles and plasma membrane rupture with a consequential localized inflammatory response (Fink and Cookson, 2005; Kroemer *et al*., 2009). Autophagy is a pro-survival stress response characterized by vast autophagic vacuolization of the cytoplasm but occurs in the absence of chromatin condensation (Kroemer *et al*., 2009).

Apoptosis is a highly selective form of programmed cell death that is crucial in the development and homeostasis of normal tissues. Compromised apoptosis contributes to the survival of precancerous cells. Uncontrolled apoptosis results in accelerated cell death causing degenerative diseases, immunodeficiency and infertility (Hassan *et al.*, 2014; Wong, 2011). Cancer cells manage to evade apoptotic signaling pathways enabling malignant tumor development and metastasis.

Apoptotic cells are characterized by distinctive morphological and biochemical changes from initiation of apoptosis to the formation of apoptotic bodies. The early phase of apoptosis is characterized by cell shrinkage, a decrease in cell volume, pyknosis as a result of chromatin condensation and nuclear fragmentation. Phosphatidylserine, a negatively-charged phospholipid is translocated from the inner to the outer surface of the cell membrane. This membrane alteration permits the early recognition of apoptotic cells by macrophages thereby promoting their phagocytosis, resulting in minimal inflammation (Hassan *et al.*, 2014; Wong, 2011), unlike necrotic forms of cell death that is associated with inflammation (Wong, 2011). Membrane blebbing and a loss of membrane integrity are characteristic features of late apoptosis (Wong, 2011; Elmore, 2007). Biochemical alterations include DNA breakdown, caspase activation, intracellular substrate cleavages by proteolysis, protein cross-linking and membrane changes resulting in phagocytic recognition (Elmore, 2007; Ouyang *et al*., 2012).

Dysregulation of apoptosis facilitates tumor development and is implicated in the resistance to treatment. Modern treatment strategies seek to restore the apoptotic signaling pathways, by either activating an inactive pathway or rectifying a defective one (Hassan *et al.*, 2014; Wong, 2011).

3.2 The apoptotic pathways

3.2.1 The extrinsic (death receptor) pathway

The extrinsic pathway occurs at the plasma membrane and is triggered via transmembrane mediated-receptor interactions, through the interaction of death receptors, belonging to the tumor necrosis factor receptor (TNFR) superfamily to their respective ligands (Elmore, 2007; Pistritto *et al*., 2016). The most common death receptors are the type 1 tumor necrosis factor (TNFR1) and CD95 (Fas) and their ligands, TNF and Fas ligand (FasL), refer to Figure 1.3. Death receptors, located on the surface of the cell, possess a protein-protein domain known as the death domain (DD) which transmit signals from the cell surface to intracellular signaling pathways (Pistritto *et al*., 2016; Wong, 2011). The death domains bind to adaptor proteins forming the TNFR-1 associated DD (TRADD) and the Fas-associated DD (FADD). The binding of ligands to death receptors forms a binding site for the cytoplasmic adaptor proteins referred to as the death-inducing signaling complex (DISC). The DISC activates procaspase-8 to its activated initiator caspase-8. This results in the direct cleavage of effector caspases -3, -6 and -7. (Elmore, 2007; Wong, 2011).

3.2.2 The intrinsic (mitochondrial) pathway

Internal stress stimuli, such as irreparable genetic damage and hypoxia, trigger intracellular signals that initiate the intrinsic pathway. The signals elicit changes within the mitochondria resulting in a disruption of mitochondrial outer membrane permeabilization (MOMP) and the release of pro-apoptotic proteins from the intermembrane space to the cytosol (Pistritto *et al*., 2016). The pathway is regulated by members of the Bcl-2 protein family and consist of pro-apoptotic proteins (Bax, Bak, Bad, Bcl-xS, Bid) and anti-apoptotic proteins (Bcl-2, Bcl-x, Bcl-xL). Under normal physiological conditions, the anti-apoptotic proteins stabilize the mitochondrial outer membrane to prevent the release of cytochrome c into the cytosol. As shown in Figure 1.3, pro-apoptotic proteins initiate the release of cytochrome c which triggers the formation of an apoptosome by binding and activating initiator caspase-9 and Apaf-1 (apoptotic protease-activating factor 1) which in turn, activates effector caspases 3, 6

and 7 (Pistritto *et al*., 2016). Effector caspases cleave structural proteins resulting in morphological changes associated with apoptosis. Other common proteins released into the cytosol are the apoptosis inducing factor (AIF), second mitochondria-derived activator of caspase (Smac), direct inhibitor of apoptosis binding protein with low pI (DIABLO) and the serine protease high temperature requirement protein A (HtrA2/Omi) (Figure 1.3) (Wong, 2011). Smac/DIABLO and HtrA2/Omi inhibit the inhibitors of apoptosis protein (IAPs) thus promoting caspase activation (Figure 1.3) (Elmore, 2007; Pistritto *et al*., 2016).

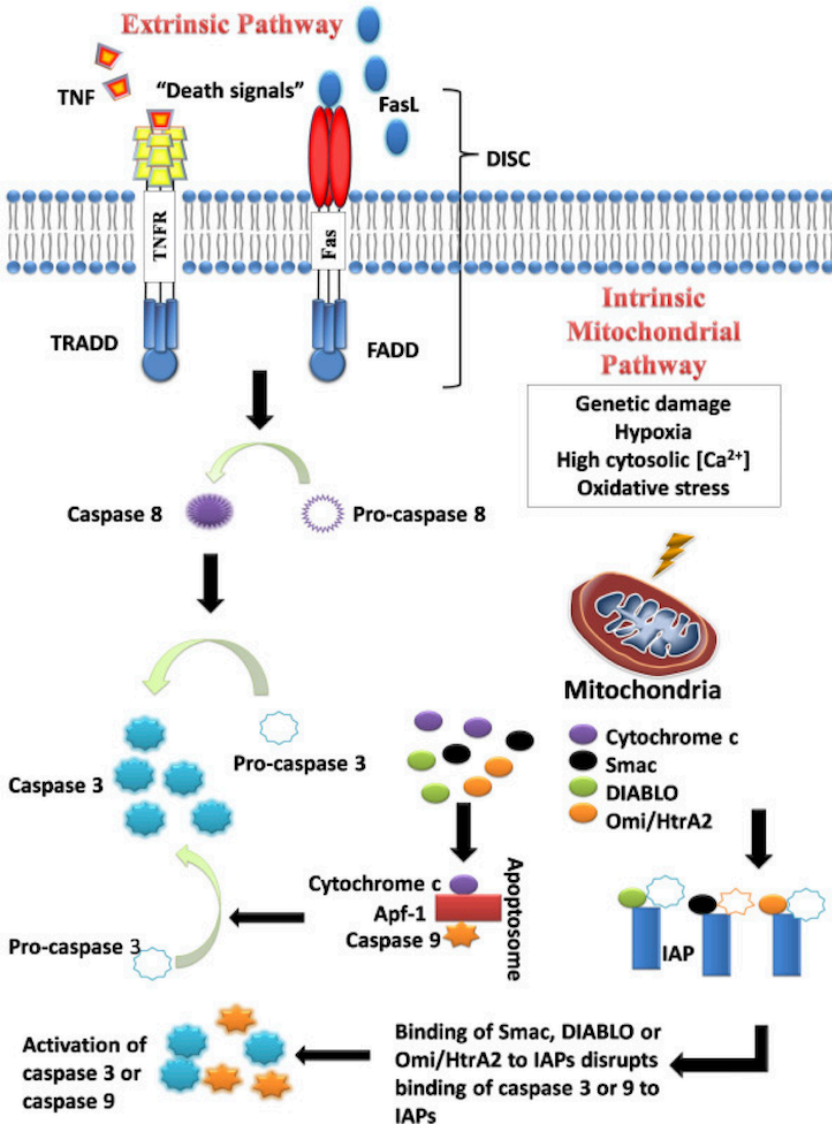


Figure 1.3 A schematic diagram of the two major pathways of apoptosis (Wong, 2011). *The death receptor pathway:* the FasL/TNF death ligand binds to their corresponding death receptors, Fas and TNFR. Death receptors recruit adaptor proteins FADD and TRADD, respectively and caspase-8 through intracellular death domains. The ligand-receptor forms the DISC binding site for adaptor proteins. DISC recruits and activates procaspase-8 to its active form, caspase-8 which directly cleaves downstream effector caspase 3 or cleaves the pro-apoptotic protein Bid to tBid which subsequently releases cytochrome c (Elmore, 2007; Wong, 2011).

The intrinsic pathway: internal stress such as hypoxia, oxidative stress and irreparable genetic damage triggers the mitochondrial pathway. Increased mitochondrial permeability causes the release of the pro-apoptotic proteins cytochrome c, Smac/DIABLO and HtrA2/Omi. Cytochrome c facilitates the formation of an apoptosome consisting of Apaf-1 and caspase-9 which causes the activation of caspase-3. Smac/DIABLO and HtrA2/Omi bind to inhibitor of apoptosis proteins (IAPs) causing the activation of effector caspase-3 and caspase-9 (Wong, 2011).

3.2.3 Convergence between the extrinsic and intrinsic pathway

The intrinsic and extrinsic pathways converge to activate the effector caspases which results in the biochemical and morphological changes characteristic of apoptosis (Pistritto *et al*., 2016). However, the pathways also converge by means of the pro-apoptotic protein, Bid. The Fas pathway causes mitochondrial damage mediated by the cleavage of Bid by caspase-8. Caspase-8 cleaves Bid to truncated Bid (tBid) and tBid initiates oligomerization of Bax or Bak which causes the mitochondria to release cytochrome c (Kantari and Walczak, 2011; Weinburg, 2014; Zeestraten *et al*., 2013). This is an example of crosstalk between the intrinsic and extrinsic pathways.

3.2.4 Caspases

The activation of caspases is a key feature of apoptosis. Caspases belong to a family of cysteine proteases that cleave the aspartic acid residues of a variety of proteins resulting in controlled cell death (Wong, 2011). Caspases are synthesized as inactive zymogens that are activated by proteolytic cleavage (Li and Yuan, 2008). Caspases can be categorized into three groups based on their function: initiator caspases (2, 8, 9 and 10), executioner caspases (3, 6 and 7) and inflammatory caspases (1, 4, 5, 11 and 12) (Elmore, 2007; Li and Yuan, 2008;). Caspase 8 and 9 are the key initiator caspases. Once activated through apoptotic signaling, they cleave and activate downstream executioner caspases (Olsen and Zhivotovsky, 2011). In turn, executioner caspases cleave key substrates essential for cell death (Pistritto *et al*., 2016).

The aim of anticancer treatments is to restore normal apoptotic function. Cytotoxic agents aim to induce caspase activation by stimulating the intrinsic or extrinsic apoptotic pathways (Hensley *et al*., 2013).

3.2.5 The execution phase of apoptosis

Cleaved caspase 8, from the extrinsic pathway and caspase-9 from the intrinsic pathway directly cleave and activate caspase-3. This is where the two initiating pathways converge,

triggering the execution phase of apoptosis (Wong, 2011). Activated caspase-3 is an executioner caspase that further activates downstream effector caspases 6 and 7. In apoptotic cells, caspase-3 cleaves the inhibitor of the caspase-activated deoxyribonuclease (ICAD), releasing caspase-activated deoxyribonuclease (CAD), thereby causing chromatin condensation by degrading chromosomal DNA within the nuclei (Wong, 2011). Caspase-3 also causes the cytoskeleton of apoptotic cells to degrade, forming apoptotic bodies. In addition, caspase-3 degrades nuclear and structural proteins that together with the aforementioned characteristics, contribute to the biochemical and morphological changes consistent with apoptosis (Wong, 2011).

4.1 Apoptotic pathways and colorectal cancer

Colorectal cancer development is augmented by the imbalance between the rates of cell growth and cell death by apoptosis that maintains intestinal epithelial cell homeostasis. The apoptotic pathways are deregulated in cancer cells. Abnormalities in these pathways promote CRC tumorigenesis and its resistance to chemotherapy and radiation therapy (Abraha and Ketema, 2016).

4.2 The extrinsic pathway in colorectal cancer

Aberrations in the death receptor (extrinsic) pathway can cause evasion of malignant cells to apoptosis. Examples include impairment and downregulation of death receptor function and expression of decoy receptors (DcR1 and DcR2) which have been shown as a mechanism of acquired drug resistance. Potential treatments that initiate the extrinsic pathway can induce apoptosis of cancer cells due to the independent triggers activating the extrinsic pathway (Abraha and Ketema, 2016; Wong, 2011).

4.2.1 The TRAIL ligand and its receptors

During normal functioning of the extrinsic pathway, the pro-apoptotic (TNF)-related apoptosis-inducing ligand (TRAIL) binds to two receptors: DR4 (TRAIL-R1) and DR5 (TRAIL-R2). The binding of the ligand and receptor forms the DISC, consisting of FADD thereby activating caspase-8. However, TRAIL may also bind to decoy receptors DR3 and DcR1(TRAIL-R3) and DcR2 (TRAIL-R4). Downregulation of DR4 and DR5 and upregulation of decoy receptors can cause TRAIL to bind to decoy receptors resulting in

dysregulated apoptosis signaling (Nahacka *et al*., 2018; Zeestraten *et al*., 2013). A study by Nahacka *et al* (2018) showed that the DR5 receptor is vital in the induction of apoptosis in HT-29 colorectal cancer cells resistant to TRAIL-induced apoptosis. When enhanced by ABT-737, an inhibitor of the Bcl-2 family, TRAIL-induced apoptosis continued through the DR5 receptor (Nahacka *et al*., 2018).

4.2.2 c-FLIP

Colorectal cancers display increased expression of the cellular Flice-like inhibitory protein (c-FLIP) isoforms and is associated with its poor clinical outcome (Safa, 2012). c-FLIP is an anti-apoptotic protein that inhibits apoptosis induced by TRAIL and FasL. c-FLIP binds to DR5, FADD or caspase-8 thereby preventing the formation of DISC and ultimately inhibiting the activation of the caspase cascade (Safa, 2012). The c-FLIP isoform shows similarities of procaspase-8 and is considered a strong inhibitor of the extrinsic pathway (Zeestraten *et al*., 2013).

4.2.3 The Fas receptor and FasL

The Fas receptor (Fas, APO-1/CD95) and its ligand FasL (CD95L) are transmembrane proteins that belong to the tumor necrosis factor receptor and ligand family (Peter *et al*., 2015). Fas-mediated apoptosis occurs via the extrinsic pathway, as described in Figure 1.3. Normal colon cells express Fas and are sensitive to Fas-mediated apoptosis. Colon cancer cells express FasL; downregulation of Fas and upregulation of FasL enables these cells to evade apoptosis signaling, thereby "counterattacking" activated tumor infiltrating lymphocytes (Elmore, 2007; Houston *et al*., 2003; Zeestraten *et al*., 2013). Potential explanations for the decreased sensitivity of tumor cells to FasL mediated apoptosis include, upregulation of c-FLIP or Bcl-2 and mutation of p53 (Houston *et al*., 2003).

4.3 The intrinsic pathway in colorectal cancer

4.3.1 Bcl-2 family proteins

The imbalance of anti-apoptotic and pro-apoptotic proteins can potentiate malignant cell survival due to the over- and under-expression of anti- and pro-apoptotic proteins, respectively. Overexpression of the Bcl-2 anti-apoptotic proteins are associated with a poor prognosis and chemo-resistance. Approximately 30-94 % of colorectal cancers overexpress

Bcl-2 (Abraha and Ketema, 2016). During the early stages of CRC tumor progression, Bcl-2 expression is increased and decreases, lowering the rate of tumor proliferation in the late stages of CRC (Zeestraten *et al*., 2013). Micro RNAs, miR-195, miR-24-2 and mrR-365-2 act as negative regulators of Bcl-2 by directly binding to the 3'-UTR of the *Bcl-2* gene, initiating apoptosis and causing a decrease in tumor proliferation (Abraha and Ketema, 2016). Oblimersen is a Bcl-2 antisense oligodeoxyribonucleotide that has been preliminarily tested in experimental therapy against CRC. When used alone, Oblimersen had limited therapeutic efficacy. It can however, sensitize CRC cells to other chemotherapeutic agents (Abraha and Ketema, 2016).

4.3.2 p53 and apoptosis

The p53 protein activates the transcription of pro-apoptotic proteins such as Bax, Bid and Apaf-1, that initiate the intrinsic pathway as well as the pro-apoptotic factors, Fas, Fas-L, DR-4 and DR-5 that induce the extrinsic pathway of apoptosis (Redza-Dutordoir and Averill-Bates, 2016). p53 can translocate from the cytosol to the mitochondria where it enhances mitochondrial membrane permeabilization releasing pro-apoptotic proteins from the mitochondria, thereby facilitating apoptosis (Redza-Dutordoir and Averill-Bates, 2016).

Fifty percent of CRCs express absent or mutated p53 (Zeestraten *et al*., 2013). According to the World Health Organization's International Agency for Research on Cancer (WHO IARC) TP53 database, p53 is mutated in HT-29 cells. A potential target involves the inactivation of the p53-MDM2 (mouse double minute 2 homolog) interaction (Abraha and Ketema, 2016). p53 and MDM2 form an autoregulatory feedback loop; p53 stimulates MDM2 which inhibits p53, by inhibiting its transcriptional activity, promoting its degradation and favoring its nuclear export (Chene, 2004). In normal cells, MDM2 is a ubiquitin ligase that targets p53 for proteosomal degradation (Zhang and Lozano, 2017). After p53 synthesis, MDM2 marks p53 by attaching a ubiquitin moiety to the protein, exports it from the nucleus to the cytoplasm where its polyubiquinated to ensure its degradation. This action results in the short 20-minute half-life of p53 in normal cells (Weinburg, 2014).

In response to DNA damage, p53 must be protected from MDM2 ubiquination and degradation. Phosphorylation of p53 on amino acid residues by kinases such as Checkpoint kinase (Chk) 1 and 2 and ataxia-telangiectasia mutated (ATM) alters the domain which MDM2 recognizes thereby preventing the p53-MDM2 interaction. MDM2 is therefore unable

to initiate ubiquitinylation of p53, p53 manages to escape degradation and is present in increased concentrations within the cell (Weinburg, 2014).

Inactivation of the contact between p53 and MDM2 using small molecule MDM2 inhibitors is a promising target in cancer therapy as it may cause senescence in colorectal tumor cells and is currently under clinical investigation (Abraha and Ketema, 2016).

4.4 Inhibitors of apoptosis proteins (IAPs)

The most common inhibitors of apoptosis proteins (IAPs) are livin, survivin and X-linked inhibitor of apoptosis (XIAP), which regulate the caspase cascade through binding of activated caspases (Zeestraten *et al*., 2013). IAPs are overexpressed in colorectal cancer and are associated with a poor prognosis (Krieg *et al*., 2013). IAPs are tightly regulated by the inhibitors Smac/DIABLO and HtrA2/Omi. Smac/DIABLO are released from the mitochondria into the cytosol and inhibit the IAPs to release bound caspases upon apoptotic activation (Zeestraten *et al*., 2013). XIAP inhibits both intrinsic and extrinsic pathways by binding and inhibiting caspase-9, caspase-3 and caspase-7 (Wong, 2011).

Survivin is an apoptotic cell death antagonist that inhibits caspase activation with XIAP (Krieg *et al*., 2013). Survivin is overexpressed in colorectal cancer cells and is absent in healthy adult cells (Zeestraten *et al*., 2013). Survivin is located in the cytoplasm and nucleus of a cell where it regulates cell viability and cell division.

Studies are investigating novel approaches targeting malignant cells with minimal effects on healthy cells; since healthy cells are less dependent on IAPs (Abraha and Ketema, 2016). Small molecules that bind IAPs decrease the activation threshold of caspase-3 and sensitizes malignant cells to chemotherapeutic agents (Abraha and Ketema, 2016). Polyphenylurea XIAP chelators were shown to antagonize the inhibitory effects of XIAP on caspase-3 and caspase-7 thereby activating apoptosis in cancerous cells (Abraha and Ketema, 2016). RNA interference (RNAi) is used to decrease IAP overexpression by producing and transferring small interfering RNAs (siRNAs) into tumor cells. Experimental trials with established chemotherapy and XIAP siRNA have shown to reduce XIAP synthesis and initiating apoptosis (Abraha and Ketema, 2016).

4.5 Heat shock proteins (HSPs)

Heat shock proteins (HSP) are overexpressed in colorectal cancer cells (Gunaldi *et al*., 2015) and facilitate carcinogenesis through the regulation of angiogenesis, metastasis and apoptosis mediation (Wu *et al*., 2017a). HSPs reverse or inhibit unfolding or denaturation of proteins in response to high temperatures or stress (hypoxia, anoxia, drugs; specifically, chemotherapeutics). HSPs are also vital in regulating molecular mechanisms during tumorigenesis. They are classified according to their molecular weight and include HSP27, HSP40, HSP60, HSP70, HSP90 and large HSPs. The HSPs play a vital role in cancer biology and are therefore considered to be potential therapeutic targets. (Wu *et al*., 2017a).

HSP27 is a key regulator in cancer development, apoptosis and drug resistance, indicative of poor disease prognosis. HSP27 inhibits the p53 induction of p21 (a cyclin-dependent kinase inhibitor protein) in cancer cells thereby suppressing cellular senescence. Additionally, HSP inhibits caspase activation by binding to cytochrome c thus preventing the formation of the apoptosome with Apaf-1 and caspase-9. Suppression of HSP27 has been shown to increase the sensitivity of colon cancer to 5-FU (Wu *et al*., 2017a).

HSP60, known as chaperonin, is located in the mitochondria, on the cell surface, cytosol and extracellular space and directly interacts with HSP70. HSP60 is increased in colorectal cancer and has a cytoprotective effect against chemotherapeutic agents. HSP60 regulates and stabilizes survivin in the mitochondria, maintaining its anti-apoptotic function. HSP60 also forms a complex with and stabilizes p53, inhibiting the pro-apoptotic function of p53 in cancer cells. HSP60 mediates 5-FU resistance; inhibiting HSP60 expression has been shown to reverse drug resistance in 5-FU-resistant SW480 CRC cells (Wu *et al*., 2017a).

HSP70, also known as mortalin, is overexpressed in colon cancer cells and inhibits both the extrinsic and intrinsic pathways by:

i.) Binding to the pro-apoptotic protein Bax, inhibiting its translocation from the cytosol to the mitochondria, thus disabling its pro-apoptotic function

ii.) Preventing Apaf-1 from forming the apoptosome

iii.) Binding to and inhibiting the function of AIF

In addition, HSP70 antagonizes p53-dependent and independent regulation (Wu *et al*., 2017a).

5. Phenotypic and targeted based novel compounds for cancer

5.1 Novel nucleoside analogues

Nucleoside analogues are used in the treatment of cancer by incorporating into DNA thus interrupting DNA replication. They can also initiate apoptosis by activating the apoptosome in the intrinsic pathway (Ewald *et al*., 2008). Nucleoside analogues are extensively used in the treatment of cancer since they bind and inhibit enzymes responsible for the copying of DNA. They are also incorporated as faulty bases in the DNA chain and can trigger apoptosis (Chabner *et al*., 2011).

5.2 Small molecule epidermal growth factor receptor kinase inhibitors (EKIs)

Epidermal growth factor receptors mediates cell growth, metastasis and inhibits apoptosis and plays a significant role in the development of metastatic CRC (Wee and Wang, 2017). There are two classes of EGFR agents: EGFR monoclonal antibodies that prevent ligand binding to receptors and small molecule EGFR tyrosine kinase inhibitors (TKI) that compete for ATP binding to the tyrosine kinase receptor (Saletti *et al*., 2015). Cetuximab, a small molecule monoclonal antibody is currently used in the treatment on mCRC (Chapter I. Section 2.5.2.2). CRC patients with mutated EGFR benefit from TKI treatment as TKIs are limited to EGFR mutated cases (Saletti *et al*., 2015).

5.3 Copper-imidazo[1,2-a]pyridines

Increased levels of intracellular copper are associated with cancer. Copper plays a key role in upregulating angiogenesis by directly binding to the angiogenic growth factor, angiogenin, enhancing its affinity for cells or by regulating the secretion of angiogenic molecules, sustaining tumor development and metastasis (Denoyer *et al*., 2015; Tardito *et al*., 2011). The abnormal accumulation of copper by cancer cells makes it potential target for the development of novel anticancer agents (Tisato *et al*., 2010).

Organic complexes containing copper as a metal has been receiving some attention as potential anticancer agents (McGivern *et al*., 2018). Tardito *et al* (2011), postulates that the organic component of copper complexes directs the metal to different molecular targets. The anticancer activity of copper complexes is attributed to its ability to produce reactive oxygen species (ROS) and cause oxidative stress. ROS consist of hydrogen peroxide, the superoxide ion, and the hydroxyl radical; which causes DNA damage (Tardito and Marchio, 2009).

Metallo-drugs such as cisplatin are included in over 50 % of anticancer treatments. However, its toxic side effects contribute to acquired or intrinsic drug resistance (McGivern *et al*., 2018). This warrants the development of novel compounds with improved effects. Copper-complexed compounds may have alternate mechanisms of action and may manage to evade chemoresistance and toxicity associated with platinum-based compounds (Tisato *et al*., 2010). Current clinical data display substantial results to merit the investigation of copper as anti-cancer agents. Additional research is required to further understand the role copper plays in the etiology of cancers to define specific treatment targets and to categorize the types of copper coordination compounds (Denoyer *et al*., 2008).

6.1 Colorectal cancer cell lines

Cancer cell lines are used to understand the biology of a cancer sub-type and to investigate the efficacy of anti-cancer agents (Gillet *et al*., 2013).

6.2 The HT-29 cell line

The adherent HT-29 human colorectal adenocarcinoma cell line was isolated from a primary tumor of a 44-year-old female in 1964 by Fogh and Trempe (1975) (Martinez-Macqueda *et al*., 2015) and is a Dukes' C colorectal adenocarcinoma (Ahmed *et al*., 2013). Under standard culture conditions, HT-29 cells form an apical brush border with tight junctions between cells. In standard culture medium, HT-29 cells secrete growth factors, cytokines and metabolites which stimulate cell survival (Martinez-Macqueda *et al*., 2015). The structure of the HT-29 cell is similar to enterocytes of the small intestine due to the presence of a brush border-associated hydrolases and a similar amount expressed villin in colonocytes (Martinez-Macqueda *et al*., 2015).

6.3 The DLD-1 cell line

The DLD-1 human colorectal adenocarcinoma is an adherent cell line and is a Dukes' C colorectal adenocarcinoma (American Type Culture Collection, 2016).

7. Aims and objectives of this study

Despite recent advances in the understanding of molecular mechanisms and treatment of cancer, there has been a notable increase in the global cancer burden and incidence of

colorectal cancer in South Africa. In Sub-Saharan Africa, colorectal cancer is associated with late-stage diagnosis, poor prognosis and limited chemotherapeutic efficacy. The discovery of novel agents aimed at targeting specific mechanisms involved in apoptotic cell death can be manipulated into chemotherapeutic drugs used in cancer treatment.

Aim:

This study aims to evaluate the efficacy of novel test compounds on the HT-29 and DLD-1 colorectal cancer cell lines.

Objectives:

- To identify the active compounds that inhibit the growth of colorectal cancer cell lines, HT-29 and DLD-1 in a viability screening procedure.
- To determine the relative potencies (IC_{50} values) of active test compounds.
- To determine if active compounds cause necrotic or apoptotic cell death by morphological evaluation.
- To evaluate the mechanism of cell death induced by test compounds by measuring the effects of active test compounds on specific apoptotic markers such as, annexin-V, caspase-3/7, mitochondrial membrane potential and caspase-9.
- To determine the effect of the most active compounds on global apoptotic protein expression in the most sensitive cell line.

Chapter II. Materials and Methodology

2.1 Cell culture

HT-29 cells were purchased form the Fox Chase Cancer Institute. DLD-1 cells were obtained from the Japanese Culture collection and were gifted by Dr. Clem Penny. Both cells lines were evaluated for authenticity by short tandem repeat analysis (Inqaba Biotech). HT-29 and DLD-1 cells are both characterized as Dukes' C stage colorectal adenocarcinomas (Ahmed *et al*., 2013; American Type Culture Collection, 2016). All solutions, buffers, and culture media were prepared with ultrapure MilliQ water. Cells were observed daily with an OlympusDP72 inverted phase contrast microscope to monitor growth and to evaluate for microbial contamination.

2.1.1 Cell culture reagents

Cells were maintained in culture medium specific to each cell line. Culture media was obtained from Sigma Aldrich and foetal bovine serum (FBS) from Biocom Africa. Cells were grown and maintained aseptically in antibiotic-free media. HT-29 cells were routinely cultured in Roswell Park Memorial Institute (RPMI) culture media (Sigma-Aldrich) and DLD-1 cells were cultured in a 1:1 (v/v) solution of Dulbecco's Modified Eagles Medium (DMEM) (Sigma-Aldrich) and Hams F-12 culture media (Sigma-Aldrich). Complete culture media was supplemented with 10 % FBS and sterile filtered before use. All solutions were stored at 4 °C until required. Culture medium was warmed to room temperature prior to use in culture.

FBS, which stimulates attachment, growth and proliferation of cells (Brunner *et al*., 2010) was heat-inactivated at 56 °C in a water bath for 60 minutes to inhibit the proteolytic activity of complement proteins (Rahman *et al.,* 2011). Thereafter, FBS was aliquoted into 50 ml test tubes and stored at -20 °C until required.

Phosphate buffered saline (PBS) was used to rinse cultures and to remove residual media that would inhibit the trypsinization process. PBS (1.37 mM NaCl ,27 mM KCl, 100 mM Na_2HPO_4 and 18 mM KH_2PO_4 (pH 7.2-7.4) was autoclaved and stored

at 4 ˚C until required. All media and solutions were warmed to room temperature before used in culture

Trypsin is an enzyme used in cell culture to dissociate adherent cells from the growth surface or from cell clusters to form single-cell suspensions. Trypsin ethylenediamine tetraacetate (trypsin-EDTA) (Sigma-Aldrich) was used in cell culture since both HT-29 and DLD-1 cell lines were adherent.

2.1.2 Cell maintenance and sub-culture

Cells were grown aseptically in 75 cm^3 culture flasks (Greiner Bio-one) in 20 ml complete medium. The cells were maintained, with a fractionally opened lid at 37 °C in a humidified incubator with an atmosphere of 5 % CO_2. When the cells had reached a confluency of 85 % they were sub-cultured as follows:

The culture media was aspirated and discarded. Cells were washed twice with 20 ml of a 1 X PBS solution (pH 7.4) which was discarded after each wash. This was followed by incubation with 3 ml of 0.25 % trypsin-EDTA for 3-5 minutes. Once the cells had detached, 5 ml complete culture media was added to the suspension and gently pipetted repeatedly to dissociate any clusters of cells that formed during trypsinization. Generally, 1 ml of the suspension was resuspended in 20 ml of complete culture medium and returned to the incubator. The culture media was replaced every second day until the cells reached confluency.

2.1.3 Determination of cell numbers and cell viability before use in experiments

The number of viable cells in the cell suspension was determined using the trypan blue exclusion assay. Trypan blue is a dye which crosses the cell membrane of dead cells, staining them blue while leaving living cells unstained (Avelar-Frietas *et al.,* 2014). This was carried out by adding 20 µl 0.4 % trypan blue (Sigma-Aldrich) to 20 µl of the cell suspension and mixed. Twenty microliters of the suspension was then added to and counted in a hemocytometer. Cells were only used in experiments if their viability exceeded 97 %.

2.1.4 Cryopreservation

Cryopreservation preserves the structural characteristics of cells at low temperatures and protects cells from contamination and damage until required in culture (Ramos *et al.,* 2014). Cell lines were cryopreserved in 74 % complete culture media specific to each cell line, 20 % FBS and 6 % of the cryoprotective agent, dimethyl sulfoxide (DMSO). Cell culture grade DMSO (Monitoring and Control Laboratories) was used. Following trypsinisation, cells were placed in 15 ml centrifuge tubes and were centrifuged (Thermo Scientific™ Heraeus Megafuge 40, Rotor 75003607) for 5 minutes at 1500 rpm. The supernatant was removed and discarded and the pellet was resuspended in 10 ml freezing media. Thereafter, 1.8 ml of the cell suspension was aliquoted into 2 ml cryotubes (Greiner Bio-One) and left at room temperature for 5-10 minutes. The cryotubes were placed in a -77 °C freezer for 72 hours in a cryobox that allows for a controlled freezing rate of 1 °C/min to retain structural integrity and optimal cell viability (Yokoyama *et al.,* 2012). Once frozen, the cryotubes were stored in liquid nitrogen at -196 °C.

2.2 Test Compounds

Three groups of compounds were evaluated against the two cells lines. They included copper-imidazo[1,2-*a*]pyridine complexes, nucleoside analogues and epidermal growth factor receptor kinase inhibitors. All compounds were synthesized by researchers in the School of Chemistry at the University of the Witwatersrand. All compounds were evaluated for purity and their structures verified by elemental analysis (copper-imidazo[1,2-*a*]pyridines) or nuclear magnetic resonance (NMR) spectroscopy. The groups of test compounds, JDs and JLPs were named after the initials of the scientist who created the compounds. Stock solutions of 2 mM of test compounds and camptothecin were prepared in 100 % ethanol (v/v). The structures of the compounds evaluated in this study are shown in Chapter III. Table 3.1 and Appendix A, Table A1 and A2.

The test compounds were evaluated for their ability to inhibit cell growth at a concentration of 50 μM. The fifty percent inhibitory concentration (IC_{50}) were obtained for compounds that caused more than 80 % inhibition at 50 μM. The

compounds which were the most potent were further assessed for their ability to induce apoptosis. This was done using assays which measured specific apoptotic characteristics. All screening assays were performed in triplicate and individual data points were obtained in quadruplicate. Each experiment included an untreated control and a positive control using either camptothecin or staurosporine. A 5 mM stock solution of staurosporine was prepared in dimethyl sulfoxide (DMSO).

2.3. The 3-[4,5-dithylthiazol-2-yl]-2,5 diphenyl tetrazolium bromide (MTT) cell viability assay

The 3-[4,5-dimethylthiazol-2-yl]-2,5 diphenyl tetrazolium bromide (MTT) assay is a rapid, quantitative, colorimetric assay that detects metabolic activity and is used in the measurement of cellular viability, proliferation or cytotoxicity (Mosmann, 1983). The assay is based on the principle that in healthy viable cells, the mitochondrial enzyme succinate dehydrogenase cleaves the yellow tetrazolium salt, MTT, into an insoluble purple formazan crystal (Price and McMillan, 1990). The water-insoluble formazan crystals are dissolved in an organic solvent, such as DMSO (Stepanenko and Dmitrenko, 2015) before optical density is measured at a test wavelength of 540 nm and a reference wavelength of 690 nm (Mosmann, 1983). A calibration curve of absorbance versus cell number for each cell line were determined, shown in Appendix B, Figure B1 and Figure B2.

In the screening assays, HT-29 and DLD-1 cell lines were exposed to 50 μM of test compound, 50 μM of camptothecin, 200 nM of staurosporine and a negative control containing no treatment for 48 hours and screened using the MTT assay. Preliminary studies showed a 100 % cell death at a concentration of 5 μM of staurosporine after 24 hours in both cell lines, therefore the concentration was further reduced to 2 μM.HT-29 and DLD-1 cells were seeded in 96-well microtiter plates (NEST Bio-tech Co., Ltd) at a density of 6 000 (HT-29) and 7 000 (DLD-1) cells per well in 180 μl culture media and incubated for 24 hours to allow attachment before exposure to test compounds. The test compounds were then added to the wells in a volume of 20 μl to give a final test compound concentration of 50 μM/well. The plates were then incubated in a partially closed plastic container at 37 °C and 5 % CO_2 for 48 hours.

MTT (5 mg/ml) (w/v) was prepared in sterile PBS and sterile filtered through a 0.22 μm membrane. A volume of 40 μl of MTT was added to each well and incubated for 3-5 hours. The culture medium and MTT was carefully aspirated from each well and 200 μl DMSO was added, to dissolve the formazan crystals. The 96-well plates were shaken on an orbital plate shaker (Thermoshaker MRC) at 1000 rpm for 5 minutes to ensure complete solubilization of the formazan crystals. The absorbance was measured using the Lab Systems Multiskan iEMS plate reader at a wavelength of 540 nm and a reference wavelength of 690 nm. The negative control consisted of cells with medium and a blank with only medium. Camptothecin and staurosporine were used as positive controls.

IC_{50} values were obtained by exposing cells to a range of concentrations (0.05 – 100 μM). At least five MTT assays were performed to obtain each average IC_{50} value and each data point was performed in quadruplicate. Sigmoidal dose response curves were constructed using the GraphPad Prism Version 5.0 Software package. The statistical significance comparing the average IC_{50} values of the control and test compounds were determined using the Mann-Whitney U-test on GraphPad Prism with a significance set at $p < 0.05$.

2.4 Cell Morphology

2.4.1 Preparation of cells for morphology studies

Glass coverslips were heat sterilized by soaking in 100 % analytical grade ethanol followed by immediate flaming. Sterile coverslips were then placed in each well of a six-well plate (Greiner Bio-One). Trypsinized and counted, cells were seeded at 50,000 cells per coverslip in a total volume of 2 ml complete culture media and incubated overnight at 37 °C in a humidified incubator with 5 % CO_2. After 24 hours, the culture media was removed and replaced with media containing the appropriate amount of test compound. Exposure periods varied according to experimental protocols. Cells were then prepared for phase contrast or fluorescence studies based on experimental protocols.

2.4.2 Phase contrast images

Cells were treated in six-well plates with 10 μM of test compound in a volume of 2 ml complete culture media respective to each cell line and examined for major morphological changes using an Olympus DP72 microscope. Phase contrast images of cells were captured over the course of 48 hours.

2.4.3 Vital dye staining using a combination of Acridine Orange/Ethidium Bromide/Hoechst (AO-EtBr-HO)

Specific stains are used in combination to distinguish between viable, early and late apoptotic and necrotic cells (Monga *et al*., 2013) and can provide clues to the presence of apoptosis. Due to apoptosis-associated changes of cell membranes that occur during the apoptotic process (Liu *et al.,* 2015b), analysis of changes in cell morphology was evaluated using a combination of the fluorescent stains, acridine orange (AO), ethidium bromide (EtBr) and Hoechst 33342 (HO).

Acridine orange permeates both viable and non-viable cells and emits a green fluorescence when bound to DNA. In addition, it causes acidic granules to fluoresce red and, in this context, is a preliminary indicator for autophagy (Karna *et al*., 2014). Ethidium bromide only penetrates cells with a compromised cell membrane and emits an orange-red fluorescence when bound to DNA (Ribble *et al*., 2005). In late apoptotic cells, EtBr penetrates the cell membrane and predominates over AO, staining the DNA orange-red (Ribble *et al*., 2005). Orange EtBr staining of the nucleus thus indicates that cells are necrotic unless the DNA shows the typical globular pattern indicative of apoptosis as shown in Figure 2.1. The DNA specific dye, Hoechst 33342 (HO), crosses membranes and stains a viable nucleus uniformly blue when viewed under UV light (Mpoke and Wolfe, 1997). If the nucleus is compromised, it shows typical structures associated with chromatin condensation or if the nucleus is apoptotic, the intensity of the blue fluorescence increases and shows the characteristic pattern of a fragmented nucleus, as shown below in Figure 2.1.

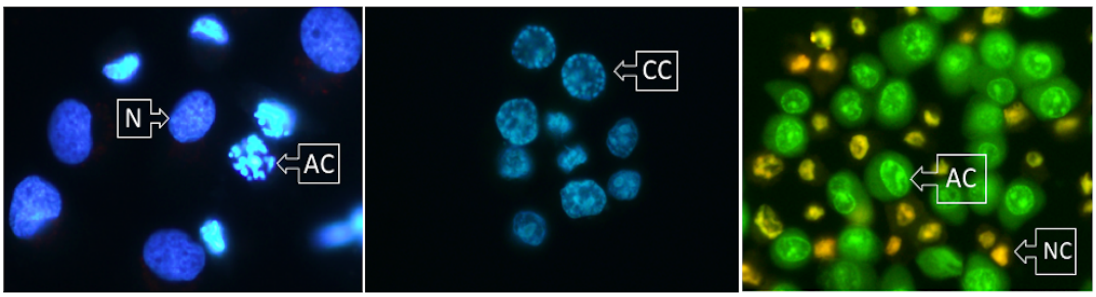


Figure 2.1 Fluorescent micrographs showing normal and apoptotic nuclei and necrotic cells as stained by vital dyes, HO, AO and EtBr. Images were viewed on an Olympus BX41 epifluorescence microscope and captured on an Olympus DP72 camera (Magnification: 400 X, exposure time= 11.0 ms and ISO= 400) (Scalebar: 20 µM). Legend: AC= apoptotic cell, CC= chromatin condensation, N= normal cell and NC= necrotic cell

This combination of dyes distinguishes between apoptotic, necrotic or healthy cells by clear color differentiation. A combination of these stains is advantageous as it permits a more distinctive identification of the types of nuclei than either stain alone (Mpoke and Wolfe, 1997). The commonly used PI does not work well when combined with HO and AO, therefore EtBr was used.

2.4.3.1 Staining procedure:

Preparation of the combination dye:

Cells grown overnight on coverslips in six-well plates were exposed to 10 µM of test compound. A concentration of 10 µM was chosen as it was roughly ten times the IC_{50} value of the most active compounds against HT-29 cells. The same concentration was used between the two cell lines to allow for a direct comparison. Ten times the IC_{50} value for DLD-1 cells required between 80 - 100 uM at which this concentration results in solubility concerns. Staurosporine (200 nM) was used as a positive control. The media was gently aspirated and discarded. Each well was rinsed twice with 2 ml of a 1 x PBS solution (pH 7.4). Stock solutions of AO (3 µl/ml), EtBr (0.4 µl/ml) and HO (3 µl/ml) were prepared in microcentrifuge tubes. One ml of each dye was combined in a microcentrifuge tube and the remaining stock solution was refrigerated at 4 ºC until required for use. The PBS was aspirated and the coverslip incubated with 500 µl of dye mixture in the dark, at room temperature for 20 minutes. This was followed by a PBS wash with 1 ml after which the coverslip was removed and

mounted in a drop of Fluoromount (Sigma-Aldrich), cells facing down on a microscope slide. Cells were viewed using an Olympus BX41 epifluorescence microscope. AO/EtBr detection was acquired using the filter cube U-MNIBA3 (excitation: 470 – 490 nm ± 20; emission: 510 – 550 nm). The long pass UV filter cube U-MWU2 was used for acquiring HO images (excitation: 330 - 385 nm ± 10; emission: 420 nm). Images were captured with an Olympus DP72 camera. All images were analyzed with the Olympus CellSens Software package. Where required, the brightness and contrast were increased.

2.5 Evaluation of Apoptosis

Specific apoptosis assays assess the mechanism of cell death based on the activation of specific markers characteristic of the apoptotic process. In this study, the exposure of phosphatidylserine (PS) on the external surface of the cell was assessed using Alexa Fluor-488 conjugated to annexin-V and examined under fluorescence microscopy. The detection of caspase-3 activity was analyzed using a fluorometric assay. Changes in the mitochondrial membrane potential were identified with the JC-1 cationic dye and evaluated using fluorescence microscopy. Caspase-9 was assessed using a live staining kit and viewed under fluorescence microscopy.

2.5.1 Annexin-V

Cells undergoing apoptosis lose the phospholipid asymmetry of their plasma membrane. Phosphatidylserine (PS), a negatively charged phospholipid is translocated from the inner leaflet of the cell and is exposed on the external surface of the membrane (Vermes *et al.,* 1995). Annexin V, a Ca^{2+} dependent phospholipid-binding protein belonging to the annexin group, detects apoptotic cells by preferentially binding to PS. The translocation of PS occurs in both apoptosis and necrosis; the difference is during early apoptosis, the cell membrane remains intact, whereas during necrosis, the cell membrane integrity is lost (Vermes *et al*., 1995). Annexin-V was therefore used in conjunction with propidium iodide (PI), a nucleic acid binding dye, in a dye exclusion test in order to determine the integrity of the cell membrane. PI is impermeable to cells with intact cell membranes. Late apoptotic or

necrotic cells have compromised membrane integrity, PI therefore intercalates with their DNA displaying a red fluorescence (Rieger *et al*., 2011; Vermes *et al*., 1995).

The ThermoFisher Alexa Fluor® 488 Annexin V/ Dead Cell Apoptosis Kit was used to detect translocated phosphatidylserine. The kit contained recombinant annexin-V conjugated to the Alexa Fluor® 488 dye. Cells grown on coverslips in six-well plates were treated with test compounds and incubated for various time periods. An untreated negative control and a positive control using staurosporine was included. Annexin-binding buffer was prepared using MilliQ water. A 100 µg/ml working solution of PI was prepared by diluting the stock solution in the annexin-binding buffer. The annexin-V detection reagent was then prepared by adding the Alexa Fluor® 488-annexin-V conjugate and PI working solution to 1 x annexin-binding buffer. The cover slips were washed with a 1 x PBS solution (pH 7.4). Thereafter, 100 µl of a solution containing Alexa Fluor® 488-annexin-V (6 % v/v) and propidium iodide (1 % v/v) was placed on the microscope slide. The cover slip was carefully placed, downwards onto the solution and was incubated at room temperature, in the dark for 15 minutes. Cells were viewed with an Olympus BX41 epifluorescence microscope. Alexa Fluor® 488 conjugated to annexin-V was detected using the U-MNIBA3 filter cube (excitation: 470 – 490 nm ± 20; emission: 510 – 550 nm). Images were captured with an Olympus DP72 camera and analyzed with the Olympus CellSens Software package.

2.5.2 Measurement of caspase-3/7 activity

Once apoptotic signaling occurs, initiator caspases cleave and activate downstream executioner caspases causing apoptosis. Upon activation by initiator caspases, the effector caspase-3 is responsible for proteolytic cleavage of structural and repair proteins in the execution phase of apoptosis (Slee *et al*., 2001 and Shi, 2002). HT-29 and DLD-1 cells were plated in six-well microtiter plates at a density of 50,000 cells per well and were incubated at 37 ˚C for 24 hours, allowing the cells to adhere. Each experiment included an untreated control comprising of complete culture medium and 200 nM staurosporine as a positive control.

The assay was performed as per the Abcam Caspase-3/7 Fluorometric Kit (Ab39383). Caspase-3/7 cleaves proteins containing the amino acid sequence Asp-Glu-Val-Asp (DEVD). The assay is based on the detection of the cleavage of the substrate DEVD-AFC (AFC: 7-amino-4-trifluoromethyl coumarin) and is quantified using a spectrofluorimeter. Upon cleavage of the substrate by caspase 3, DEVD-AFC emits a blue light and free AFC emits a yellow-green fluorescence. HT-29 and DLD-1 cells were treated with 10 µM of test compound for 20 hours. Staurosporine (200 nM) was used as a positive control. Following exposure, the media was aspirated and cells were washed gently with 2 ml of 1 x PBS solution (pH 7.4). Thereafter the PBS was aspirated and cells were trypsinized with 1 ml trypsin-EDTA for 10 minutes in a humidified incubator at 37 ºC. One ml culture media was added to inhibit the trypsin reaction and thereafter transferred to sterile 2.0 ml microcentrifuge tubes. Cells were centrifuged in a micro-centrifuge (Microcentaur MSE) at 1000 rpms for 5 minutes, washed twice with 2 ml PBS and centrifuged after each wash at 1000 rpm for 5 minutes. The supernatant was discarded after each centrifugation.

HT-29 and DLD-1 cell pellets were re-suspended in 60 µl chilled Lysis Buffer and incubated on ice for 10 minutes. Ten microliters of DTT (Dithiothreitol) was added to 1.0 ml of 2 X reaction buffer (to obtain a final concentration of 10 mM). The protein concentration of cell lysates was then determined using the Bradford assay, as described in section 2.5.3. Thereafter, 200 µg of cell lysates and 5 µl of the 1 mM DEVD-AFC substrate was added to each well of a 96-well black-fluorescence plate followed by the addition of 50 µl of 2 X reaction buffer (containing DTT) to each well to ensure adequate mixing. This was followed by incubation at 37 ˚C for 2 hours. The relative fluorescence was read with the Molecular Devices FilterMax F5 Multi-Mode Microplate Reader equipped with Softmax Pro Microplate Data Acquisition and Analysis Software. (Excitation: 405 nm and emission: 535 nm). The protein concentration was determined from the standard curve. Specific activity of the caspase-3/7 protein was calculated and the caspase-3/7-fold increase was determined by comparing the obtained results to an untreated control (Appendix E, Table E1 and Table E2).

2.5.3 Protein estimation

The protein concentration in cell lysates were measured using the Bradford protein assay (BIO-RAD). This dye-binding assay is based on a color change of the Coomassie Brilliant Blue G-250 dye when bound to proteins of various concentrations. When bound to proteins, there is a change in the absorption maximum from 465 nm to 595 nm (Bradford, 1976).

Standardized bovine serum albumin (BSA) (1.0 mg/ml) (Fluka ™) was used to construct a standard curve. Two hundred microliters of diluted dye reagent (1 part dye in 4 parts ddH_2O) was then added to each well.

Ten µl of each test sample was pipetted into individual wells of a 96-well microtiter plate, in duplicate followed by 200 µl of dye reagent. Using the Multiskan^{TM} GO Microplate Spectrophotometer (Thermo Scientific^{TM}), each well was shaken at 300 rpm for 5 minutes and absorbance was measured at 595 nm. A standard curve was constructed with concentrations for each protein determination. Standard curves are shown in Appendix D, Figure D1-3.

2.5.4 Mitochondrial membrane potential assay

The disruption of mitochondrial membrane potential is characteristic of the apoptotic process. The electron transport chain produces an electrochemical gradient by means of oxidative reactions which generates a mitochondrial membrane potential ($\Delta\psi m$) (Sakamuru *et al.,* 2016). $\Delta\psi m$ is essential in many mitochondrial processes and is a feature of mitochondrial function. Mitochondrial function can be evaluated by observing the mitochondrial membrane potential (Sakamuru *et al.,* 2016). Depolarization of the mitochondrial membrane was assessed using the cationic carbocyanine 5',6,6'-tetrachloro-1,1',3,3'-tetraethyl-benzimidazolyl-carbocyanine iodide (JC-1) dye (Smiley *et al*., 1991). The JC-1 dye facilitates differentiation between low and high membrane potential. At low concentrations (due to a low $\Delta\psi m$), the dye remains in its monomeric form, displaying a green fluorescence. At high concentrations (due to a high $\Delta\psi m$), in healthy cells the dye accumulates in the mitochondria forming JC-1 aggregates, causing a shift in the fluorescence spectrum from green to red.

The assay was carried out as per the Molecular Probes ™ protocol. The HT-29 and DLD-1 cells were seeded on coverslips in six-well plates at a density of 50,000 cells per well and left to adhere for 24 hours at 37 ˚C in a humidified incubator. The cells were treated with test compound and were incubated for 12 hours. Results obtained in HT-29 and DLD-1 cells before 12 hours showed red fluorescence with JC-1 aggregates indicative of an intact mitochondrial membrane potential. A negative control consisted of untreated cells in culture medium. Staurosporine (200 nM) was used as a positive control. Following exposure of test compounds, the media was aspirated and the cells were washed twice with 1 ml of a 1 x PBS solution (pH 7.4). Cells were stained with 500 µl of 5 µg/ml (5 mg/ml stock) JC-1 for 20 minutes at room temperature in the dark. The dye was then aspirated and wells were washed twice with PBS. The coverslips were mounted on microscope slides with the cells facing downwards and were viewed with an Olympus BX41 epifluorescence microscope using the filter cube U-MNIBA3 for FITC (excitation: 470 – 490 nm ± 20; emission: 510 – 550 nm). Images were captured with an Olympus DP72 camera and analyzed with the Olympus CellSens Software package.

2.5.5 Caspase-9 detection

The assay was performed as per the Abcam Caspase-9 Active FITC Staining Kit (ab65615) protocol which detects activated caspase-9 in living cells. Caspase-9 cleaves proteins containing the amino acid sequence Leu-Glu-His-Asp (LEHD). The assay uses the caspase-9 inhibitor LEHD-FMK (fluoromethylketone) conjugated to FITC (FITC-LEHD-FMK) as a fluorescent marker. FITC-LEHD-FMK irreversibly binds to activated caspase-9 in apoptotic cells. When observed using the U-MNIBA3 filter for FITC detection, caspase-9 positive cells fluoresce bright green.

HT-29 and DLD-1 cells were grown on coverslips in six-well plates at a density of 50,000 cells per well and left to adhere for 24 hours at 37 ˚C in a humidified incubator. Cells were treated with 10 µM of test compound and incubated for 18 hours. Staurosporine (200 nM) was used as a positive control and the negative control consisted of untreated cells in culture medium. Following treatment of cells, the media was discarded and cells were washed twice with 2 ml of a 1 x PBS solution

(pH 7.4). Nine hundred microliters of Wash Buffer and 3 µl FITC-LEHD-FMK were aliquoted into a sterile microcentrifuge tube and gently pipetted to ensure mixing. One hundred and fifty microliters of the prepared solution was added to each well containing treated cells and control samples and incubated for 1 hour at 37 ˚C. Using a sterile blade and a pair of forceps, cover slips were carefully lifted and washed three times with PBS before mounting, cells facing down on a microscope slide. Caspase positive cells have brighter green signals and caspase negative cells have weaker signals. Cells were viewed with an Olympus BX41 epifluorescence microscope using the U-MNIBA3 filter cube for FITC detection (excitation: 470 – 490 nm ± 20; emission: 510 – 550 nm). Images were captured with an Olympus DP72 camera and analyzed with the Olympus CellSens Software package.

2.6 Expression of apoptosis-related proteins using a proteome array

Since it was not feasible to test the effects of active test compounds on all the proteins involved in apoptosis, it was hoped that an apoptotic proteome array would be able to provide some insight into changes of apoptotic protein expression. In the context of this study, the active copper-imidazo[1,2-*a*]pyridines were selected to determine their effect on the expression levels of some of the proteins involved in the regulation of the apoptotic pathway.

The Proteome Profiler ™ Human Apoptosis Array Kit (R&D Systems), is a membrane-based antibody array used to simultaneously detect the expression of 35 apoptosis-related proteins. Capture antibodies are spotted in duplicate onto nitrocellulose membranes. Proteins present in cell lysates are incubated with the array and the apoptotic proteins bind to their corresponding antibodies. After washing to remove any unbound protein, membranes are incubated with a cocktail of biotinylated detection antibodies to detect captured proteins. The signal of streptavidin is amplified when conjugated to horse radish peroxidase (HRP). Streptavidin has a high binding affinity to the biotinylated antibodies and the HRP enzyme allows for chemiluminescent detection at each capture spot. The resultant signal produced on each capture spot on the nitrocellulose membrane corresponds to the amount of bound protein. The procedure is described in the flow diagrams, Figure 2.2A and 2.2B

below. The assay was performed to investigate possible changes in the expression profile of apoptosis-related proteins in HT-29 cells treated with the active copper-imidazo[1,2-*a*]pyridines.

Procedure: Ten million cells/flask per treatment were seeded in 75 cm^3 flasks and were allowed to adhere overnight. The following day, the cells were treated with 5 µM of test compound for 18 hours. Treated cells were washed three times with 2 ml of a 1 x PBS solution (pH 7.4) and the cells harvested with a cell scraper. Thereafter, cells were solubilized in 2.5 ml Lysis Buffer 17, to which was added a protease inhibitor cocktail. One Roche protease inhibitor mini tablet was added per 10 ml of lysate (catalogue number: 11 836 170 001). The cell lysate was pipetted until no cell clumps were visible and then incubated for 30 minutes on a rocking platform at 4 ºC. Lysates were then centrifuged in a Joaun Centrifuge, open-angled rotor (catalogue number 11174588) at 15 000 rpms for 5 minutes. The supernatant was transferred into a new microcentrifuge tube and stored on ice while the protein determination was performed for each cell lysate using the Bradford protein assay, as described in section 2.5.3. The lysates were diluted 1:4 with water to reduce the concentration of substances that may interfere with the Bradford assay. All reagents were kept on ice for the duration of the experiment and reagents were prepared immediately prior to usage. Reagent preparation is described in Table 2.1.

While the lysate was being prepared, one array per treatment was placed into each well of the supplied 4-well multi-dish together with 2 ml Array Buffer 1 and incubated on a rocking platform for at least 60 minutes at 4 ºC. This step served as a membrane blocking step. Following the protein determination, lysate samples containing 400 µg of protein were added to Array Buffer 1 to a total volume of 2 ml per array (obtained from protein quantification). Once the blocking step was completed, Array Buffer 1 was aspirated from the well and the lysate samples were added and incubated overnight on a rocking platform at 4 ºC.

Each array was removed from the multi-dish and placed in individual containers with 20 ml Wash Buffer. Arrays were washed three times with 20 ml 1 X Wash Buffer for 10 minutes on a rocking platform. Following the washing steps, the arrays were returned to the cleaned multi-well dish and incubated with the 1.5 ml of detection

antibody cocktail for 1 hour on a rocking platform. This was followed by another washing step as described above. After washing the membranes, they were incubated for 30 minutes with 2 ml of streptavidin-HRP on a rocking platform at 4 ºC. The washing step was thereafter repeated for a total of three washes, as described above.

Membranes were removed from respective wash containers, and briefly blotted with filter paper to remove excess wash buffer. The membranes were placed on a transparent sheet of plastic and 1 ml of freshly prepared chemiluminescence reagent was pipetted evenly onto each membrane, covered with another sheet of transparent plastic and incubated for 1 minute. This was followed by removal of the top plastic sheet and the membranes briefly blotted with filter paper to remove excess Chemi Reagent Mix. The membranes, still on the bottom transparent sheet, were covered with plastic wrap and immediately placed into a BIO-RAD ChemiDoc ™ MP Imager to detect the positive chemiluminescent signals on the membrane. Data was analyzed using the Image Lab Software Version 6.

Table 2.1: Reagents requiring preparation prior to usage

Reagents	Preparation
Lysis Buffer 17	Add 1 Protease inhibitor cocktail tablet to 10 ml of Lysis Buffer 17
1 X Wash Buffer	Dilute 20 ml of 25 X Wash Buffer Concentrate into 480 ml deionized water (check required volume)
1 X Array Buffer 2/3	Dilute 2 ml of 5 X Array Buffer 2 Concentrate into 8 ml of Array Buffer 3
Detection Antibody Cocktail	Reconstitute Human Apoptosis Detection Antibody Cocktail in 100 µl deionized water
Chemi Reagent Mix	Chemi Reagent 1 and 2 are mixed in equal volumes within 5 minutes of usage. Cover in foil to protect from light.

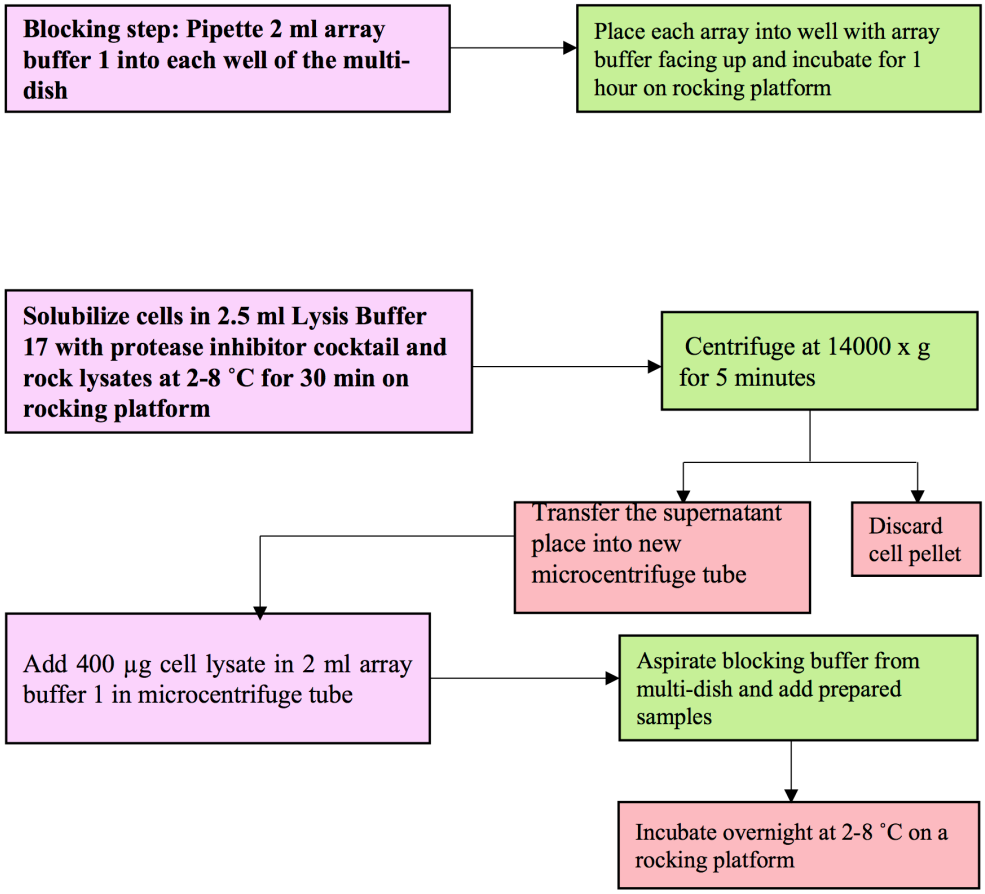


Figure 2.2 (A) Flow diagram of day one of the human apoptosis array method

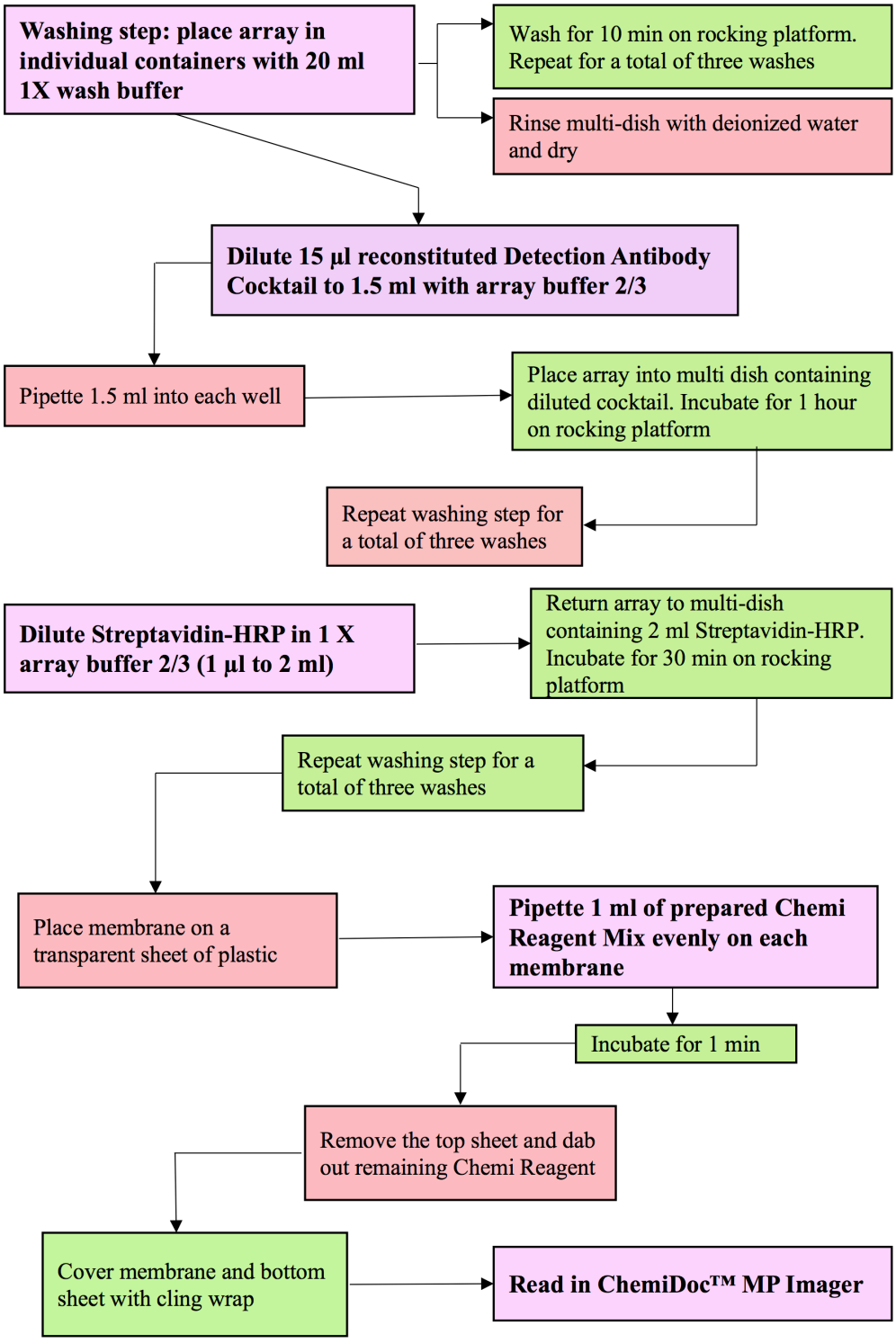


Figure 2.2 (B) Flow diagram of day two of the human apoptosis array method

Chapter III. Results

3.1 Screening of test compounds on HT-29 and DLD-1 cell lines

The novel compounds used in this study were synthesized by the Department of Chemistry at the University of the Witwatersrand. Three different classes of compounds were evaluated in this study and the results are presented below. HT-29 and DLD-1 colorectal cancer cells were exposed to nucleoside analogues (JLPs), epidermal growth factor receptor kinase inhibitors (EKIs) and copper-complexed imidazo[s1,2-*a*]pyridines (JDs) to identify active compounds. Compounds that caused more than an 80 % inhibition of cell viability at 50 µM after 48 hours were considered active and were further assessed to determine their IC_{50} values. Camptothecin and staurosporine are known inducers of apoptosis and were chosen as positive controls against both cell lines. Staurosporine is a non-selective protein kinase inhibitor and camptothecin is the parent compound of irinotecan which is currently used in the treatment of metastatic CRC. Screening results are shown below in Figure 3.1 and Figure 3.2.

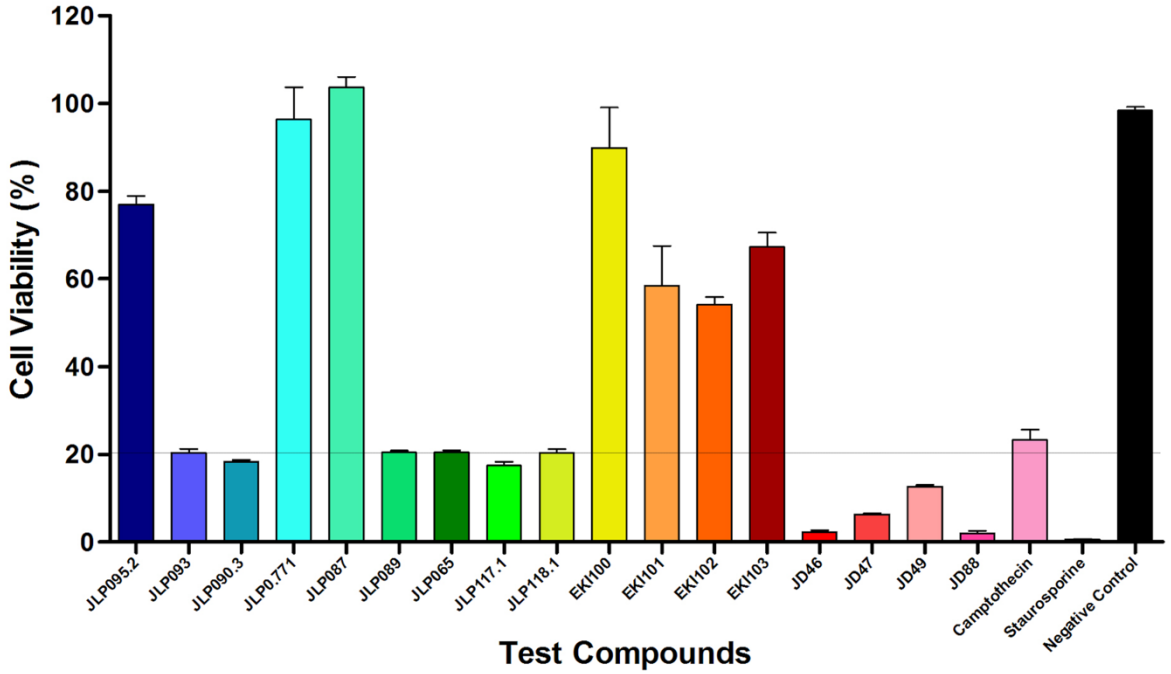


Figure 3.1 The effect of test compounds on the cell viability of HT-29 cells. HT-29 cells were exposed to nucleoside analogue (JLPs), EKIs and copper-imidazo[1,2-*a*]pyridine (JDs) test compounds and camptothecin at 50 µM, 2 µM staurosporine and a negative control with no treatment for 48 hours. Each bar represents the mean ± SEM of values obtained from four independent assays.

The results identified six JLPs (JLP093, JLP090.3, JLP089, JLP065, JLP117.1 and JLP118.1) that reduced HT-29 cell viability by more than 80 % (Figure 3.1). The EKIs were poorly active, reducing cell viability between 15 and 55 %. EKI 102 was the most active (approximately 50 % inhibition) and EKI 100 the least active, reducing cell viability by 15 % (Figure 3.1). The JDs (JD46, JD47, JD49 and JD88) were the most active, reducing cell viability by more than 85 % (Figure 3.1). The positive controls had dissimilar results; staurosporine reduced cell viability by more than 99 % and camptothecin by more than 80 % with a percent cell viability of 23.3 % (Figure 3.1).

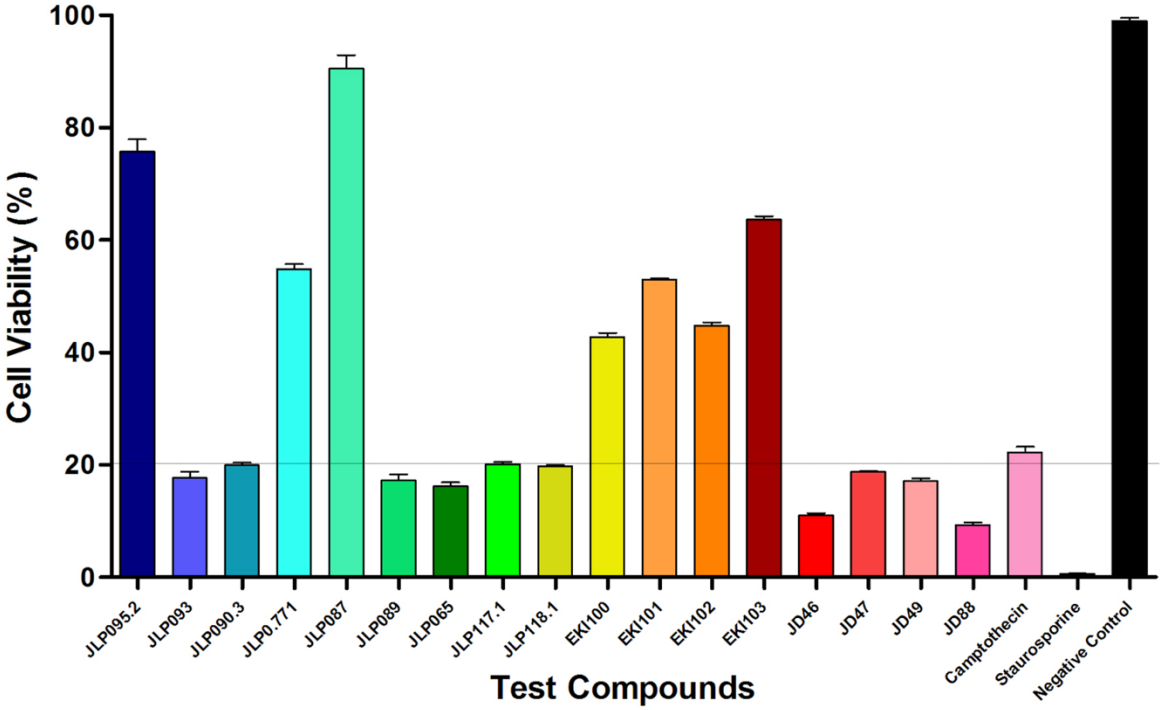


Figure 3.2 The effect of test compounds on the cell viability of DLD-1 cells. DLD-1 cells were exposed to nucleoside analogues (JLPs), EKIs and copper-imidazo[1,2-*a*]pyridine (JDs) test compounds and camptothecin at 50 µM, 2 µM staurosporine and a negative control with no treatment for 48 hours. Each bar represents the mean ± SEM of values obtained in quadruplicate from four independent assays.

Initial screening results of test compounds and positive controls showed similarities in the percent cell viability between DLD-1 and HT-29 cell. Six JLP compounds reduced cell viability by more than 80 % in DLD-1 cells (Figure 3.2). The EKIs reduced cell viability by less than 60 % (Figure 3.2). The JD compounds reduced cell viability by more than 80 % with JD88 being the most active. (Figure 3.2). Staurosporine was more active than camptothecin and reduced cell viability by more than 99 % (Figure 3.2). The compounds

selected for the determination of IC_{50} values reduced cell viability in HT-29 and DLD-1 cells by more than 80 % and were considered the most active. No further work was pursued on the EKIs since they showed poor cytotoxic activity. The structures of the EKIs and nucleoside analogues are shown in Appendix A, Table A1 and Table A2.

3.1.1 IC_{50} values of the nucleoside analogues on DLD-1 and HT-29 cells

Dose response curves were constructed from the data obtained using the MTT assay. The fifty percent inhibitory concentrations (IC_{50} values) were calculated from sigmoidal dose response curves generated by the Graph Pad Prism version 5 software. Dose response curves are shown in Appendix C, Figure C1 and C2.

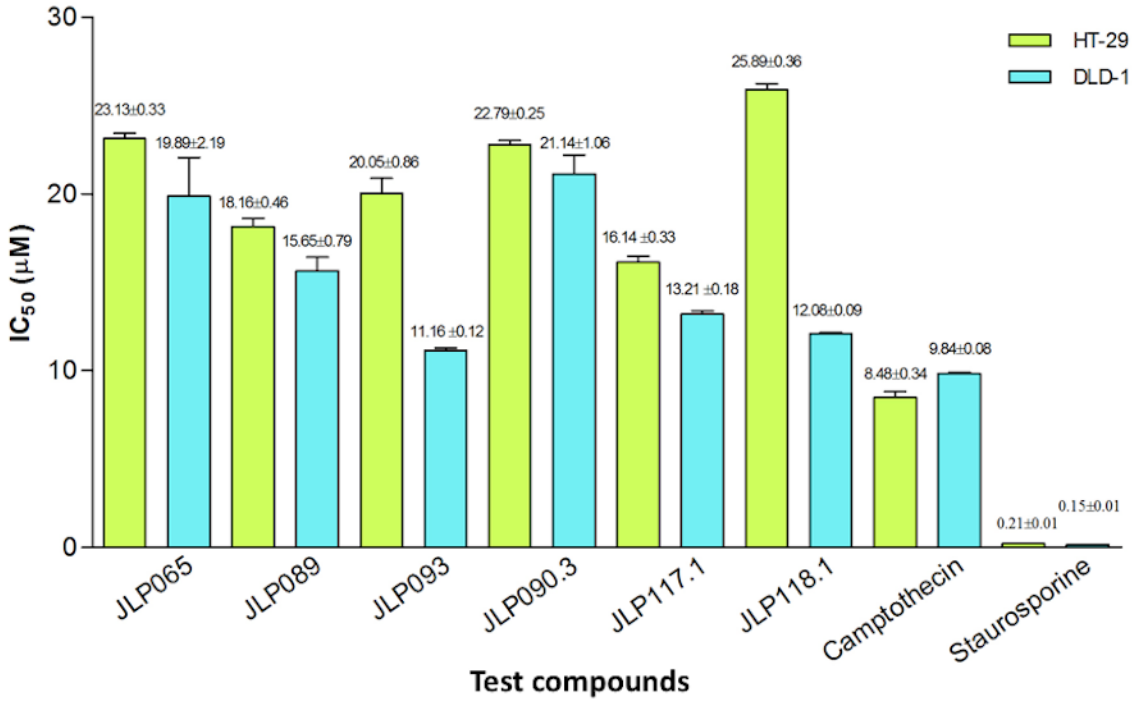


Figure 3.3 IC_{50} values of nucleoside analogues and the positive controls, camptothecin and staurosporine in HT-29 and DLD-1 cells. HT-29 and DLD-1 cells were exposed to nucleoside analogues and camptothecin at concentrations ranging from 0.05 µM to 100 µM for 48 hours. Staurosporine concentrations ranged from 0.05 µM to 2 µM. Each bar represents the mean ± SEM of IC_{50} values obtained from five MTT assays.

IC_{50} values were obtained by exposing cells to a range of concentrations of test compounds between 0.05 µM and 100 µM for 48 hours. Staurosporine concentrations ranged from 0.05 µM to 2 µM. Experiments were repeated at least five times. Figure 3.3 is a summary of IC_{50} values of the nucleoside analogues and the positive controls, camptothecin and staurosporine obtained for HT-29 and DLD-1 cells. The results are presented in Figure 3.3 and indicates

that DLD-1 cells were more sensitive to the nucleoside analogues than the HT-29 cells. The HT-29 cell line was more sensitive to camptothecin but less sensitive to staurosporine than the DLD-1 cell line. Staurosporine was most active with IC_{50} values in the 200 nM range for both cell lines.

IC_{50} values of the test compounds and positive controls, camptothecin and staurosporine were compared to determine significant differences. Statistical analysis of IC_{50} values was performed using the two-sample, unpaired Mann-Whitney U-test with significance set at $p < 0.05$ and a 95 % confidence interval. The IC_{50} values of nucleoside analogues in DLD-1 cells ranged from 11.0 μM to 21.0 μM. The DLD-1 cells were most sensitive to JLP093 (IC_{50} = 11.16 ±0.12 μM) and least sensitive to JLP090.3 (IC_{50} = 21.14 ±1.06 μM). There was no significant difference in the IC_{50} values of JLP090.3 and JLP065 ($p > 0.05$, $p = 0.49$), indicating similar efficacy of these two compounds.

The IC_{50} values of nucleoside analogues in HT-29 cells ranged from 16.0 μM to 26.0 μM. As seen in Figure 3.3, HT-29 cells were most sensitive to the positive controls, staurosporine and camptothecin, having IC_{50} values of 0.21 μM and 8.48 μM, respectively. In the test compounds, HT-29 cells were most sensitive to JLP117.1 (IC_{50} = 16.14 ± 0.33 μM) and least sensitive to JLP118.1 (IC_{50} = 25.89 ± 0.36 μM), with a significant difference of $p = 0.0079$. There was no significant difference between the IC_{50} values of JLP065 and JLP090.3 ($p > 0.05$, $p = 0.49$), indicating similar efficacy of these compounds. No significant difference was observed between JLP090.3 and JLP093 ($p > 0.05$, $p = 0.12$), indicative of similar efficacy. Statistical analysis comparing camptothecin and the JLP compounds showed a significant difference between them, ($p < 0.05$, $p = 0.03$), indicating increased potency of camptothecin against HT-29 cells. Staurosporine, compared to all the tested compounds, was the most potent with a significant difference of $p < 0.05$, $p = 0.01$ compared to all JLP compounds, suggestive of increased activity. A significant difference of $p = 0.0079$ existed between the IC_{50} values of staurosporine and camptothecin, indicative of increased staurosporine activity. In both cell lines, the nucleoside analogues were less effective than camptothecin and staurosporine.

3.1.2 IC_{50} values of the copper-imidazo[1,2-*a*]pyridines on DLD-1 and HT-29 cells

Sigmoidal log dose response curves of the copper-imidazo[1,2-*a*]pyridines against DLD-1 and HT-29 cells are shown in Appendix C, Figure C3 and C4. IC_{50} values were obtained by exposing cells to a range of concentrations of copper-imidazo[1,2-*a*]pyridines of between 0.05 µM and 100 µM for 48 hours. Staurosporine concentrations ranged from 0.05 µM to 2 µM. Experiments were repeated at least five times. Results are shown in Figure 3.4.

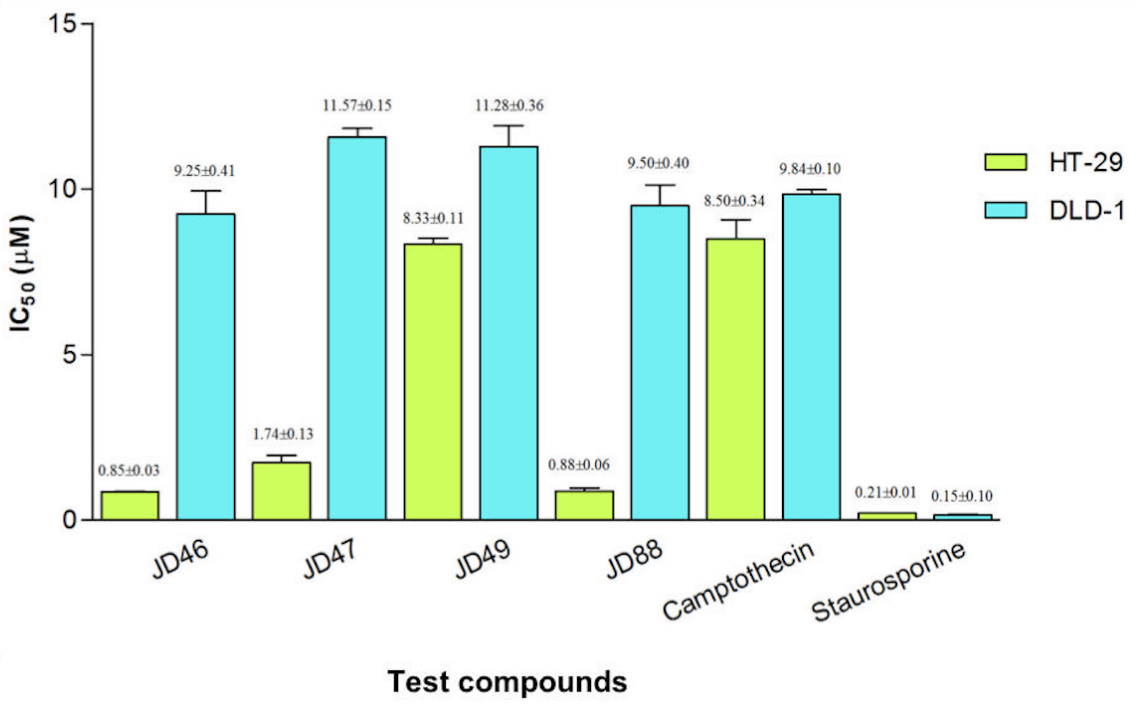


Figure 3.4 IC_{50} values of copper-imidazo[1,2-*a*]pyridines and the positive controls, camptothecin and staurosporine in HT-29 and DLD-1 cells. HT-29 and DLD-1 cells were exposed to copper-imidazo[1,2-*a*]pyridines and camptothecin at concentrations ranging between 0.05 µM to 100 µM for 48 hours. Staurosporine concentrations ranged from 0.05 µM to 2 µM. Each bar represents the mean ± SEM of IC_{50} values obtained from five MTT assays.

Figure 3.4 shows the IC_{50} values of the copper-imidazo[1,2-*a*]pyridines and the positive controls camptothecin and staurosporine, against both cell lines. The HT-29 cell line was more sensitive to the copper-imidazo[1,2-*a*]pyridines and to camptothecin (IC_{50} = 8.50 ±0.34 µM) than the DLD-1 cell line.

The IC_{50} values of the test compounds in HT-29 cells ranged between 0.85 µM to 8.33 µM. Three compounds showed IC_{50} values below 2.0 µM; JD46, JD88 and JD47 (0.85 ±0.03 µM, 0.88 ±0.06 µM and 1.74 ±0.13 µM, respectively). JD49 was the least potent with an IC_{50}

value of 8.33 ±0.11 μM. In comparison, the positive control, camptothecin had the highest IC_{50} value (8.50 μM) and staurosporine had the lowest IC_{50} value (0.21 μM) (Figure 3.4).

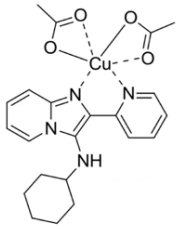
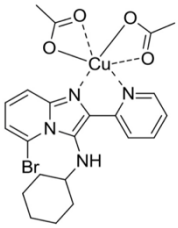
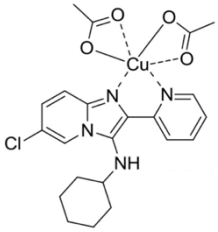
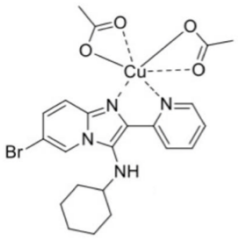
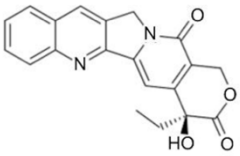
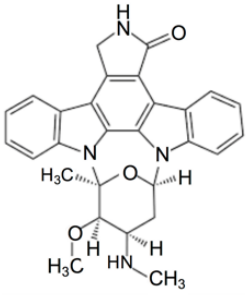
IC_{50} values of the active test compounds (JD46, JD47R, JD49, JD88) and positive controls, camptothecin and staurosporine were compared to determine significant differences. Statistical analysis of IC_{50} values was performed using the two-sample, unpaired Mann-Whitney U-test with a significance criterion set at $p < 0.05$ with a 95 % confidence interval. There was no significant difference ($p > 0.05$, $p = 0.11$) in the IC_{50} values between JD46 and JD88). Statistical analysis comparing JD46 and JD88 to JD47 showed a significant difference between them, ($p < 0.05$, $p = 0.03$), indicating increased potency of JD46 and JD88 against HT-29 cells. There was no significant difference in IC_{50} values between camptothecin and JD49 ($p > 0.05$, $p = 0.69$), indicating similar efficacy of JD49 to camptothecin (Figure 3.5).

After a 48-hour exposure of DLD-1 cells to test compounds, cells were most sensitive to JD46 and JD88 (Figure 3.4). The IC_{50} values of the test compounds in DLD-1 cells ranged between 9.25 μM to 11.57 μM and were similar to that of camptothecin which had an IC_{50} value of 9.84 μM. There was no statistically significant difference between the IC_{50} values of JD46, JD88 and camptothecin ($p > 0.05$; $p = 0.20$; $p = 0.69$ and $p = 0.34$, respectively), indicating similar efficacy between these compounds. The IC_{50} values for the least active compounds; JD47 and JD49 were significantly higher than camptothecin ($p < 0.05$, $p = 0.03$), suggesting a lower efficacy compared to camptothecin.

3.1.3 Selection of compounds for further investigation

With regard to IC_{50} values, the nucleoside analogues exhibited poor activity compared to the copper-imidazo[1,2-*a*]pyridines in both cell lines, with the exception of JLP093 in DLD-1 cells (Figure 3.3 and Figure 3.4). The four copper-imidazo[1,2-*a*]pyridines; JD46, JD47, JD49 and JD88 were considered the most active due to their low IC_{50} values in both cell lines. Therefore, no further work was pursued on the JLP nucleoside analogues. Based on information obtained regarding their respective potency, the copper-imidazo[1,2-*a*]pyridines were selected for further investigation. Copper complexed organic compounds has attracted some attention in recent years as potential anticancer agents (McGivern *et al.*, 2018). The structures of the compounds are showed below in Table 3.1. All four copper compounds were evaluated for their ability to induce apoptosis in HT-29 and DLD-1 cells.

Table 3.1: Chemical structures of active copper-imidazo[1,2-*a*]pyridines

Compound name	Compound structure	HT-29 IC_{50} (µM)±SEM	DLD-1 IC_{50} (µM)±SEM
JD46	 Molecular weight: 474.01 g/mol	0.85 ± 0.03	9.25 ± 0.41
JD47	 Molecular weight: 552.91 g/mol	1.74 ± 0.13	11.57 ± 0.15
JD49	 Molecular weight: 508.46 g/mol	8.33 ± 0.11	11.28 ± 0.36
JD88	 Molecular weight: 552.91 g/mol	0.88 ± 0.06	9.50 ± 0.40
Camptothecin	 Molecular weight: 348.35 g/mol	8.50 ± 0.34	9.84 ± 0.10
Staurosporine	 Molecular weight: 466.53 g/mol	0.21 ± 0.01	0.15 ± 0.10

3.2 Copper-imidazo[1,2-*a*]pyridines induced changes to the cell morphology of HT-29 and DLD-1 cells

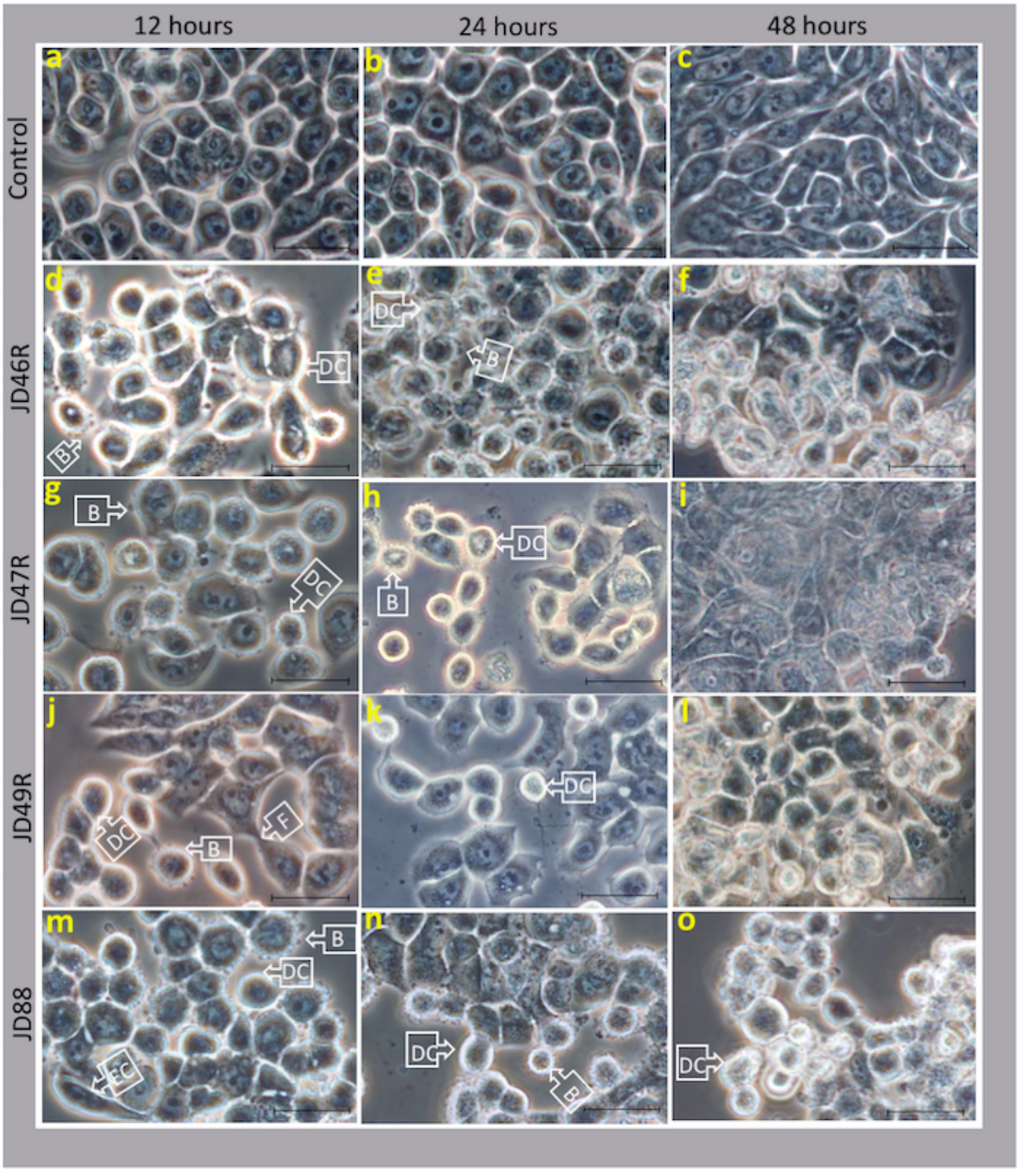
HT-29 and DLD-1 cells were grown on cover slips and treated with copper-imidazo[1,2-*a*]pyridines as described in section 2.4.1 of the Materials and Methodology. Both cell lines were treated with the copper-imidazo[1,2-*a*]pyridines; JD46, JD47, JD49 and JD88 at a concentration of 10 μM. Camptothecin and staurosporine were used as positive controls and cells were observed for morphological changes from 12 to 48 hours. Cells were viewed with an Olympus CKX41 microscope at a 200 X magnification and images were captured with an Olympus DP21 camera.

3.2.1 Phase contrast microscopy evaluation of copper-imidazo[1,2-*a*]pyridines induced morphological changes in HT-29 cells

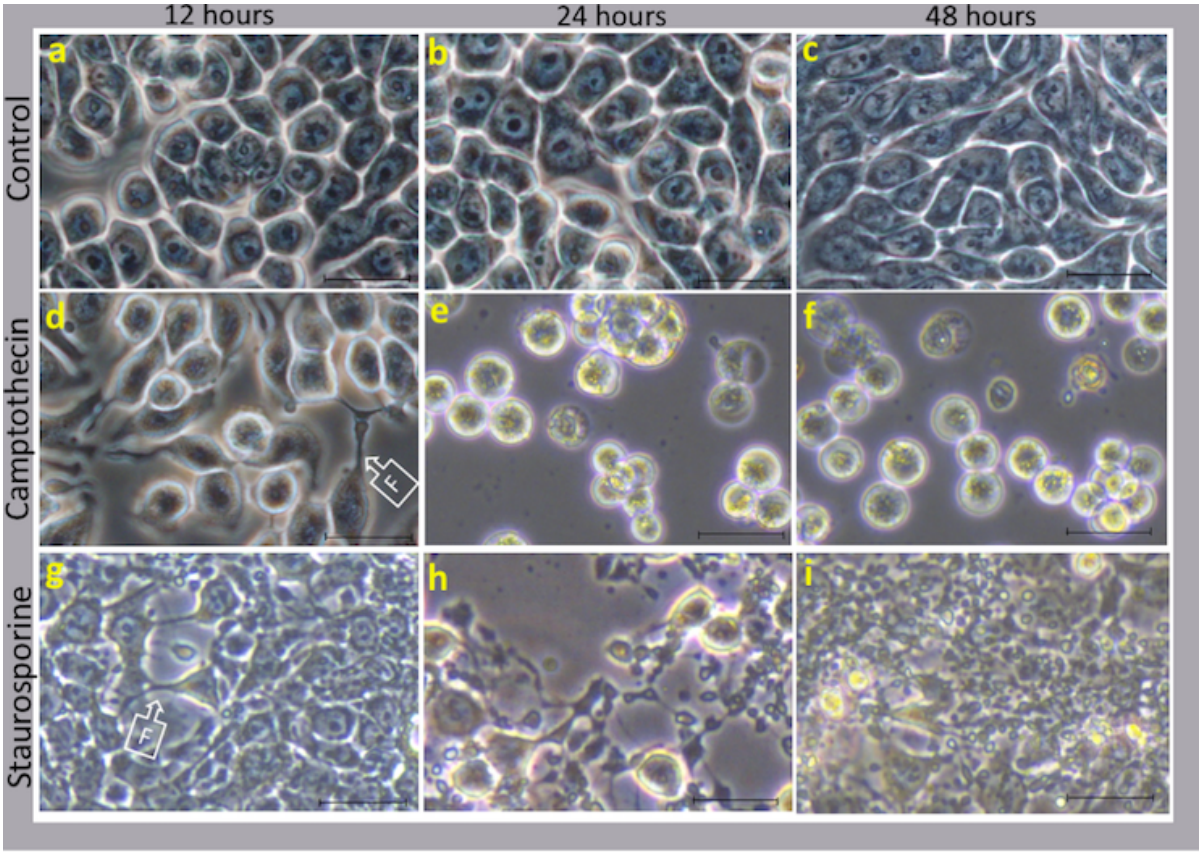
The effect of copper-imidazo[1,2-*a*]pyridines on the morphology of HT-29 cells were assessed over a period of 48 hours after treatment with 10 μM of test compound. The positive control, camptothecin was used at 10 μM and staurosporine at 200 nM. Cells were observed at various time periods between 12 and 48 hours after treatment. The effects of the copper-imidazo[1,2 *a*]pyridines are shown in Figure 3.5 (A). The effects of the negative and positive controls are shown in Figure 3.5 (B).

Cells treated with copper-imidazo[1,2-*a*]pyridines showed a change in cells shape; either more rounded or elongated at 12 hours (Figure 3.5A, panel d, g, j, m). Rounding of JD46 treated cells was observed at 12 hours and progressed until 48 hours where cells were detached from the growth surface (Figure 3.5A panel d-f). Rounded JD46, JD47 and JD49 treated cells displayed membrane blebbing at 12 hours (Figure 3.5A, panel g and j). Extensive membrane blebbing in rounded cells was present in JD88 treated cells at 12 hours (Figure 3.5A panel m). Blebbing of cell membranes is a prominent feature of apoptosis. Compared to the untreated controls, JD88 treated cells were smaller and showed cell shrinkage, another feature associated with apoptotic cell death (Figure 3.10A panel m-o).

These findings show that the copper-imidazo[1,2-*a*]pyridines induced changes consistent with apoptotic cell death, such as membrane blebbing in HT-29 cells. By comparison, during the observed time periods, morphological changes were present in JD46, JD47 and JD88 treated cells from 12 hours. At this concentration, JD49 showed changes at a later time period compared to JD46, JD47 and JD88 and both positive controls.



<u>Figure 3.5 (A)</u> Photomicrographs of HT-29 cells showing morphological changes after treatment with copper-imidazo[1,2-*α*]pyridines. HT-29 cells were treated with 10 µM of JD46, JD47, JD49 and JD88. (Magnification: 200 X, scalebar: 50 µm) Legend: B= blebbing, DC= detached cell, EC= elongated cell and F= filopodia.



<u>Figure 3.5 (B)</u> Photomicrographs of HT-29 cells showing morphological changes after treatment with camptothecin and staurosporine. HT-29 cells were treated with 10 µM of camptothecin and 200 nM of staurosporine. (Magnification: 200 X, scalebar: 50 µm) Legend: F= filopodia.

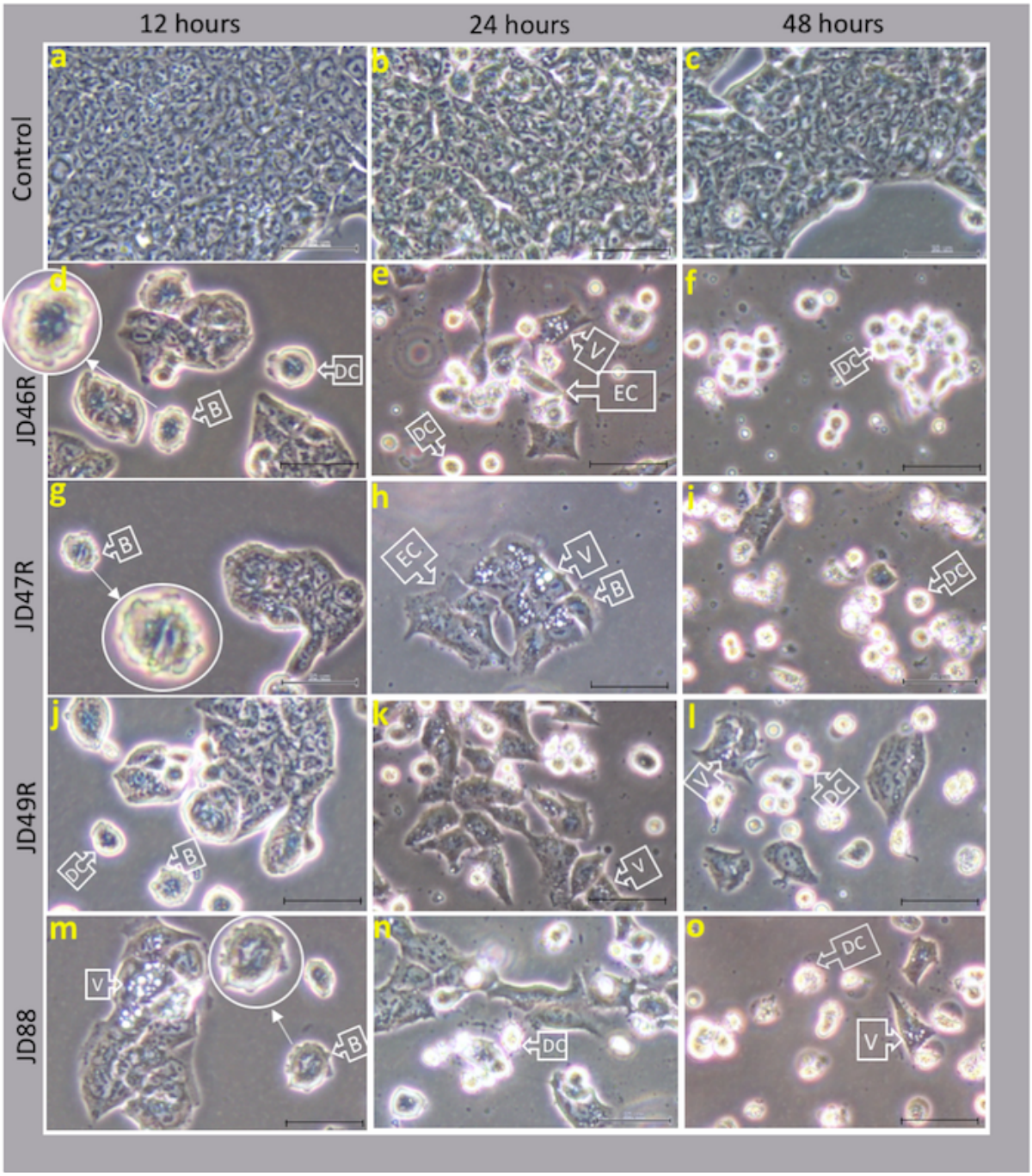
At the observed time periods, no morphological changes were observed in the untreated controls (Figure 3.5A and Figure 3.5B panel a-c). Camptothecin treated cells exhibited a spindle-like appearance at 12 hours and were rounded up and detached from the growth surface at 24 and 48 hours (Figure 3.5B panel d-f). Cells treated with staurosporine remained attached to the growth surface and appeared to be anchored to each other by filopodia from 12 to 48 hours (Figure 3.5B, panel g-i).

3.2.2 Phase contrast microscopy evaluation of copper imidazo[1,2-*a*]pyridines induced morphological changes in DLD-1 cells.

DLD-1 cells were treated with 10 µM of copper-imidazo[1,2-*a*]pyridines and positive control, camptothecin. Cells were exposed to staurosporine at a concentration of 200 nM.

Results are shown in Figure 3.6 (A). The effects of the negative and positive controls are shown in Figure 3.10 (B).
DLD-1 cells exposed to the test compounds were observed over a period of 48 hours. Photomicrographs in Figure 3.6 (A) and Figure 3.6 (B) are images captured at 12, 24 and 48-hour intervals. The DLD-1 cells grow in tightly packed clusters. Compared to the untreated control, after 12 hours, DLD-1 cells treated with test compounds and positive controls, showed a decreased growth density. At 12 hours, cells treated with JD46 displayed membrane blebbing (Figure 3.6 A, panel d). At 24 hours, vacuole formation and a change in shape from oval to spindle-like and elongated occurred (Figure 3.6 A, panel d-e). Cells were also rounded and partially detached from the growth surface. Similarly, at 12 hours, JD47 exhibited membrane blebbing. At 24 hours, extensive vacuole formation was visible with cells undergoing a change in shape from oval to elongated (Figure 3.6 A, panel g-h). Similarly, JD49 treated cells displayed cell rounding and membrane blebbing at 12 hours and elongated, spindle-like cells at 24 hours (Figure 3.6 A, panel j-k). At 12 hours, JD88 treated cells formed membrane blebs and cytoplasmic vacuoles (Figure 3.6 A, panel m). At 24 hours, elongated, spindle-like cells were visible with some cells rounded up and detached from the growth surface (Figure 3.6 A panel n).

The positive control, camptothecin caused similar morphological changes at 12 hours to JD46, JD47 and JD49, including membrane blebbing and rounding of cells however, at 24 hours, most cells had detached from the growth surface (Figure 3.6 B panel d-f). At 12 hours, staurosporine treated cells showed an alteration in shape from rounded to elongated at but still remained in their tightly bound clusters (Figure 3.6 B panel g). Cells formed spindle-like structures at 24 hours and at 48 hours, cell shrinkage occurred with cells remaining attached to the growth surface through filopodia and cytoplasmic extensions (Figure 3.6 B, panel h-i).



<u>Figure 3.6 (A)</u> Photomicrographs of DLD-1 cells showing morphological changes after treatment with 1 copper-imidazo[1,2-*a*]pyridines. DLD-1 cells were treated with 10 µM of JD46, JD47, JD49 and JD88. (Magnification: 200 X, scalebar: 50 µm). Legend: B= blebbing, DC= detached cell, EC= Elongated cell and V=vacuoles.

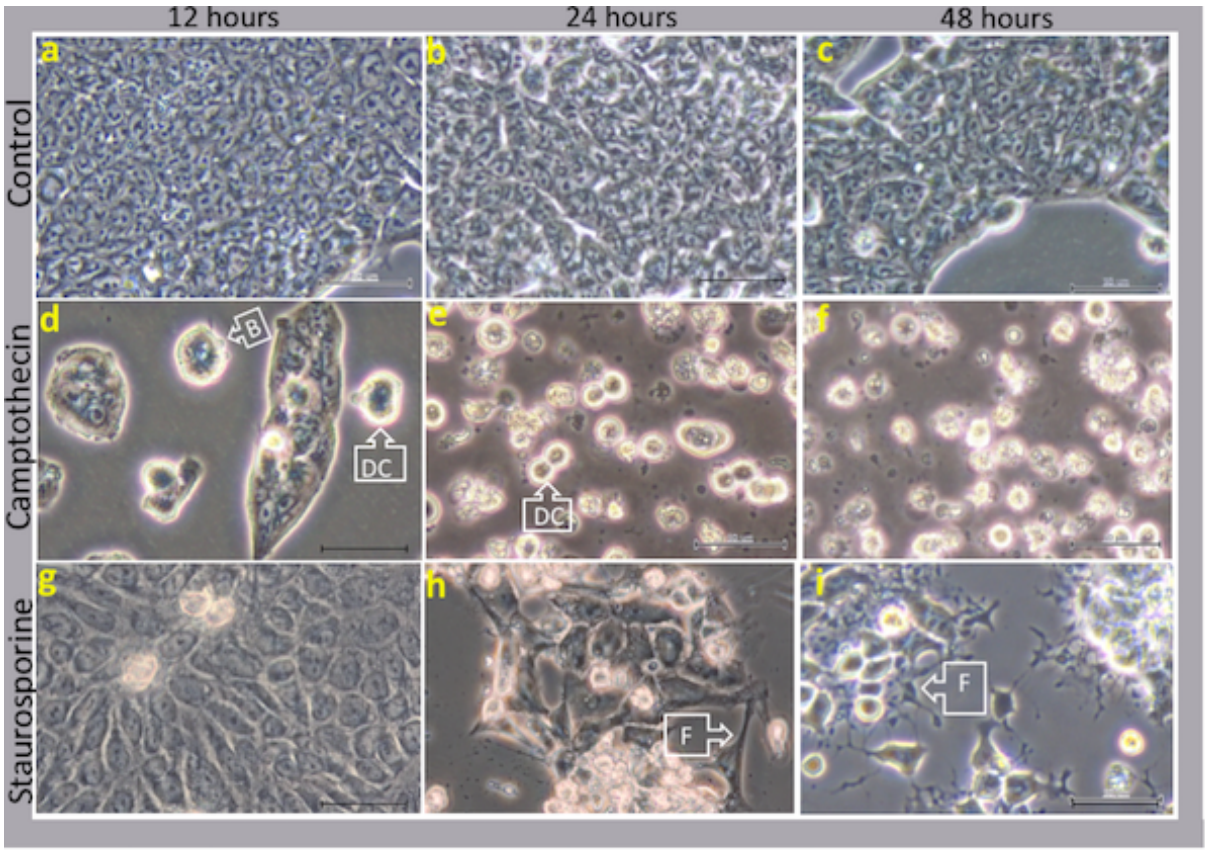


Figure 3.6 (B) Photomicrographs of DLD-1 cells showing morphological changes after treatment with camptothecin and staurosporine. DLD-1 cells were treated with 10 µM of camptothecin and 200 nM of staurosporine. (Magnification: 200 X, scalebar: 50 µm). Legend: B= blebbing, DC= detached cell, and F= filopodia.

3.2.3 Preliminary investigation of the mechanism of cell death with vital dyes

Vital dyes are useful preliminary indicators of necrotic and apoptotic cell death. This method rapidly identifies necrotic cell death and can indicate the potential of a substance to induce apoptotic cell death and is describe in detail in section 2.4.3 of Materials and Methodology. The analysis of specific changes in cellular morphology was evaluated using a combination of the vital fluorescent dyes; acridine orange (AO), ethidium bromide (EtBr) and the DNA specific dye, Hoechst 33342 (HO). The membrane integrity of a cell is assessed based on the ability of EtBr to penetrate a compromised membrane. EtBr causes the nucleus of necrotic cells to stain orange. AO crosses the membrane of cells and binds to nuclear material showing a green fluorescence. In addition, AO causes acidic granules to fluoresce red and is a preliminary indicator for autophagy. HO stains a healthy nucleus uniformly blue. An increase

in fluorescence intensity and a globular nuclear appearance indicated fragmented nuclei and is characteristic of apoptotic cells.
HT-29 and DLD-1 cells were exposed to 10 µM of the active copper-imidazo[1,2-*a*]pyridines; JD46, JD47, JD49 and JD88. The positive control of choice was staurosporine as it was very effective against both cell lines at 200 nM. Cells were observed with an Olympus BX41 camera using the U-MNIBA3 filter cube for AO/EtBr detection and the U-MWU2 filter cube was used for acquiring HO images. Fluorescent images were captured using an Olympus DP72 camera.

3.2.3.1 The effect of copper-imidazo[1,2-*a*]pyridines on the mechanism of cell death in HT-29 cells

HT-29 cells were exposed to 10 µM of copper-imidazo[1,2-*a*]pyridines: JD46, JD47, JD49 and JD88 for 16 hours. Results obtained in treated cells before 16 hours showed no apoptosis. Staurosporine (200 nM) was used as a positive control. Results are shown in Figure 3.7. Untreated control cells were stained uniformly blue by HO, maintaining their characteristic, round-oval shaped nuclei (Figure 3.7, panel b and c). In contrast, at a 16-hour exposure, the positive control, staurosporine showed fragmented nuclei, characteristic of apoptotic cells (Figure 3.7, panel p-r).

All apoptotic cells showed an increase in HO fluorescence. The nuclei of HT-29 cells treated with JD46 displayed apoptosis and chromatin condensation when stained with HO and AO (Figure 3.7, panel d-f). Similarly, JD47 treated cells showed apoptotic nuclei and the presence of chromatin condensation (Figure 3.7, panel g-h). Apoptotic cells were visible in JD49 treated cells as well as cells displayed extensive chromatin condensation (Figure 3.7, panel k). HT-29 cells treated with JD88 displayed irregularly shaped nuclei with chromatin condensation. Apoptotic cells were smaller in size and fluoresced at a higher intensity (Figure. 3.7, panel n).

Morphological changes characteristic of early apoptosis includes chromatin condensation, nuclear fragmentation and the formation of apoptotic bodies. These results indicate that compared to an untreated control, all copper-imidazo[1,2-*a*]pyridine test compounds were able to induce morphological changes consistent with apoptosis. At a concentration of 10 µM, no cells experienced necrotic cell death.

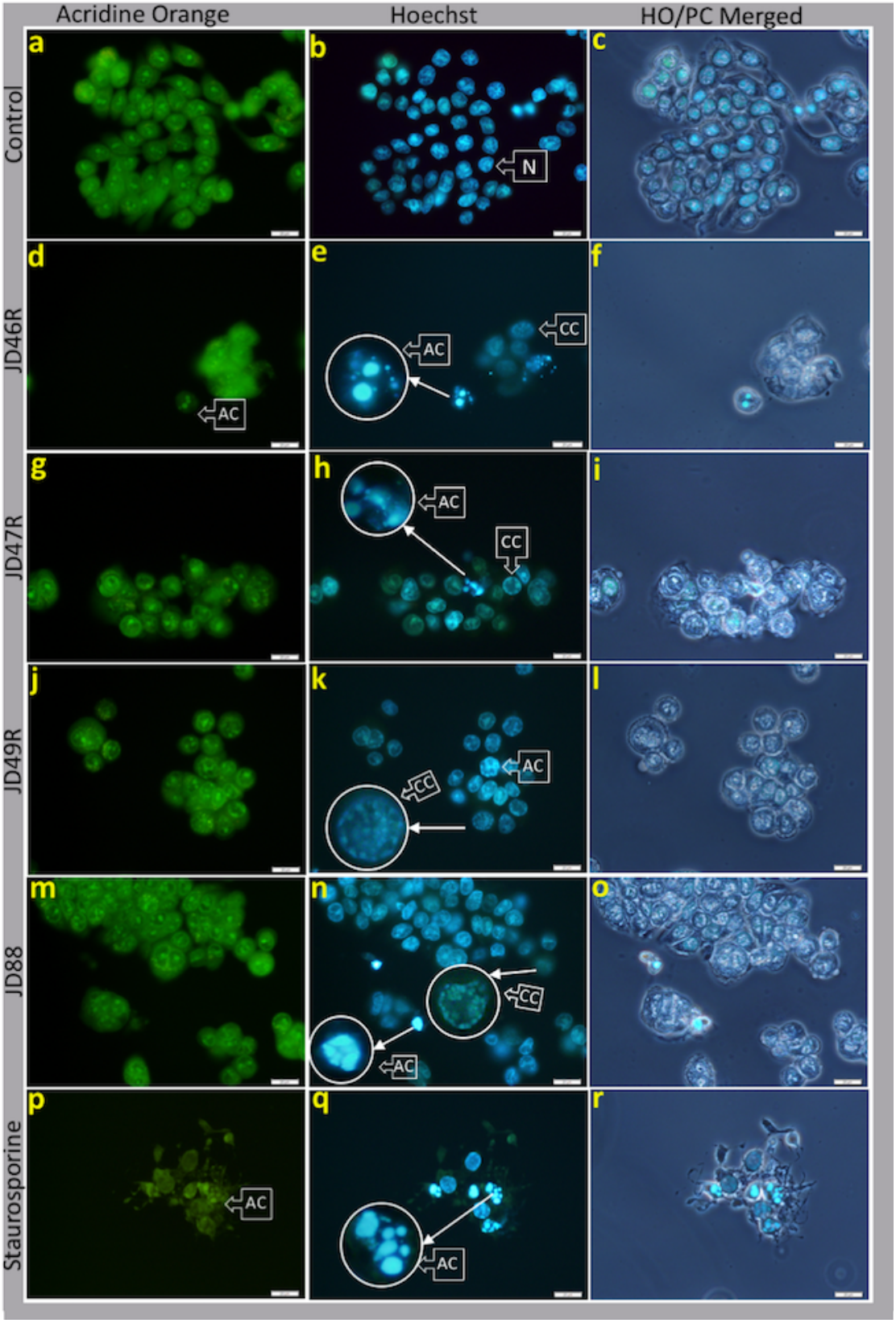


Figure 3.7 Fluorescent micrographs of HT-29 cells after treatment with copper-imidazo[1,2-*a*]pyridines and staurosporine. HT-29 cells were treated with 10 µM of JD46, JD47, JD49 and JD88 and 200 nM of staurosporine for 16 hours. (Magnification: 400 X, exposure time: 11.0 ms and ISO: 400) (scalebar: 20 µm). Legend: AC= apoptotic cell, CC= chromatin condensation, N= normal nuclei and PC=phase contrast.

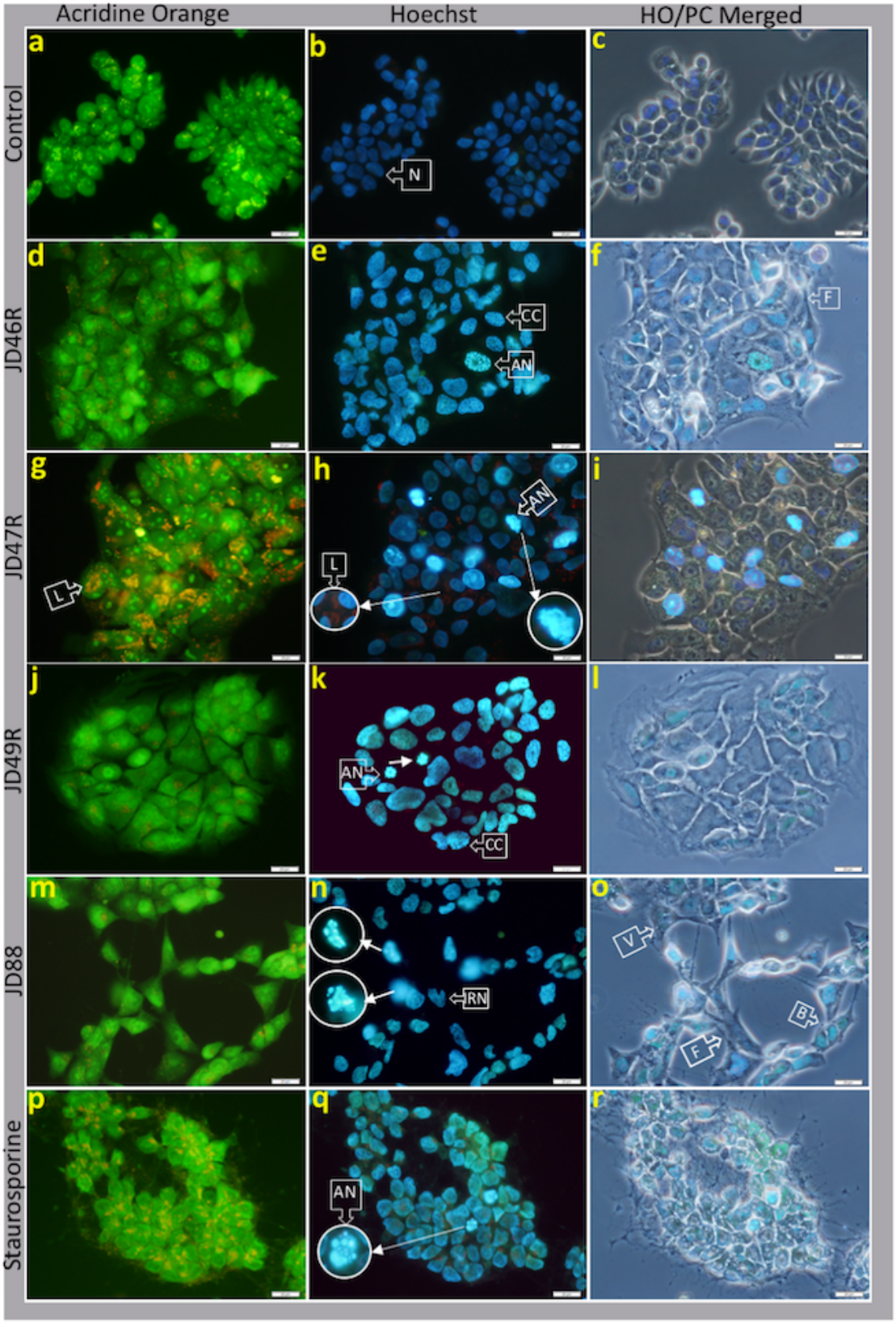
3.2.3.2 The effect of copper-imidazo[1,2-*a*]pyridines on the mechanism of cell death in DLD-1 cells

DLD-1 cells were exposed to 10 μM of the copper-imidazo[1,2-*a*]pyridines: JD46, JD47, JD49 and JD88 for 16 hours. Staurosporine (200 nM) was used as a positive control. Results are shown in Figure 3.8.

Untreated DLD-1 cells displayed a regular oval-shaped nucleus which stained uniformly blue with HO (Figure 3.8, panel b). The periphery of staurosporine treated DLD-1 cells showed extensive cytoplasmic degeneration but no necrosis was observed. This is indicative of intact cell membranes (Figure 3.8, panel p and r). HO stained cells showed the presence of apoptotic cells as well as cells with irregularly shaped nuclei (Figure 3.8, panel q).

Chromatin condensation and apoptotic cells were observed in JD46 treated cells (Figure 3.8, panel e-f). Some cells, located on the periphery were rounded up and remained attached to the growth surface by filopodia (Figure 3.8, panel d and f). JD47 caused extensive lysosomal aggregation which fluoresced red-orange when stained with AO and red when stained with HO (Figure 3.8, panel g-h). Cells did not stain red with HO however, HO staining revealed the presence of an apoptotic nucleus which was also visible in the HO/PC merged image (Figure 3.8, panel h-i). The relative increase in HO fluorescence intensity was also indicative of apoptosis (Figure 3.8, panel h). Chromatin condensation and apoptotic nuclei were present in cells treated with JD49 (Figure 3.8, panel k-l). HO staining revealed JD88 treated cells exhibited irregularly shaped nuclei (Figure 3.8, panel n). Clusters of spindle-like JD88 treated cells were held together by filopodia (Figure 3.8, panel m and o). Perinuclear vacuole formation and membrane blebbing was also visible on the phase contrast image (Figure 3.8, panel o). These results indicate that after a 16-hour treatment, all four copper-imidazo[1,2-a]pyridine test compounds were able to induce morphological changes in DLD-1 cells which are associated with apoptosis.

HT-29 and DLD-1 cells displayed similar results as apoptotic features were present in cells treated with JD46, JD47, JD49 and JD88. At the concentration tested, copper-imidazo[1,2-*a*]pyridines did not cause necrosis in HT-29 and DLD-1 cells as noted due to the absence of cells with a red-orange stained nucleus.



<u>Figure 3.8</u> Fluorescent micrographs of DLD-1 cells after treatment with copper-imidazo[1,2-*a*]pyridines and staurosporine. DLD-1 cells were treated with 10 µM of JD46, JD47, JD49 and JD88 and 200 nM of staurosporine for 16 hours. (Magnification: 400 X, exposure time: 11.0 ms and ISO: 400) (scalebar: 20 µm). Legend: AN= apoptotic nucleus, B= blebbing, CC= chromatin condensation, F= filopodia, IRN= Irregular nucleus, L= lysosomes, N= normal nuclei and V= vacuoles.

3.3 The exposure of phosphatidylserine on the surface of HT-29 and DLD-1 cells after treatment with copper-imidazo[1,2-*a*]pyridines

A combination of annexin-V conjugated to Alexa Fluor 488 and propidium iodide was used to differentiate between viable, early apoptotic, late apoptotic and necrotic cells. Each experiment was repeated at least three times. Cells were viewed with an Olympus BX41 microscope using the U-MNIBA3 filter cube for Alexa Fluor 488 detection. Images were captured using an Olympus DP72 camera with constant exposure times and ISO settings for control and treated cells. HT-29 and DLD-1 cells were treated with 10 uM of the copper-imidazo[1,2-*a*]pyridine test compounds JD46, JD47, JD49 and JD88. Staurosporine (200 nM) was used as a positive control.

3.3.1 The effect of copper-imidazo[1,2-*a*]pyridines on annexin-V binding in HT-29 cells

Annexin-V binding to phosphatidylserine in HT-29 cells was evaluated after a 12-hour exposure period and results are shown in Table 3.2, Figure 3.9 and 3.10. Results are representative of three independent experiments. After a 12-hour treatment, none of the HT-29 cells in the negative control were stained positive for annexin-V binding or PI uptake (Figure 3.9 panel a-b). The green fluorescent dots in the untreated control (Figure 3.9 panel b) was due to non-specific background binding. Cells treated with the positive control, staurosporine were positive for both annexin-V and PI, indicative of late apoptosis/early necrosis (Figure 3.9 panel k-l). No cells were PI positive without being annexin-V positive as well, indicating that the cells were undergoing apoptosis rather than necrosis (Figure 3.9 panel k-l and Figure 3.10)

Compared to the negative control, HT-29 cells treated with copper-imidazo[1,2-*a*]pyridines displayed an increase in annexin-V staining, indicative of the presence of PS on the surface of cell membranes. Annexin-V positive cells treated with JD46, JD47 and JD88 displayed bright green fluorescence whereas, the green fluorescence signal was weaker in JD49 treated cells (Figure 3.9 panel c, e, g, i). Corresponding phase contrast images showed membrane blebbing in JD49, JD88 and staurosporine treated cells (Figure 3.9 panel h, j, l).

Figure 3.10 shows the average percentage of cells positive for annexin-V and PI obtained from three independent experiments, after a 12-hour exposure to copper-imidazo[1,2-*a*]pyridines. Table 3.2 represents the combined data of three experiments, showing the average percentage of HT-29 cells positive for annexin-V and annexin-V/PI. The positive control staurosporine showed close to 100 % annexin-V+ and PI+ cells, indicating late apoptosis/early necrosis (Figure 3.10). Of the test compounds at a 12-hour exposure time, JD47 caused the highest percentage of annexin-V positive cells followed by JD88, JD49 and JD46 as shown in Table 3.2.

Table 3.2: Average percentage of HT-29 cells showing annexin-V and PI.
The data is representative of three independent experiments. The percentage cells positive for annexin-V and PI was calculated using the Olympus CellSens Software package.

Compounds	Annexin- V+ cells only (%)	Annexin-V +/ PI+ cells (%)
Control	0	0
JD46	39.4 ± 1.7	5.6 ± 0.4
JD47	71.5 ± 1.0	1.4 ± 1.0
JD49	43.0 ± 1.5	0 ± 0.0
JD88	55.8 ± 0.5	6.0 ± 1.3
Staurosporine	97.0 ± 3.0	97.0 ± 3.0

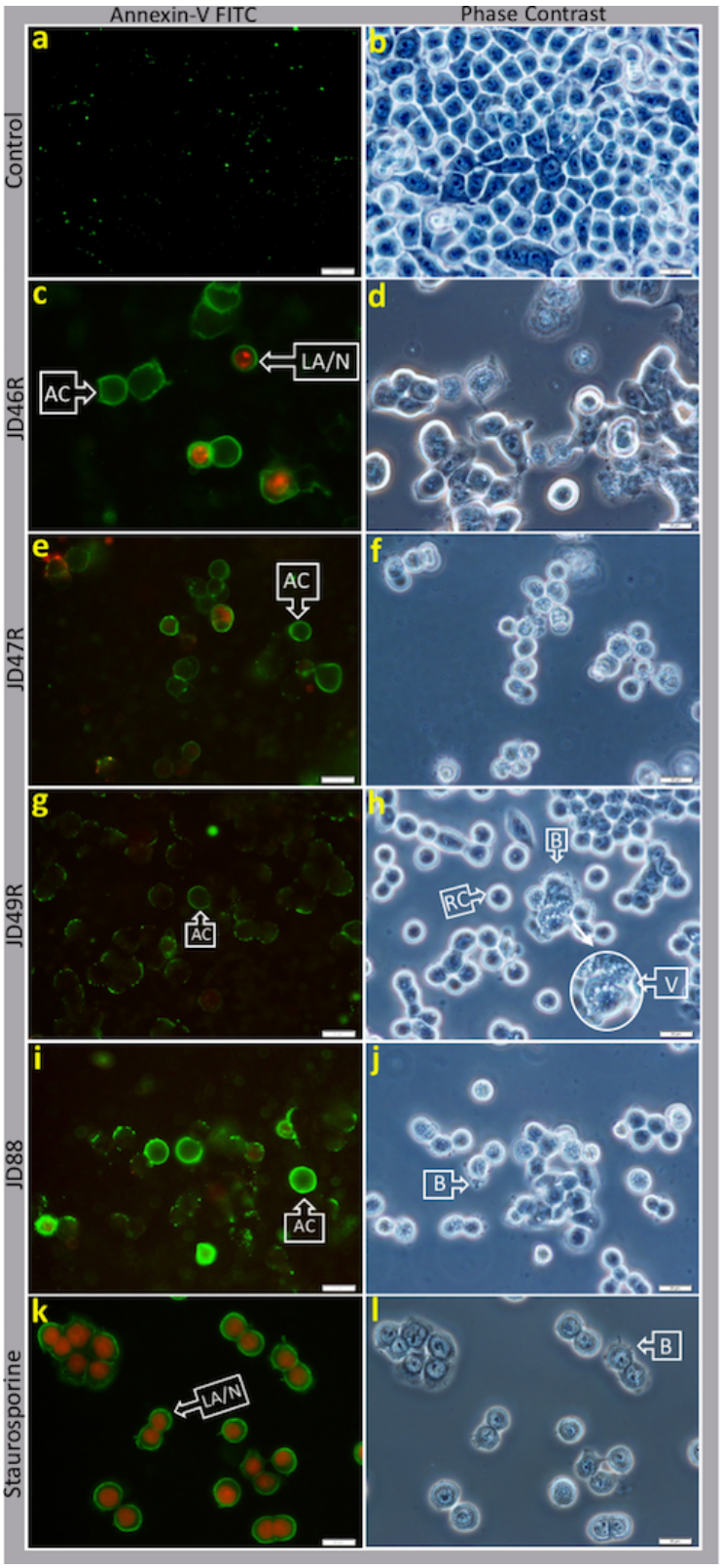


Figure 3.9 Annexin-V/PI stained HT-29 cells following exposure to active copper-imidazo[1,2-*a*]pyridines. HT-29 cells were treated with 10 µM of JD46, JD47, JD49 and JD88 and 200 nM staurosporine for 12 hours. (Magnification: 400X, exposure time: 140.0 ms, ISO: 400) (scalebar: 20 µm). Legend: AC= apoptotic cell, B=blebbing, LA/N=late apoptotic/necrotic cell, RC= rounded cell and V= vacuoles.

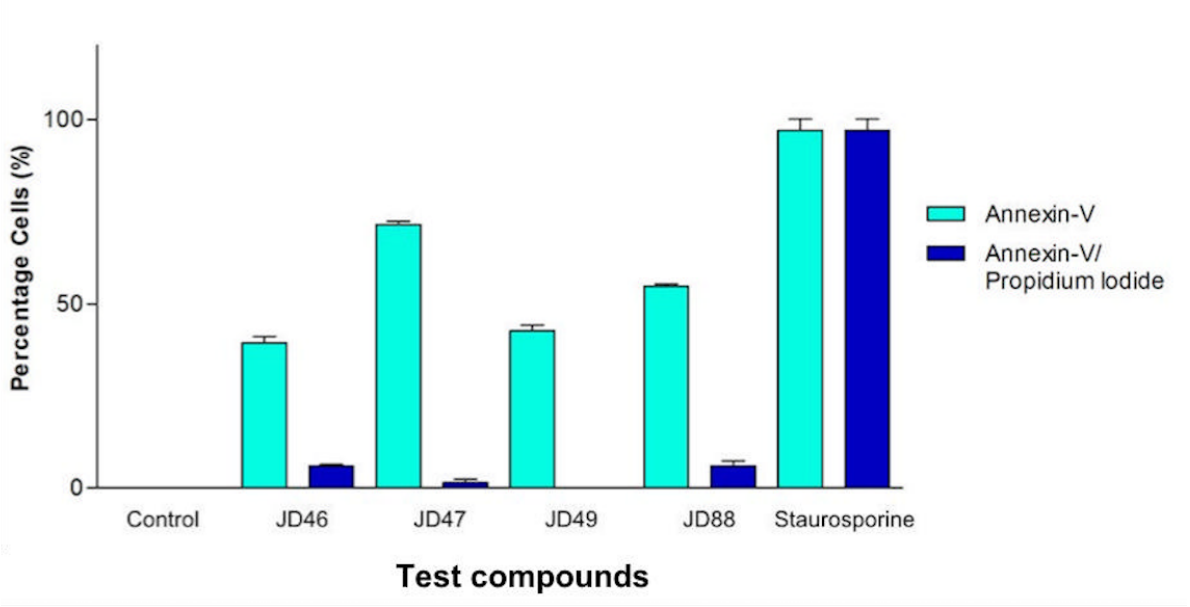


Figure 3.10 Average percentage of HT-29 cells positive for annexin-V and PI after a 12-hour exposure to copper-imidazo[1,2-*a*]pyridines. HT-29 cells were exposed to 10 µM of JD46, JD47, JD49 and JD88 and 200 nM staurosporine. Each bar represents the mean ± SEM of values obtained from three independent experiments.

In summary, all four test compounds were able to induce PS expression on the outer cell membrane in HT-29 cells. JD47 was the most effective inducer of PS translocation followed by JD88 which had the highest percentage of PI+ cells in HT-29 cells, at the conditions tested (Figure 3.10 and Table 3.2).

3.3.2 The effect of copper-imidazo[1,2-*a*]pyridines on annexin-V binding in DLD-1 cells.

Annexin-V binding to phosphatidylserine in DLD-1 cells was evaluated after the cells were treated with 10 µM of JD46, JD47, JD49 and JD88 for a period of 16 hours. No desired annexin-V or PI staining was observed in DLD-1 cells before 16 hours. Staurosporine was used at a concentration of 200 nM. Results are shown in Figure 3.11, Figure 3.12 and Table 3.3 and are representative of three independent experiments.

Untreated control DLD-1 cells showed no annexin-V binding indicating an absence of PS on the cell membranes. Background fluorescence in the negative control was due to non-specific background binding (Figure 3.11 panel a-b). The positive control, staurosporine, showed only a few cells undergoing late apoptosis/early necrosis (Figure 3.11 panel k). This was perhaps due to a discrepancy in the required time period for PS expression on the outer cell membrane

in staurosporine treated DLD-1 cells. The percentage of cells showing annexin-V binding was low in all the treated cells including staurosporine and appeared to be confined to cells that were partially dissociated from the growth surface. Figure 3.11, panel c, e, g, i, k).

Table 3.3: Average percentage of DLD-1 cells showing annexin-V- and PI activity
The data represents the average of three independent experiments. The percentage cells positive for annexin-V and PI was calculated using the Olympus CellSens Software package.

Compounds	Annexin-V + cells only (%)	PI+ cells (%)
Control	0 ± 0.0	0 ± 0.0
JD46	3.8 ± 0.01	0 ± 0.0
JD47	9.9 ± 0.3	0 ± 0.0
JD49	12.6 ± 0.1	3.6 ± 0.2
JD88	11.9 ± 0.3	0 ± 0.0
Staurosporine	4.9 ± 0.1	0 ± 0.0

In addition, JD49 showed some cells which were stained positive for PI only, an indicator of necrotic cell death. Figure 3.12 shows the average percentage of cells positive for annexin-V and PI after a 16-hour exposure to test compounds. JD46 showed the lowest annexin-V activity from the copper-imidazo[1,2-*a*]pyridines. In contrast, JD49 treated cells displayed the highest percentage of annexin-V+ and annexin-V- /PI+ fluorescence followed by JD88 which showed 11.9 % of cells positive for annexin-V (Figure 3.11, Figure 3.12 and Table 3.3).

Compared to DLD-1 cells, HT-29 cells treated with the test compounds showed increased annexin-V binding. The average annexin-V+ percentage in HT-29 cells ranged from 39.0 – 72.0 % and the average annexin-V+ percentage in DLD-1 cells ranged from 3.0 – 13.0 % (Table 3.2 and Table 3.3) This suggests a greater sensitivity of HT-29 cells to copper-imidazo[1,2-*a*]pyridine test compounds in terms of increased exposure of PS on the outer cell membrane. In addition, the HT-29 cells were more sensitive to staurosporine than the DLD-1 cells since the translocation of PS was induced in 97 % of HT-29 cells compared to 2.3 % in DLD-1 cells.

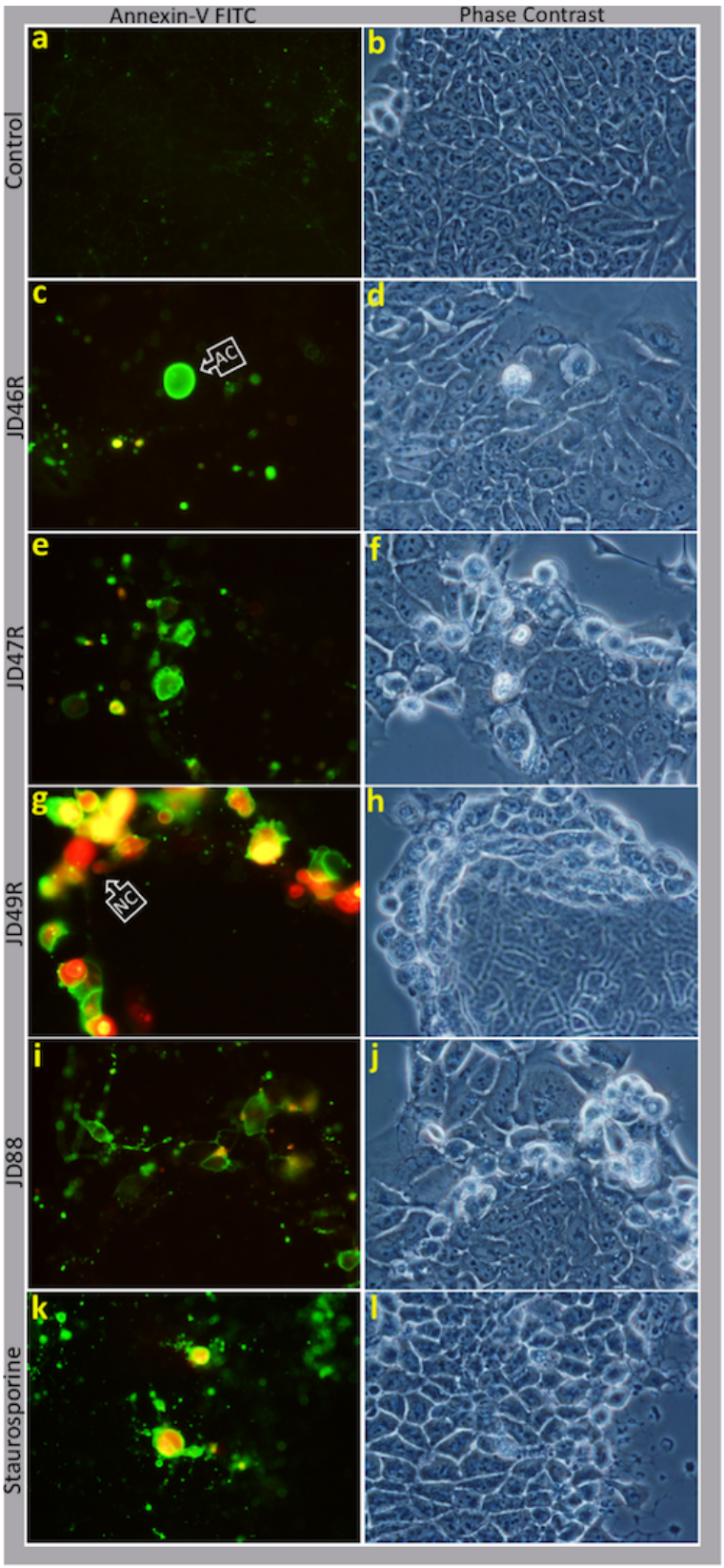


Figure 3.11 Annexin-V/PI stained DLD-1 cells following exposure to active copper-imidazo[1,2-*a*]pyridines. DLD-1 cells were treated with 10 µM of JD46, JD47, JD49 and JD88 and 200 nM staurosporine for 16 hours. (Magnification : 400X, exposure time: 140.0 ms and ISO: 400) (scalebar: 20 µm,). Legend: AC= apoptotic cell and NC= necrotic cell.

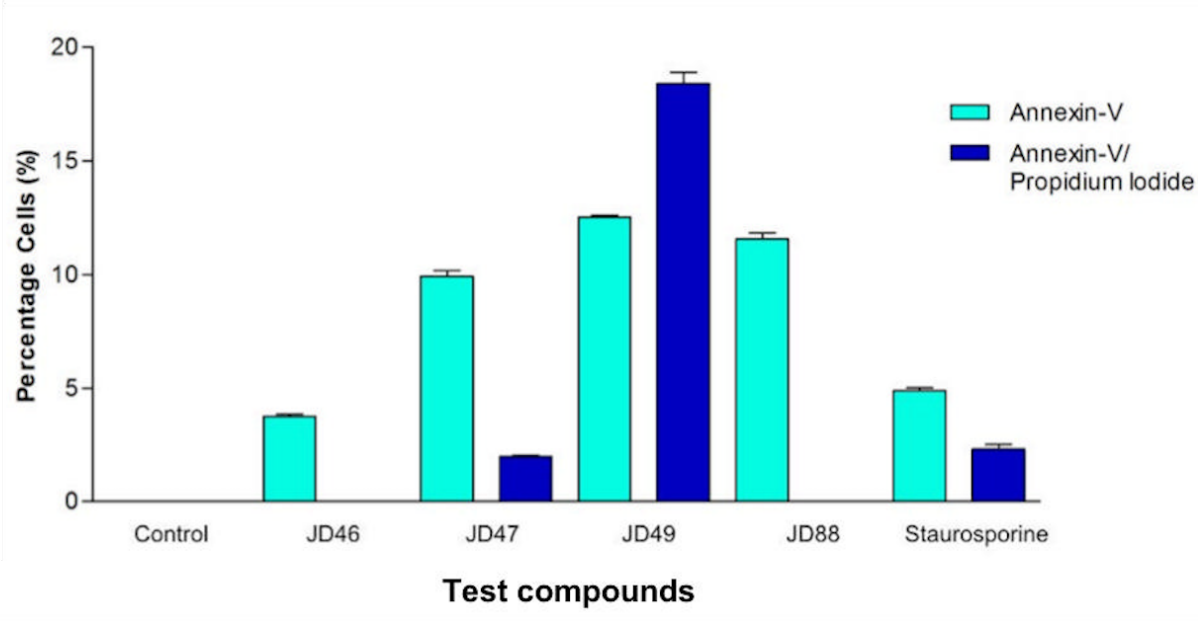


Figure 3.12 Average percentage of DLD-1 cells positive for annexin-V and PI after a 16-hour exposure to copper-imidazo[1,2-*a*]pyridines. DLD-1 cells were exposed to 10 µM of JD46, JD47, JD49 and JD88 and 200 nM staurosporine. Each bar represents the mean ± SEM of values obtained from three independent experiments.

3.4 Activation of caspase-3/7 in HT-29 and DLD-1 cells by copper imidazo[1,2*a*]pyridines

Caspases are intracellular cysteine proteases essential for the induction of apoptosis. Caspase-3/7, an executioner caspase, is responsible for cleaving cellular proteins in apoptosis. Caspase-3/7 activity was detected using the Abcam's Fluorimetric Caspase-3/7 Assay Kit (Ab39383). Caspase-3/7 cleaves proteins containing the amino acid sequence Asp-Glu-Val-Asp (DEVD). The assay is based on the detection of the DEVD-AFC (7-amino-4-trifluoromethylcoumarin) substrate cleavage and is quantified using a spectrofluorimeter. The detailed method is described in section 2.5.2 of Materials and Methodology. The specific activity of caspase-3/7, relative to the amount of protein present in the cell lysate is shown in Appendix E, Table E1 and E2. The protein concentration for each lysate was measured with the Bio-Rad protein assay (Bio-Rad SA) (materials and methods section 2.5.3). Copper-imidazo[1,2-*a*]pyridine test compounds, at a concentration of 10 µM, were evaluated for their ability to induce caspase-3/7 activity in HT-29 and DLD-1 cells. Since caspase-3/7 activation is a late apoptotic event, cells were exposed to test compounds for 20 hours. Staurosporine (200 nM) was used as a positive control. Caspase-3/7 activity relative to untreated controls

and staurosporine are summarized in Table 3.4. The data used to calculate average fold increase in caspase-3/7 activity is shown in Appendix E, Table E1 and E2. Results are representative of three independent experiments and each data point was obtained in duplicate. Results are displayed below in Figure 3.13 and Figure 3.14. Protein standard curves can be found in Appendix D, Figure D1-3.

3.4.1 Induction of caspase-3/7 activity by copper-imidazo[1,2-*a*]pyridines in HT-29 cells

HT-29 cells were treated with 10 µM of copper-imidazo[1,2-*a*]pyridines and 200 nM staurosporine for 20 hours to determine caspase-3/7 activity. Relative to the untreated control, all the copper-imidazo[1,2-*a*]pyridines and staurosporine showed an increase in caspase-3/7 activity. Compared to the negative control, JD88 exhibited the greatest fold increase in caspase-3/7 activity (3.57) in HT-29 cells, followed by JD46 (3.30). JD47 showed a 2.52-fold increase whereas JD49 increased by 2.27-fold. The positive control, staurosporine, showed the least caspase-3/7 activity, relative to the control, with a fold increase of 1.73 (Figure 3.13 and Table 3.4).

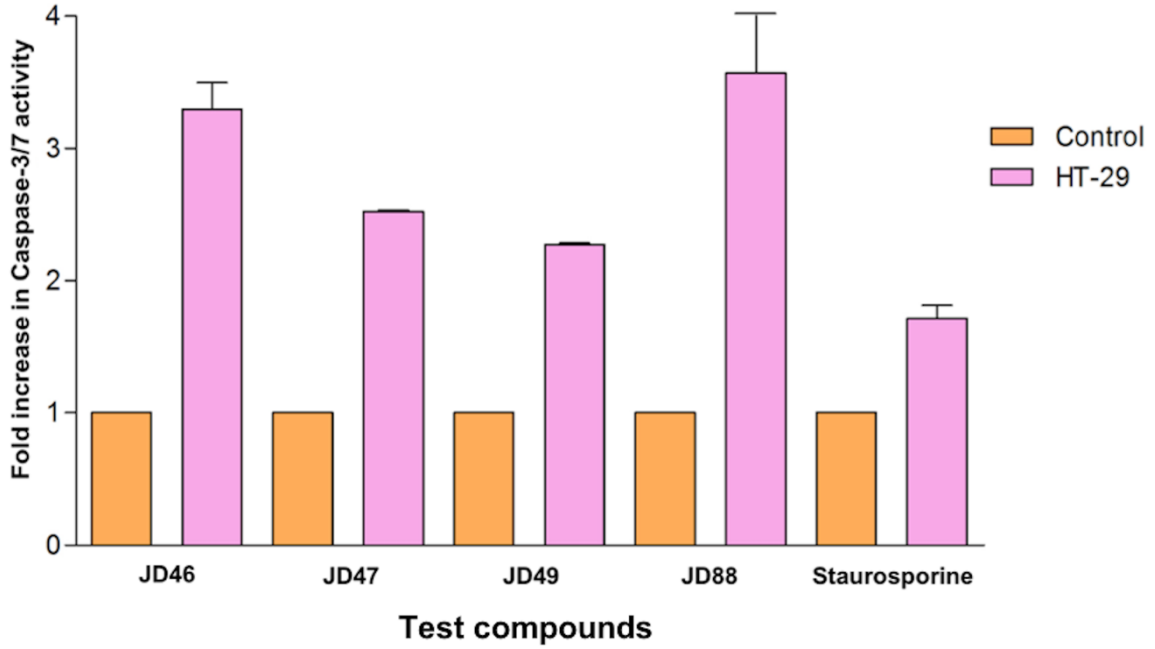


Figure 3.13 Fold increase in caspase-3/7 activity in HT-29 cells after a 20 hour exposure to copper-imidazo[1,2-*a*]pyridines. Cells were treated with 10 µM of JD46, JD47, JD49 and JD88 and 200 nM of staurosporine. Each bar represents the mean ± SEM of values obtained in duplicate from three independent experiments

3.4.2 Induction of caspase-3/7 activity by copper-imidazo[1,2-*a*]pyridines in DLD-1 cells

DLD-1 cells were treated with 10 µM of copper-imidazo[1,2-*a*]pyridines for 20 hours. Staurosporine (200nM) was used as a positive control. All compounds showed an increase in caspase-3/7 activity albeit lower than that observed for the HT-29 cells. Staurosporine and JD46 displayed similar fold increases at 2.11 and 2.12, respectively, suggesting that the test compound stimulates caspase-3/7 activity equivalent to the positive control. JD47 and JD49 showed similar caspase-3/7 inducing ability with a fold increase of 1.44 and 1.42, respectively. At the concentration tested, JD88 demonstrated the lowest activity with a marginal increase of 1.22 relative to the untreated control (Figure 3.14).

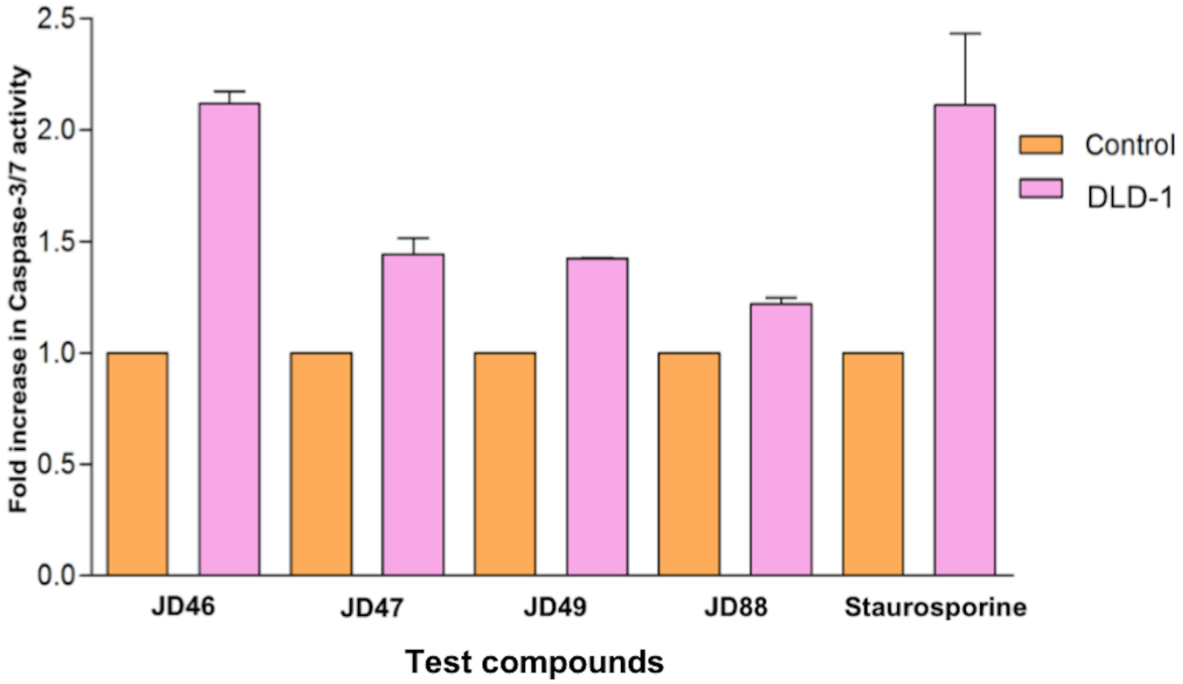


Figure 3.14 Fold increase in caspase-3/7 activity in DLD-1 cells after a 20 hour exposure to copper-imidazo[1,2-*a*]pyridines. Cells were treated with 10 µM of JD46, JD47, JD49 and JD88 and 200 nM of staurosporine. Each bar represents the mean ± SEM of values obtained in duplicate from three independent experiments.

Table 3.4. Comparison of caspase-3/7 activity in HT-29 and DLD-1 cells. Cells were exposed to 10 µM of test compounds and 200 nM staurosporine Results are representative of three independent experiments.

Compound	Fold increase in caspase-3/7 activity relative to the control	
	HT-29	DLD-1
Staurosporine	1.73 ± 0.09	2.11 ± 0.32
JD46	3.30 ± 0.12	2.12 ± 0.03
JD47	2.52 ± 0.01	1.44 ± 0.07
JD49	2.27 ± 0.01	1.42 ± 0.00
JD88	3.57 ± 0.27	1.22 ± 0.01

Caspase-3/7 is a key effector caspase involved in apoptosis and an increase in activity levels indicate apoptosis induction. These findings show that at a concentration of 10 µM, all copper-imidazo[1,2-*a*]pyridines, were able to induce caspase-3/7 activity in HT-29 and DLD-1 cells. Compared to HT-29 cells, the increase in caspase-3/7 activity in DLD-1 cells was lower (Table 3.5). JD88 caused the highest caspase-3/7 increase in HT-29 cells and conversely, the lowest increase in DLD-1 cells (3.57 and 1.22, respectively). The positive control staurosporine caused the smallest increase in caspase-3/7 activity in HT-29 cells and conversely, the highest increase in DLD-1 cells with an average activity of 1.71 and 2.11, respectively.

3.5 The effect of copper-imidazo[1,2-*a*]pyridines on the mitochondrial membrane potential of HT-29 and DLD-1 cells

Optimal functionality of mitochondria is essential in the production of ATP and the maintenance of cellular metabolism. Disruption of mitochondrial function leads to a loss of the mitochondrial membrane potential (Δψm), a feature of early apoptosis (Redza-Dutordoir and Averill-Bates, 2016). Changes to the mitochondrial membrane potential are easily detected with the use of the JC-1 dye as described in section 2.5.4 of Materials and Methodology. The quantity of JC-1 in the mitochondria is contingent to the membrane potential, thus, healthy cells with high Δψm form JC-1-aggregates which fluoresces red-orange. The JC-1 dye remains in its green monomeric form in apoptotic cells with a low Δψm (Mathur *et al.,* 2000).

The mitochondrial membrane potential in HT-29 and DLD-1 cells was evaluated after treating cells with 10 μM of the copper-imidazo[1,2-*a*]pyridines and the positive control staurosporine (200 nM). The cells were viewed with an Olympus BX41 microscope using the U-MNIBA3 long bandpass filter cube which detects green/red fluorescence. Images were captured with an Olympus DP72 camera. Exposure times and ISO settings were kept constant for all the treatments. Results are representative of at least three independent experiments and are shown below in Figure 3.15 and Figure 3.18. The Olympus CellSens Software was used to calculate the percentage of cells showing red-orange JC-1 aggregates and green JC-1 monomer aggregates in each experiment and is presented Figure 3.16 and Figure 3.18.

3.5.1 The effects of copper-imidazo[1,2-*a*]pyridines on the mitochondrial membrane potential of HT-29 cells

HT-29 cells were assessed after a 12-hour exposure to test compounds. The effect of the copper-imidazo[1,2*a*]pyridines are shown in Figure 3.15 and Figure 3.16. Untreated HT-29 control cells, showed 92.8 % red-orange fluorescence in the perinuclear area, indicating JC-1 aggregates in the mitochondria and an intact mitochondrial membrane potential (Figure 3.15, panel a and Figure 3.16). In contrast, HT-29 cells treated with staurosporine showed 86.6 % green fluorescence with JC-1 in its monomeric form (Figure 3.15 panel b and Figure 3.16). Cells treated with JD46, JD47 and JD88 showed predominantly green fluorescence indicating that JC-1 was monomeric and the mitochondrial membrane potential disrupted (Figure 3.15 panel c, d and f). Test compounds JD46, JD47, JD88 all showed a complete loss of mitochondrial membrane potential while 23.0 % of cells treated with JD49 (Figure 3.16) still had intact mitochondria with an intact mitochondrial membrane potential. Low levels of red-orange aggregates in JD49 treated cells can be seen in Figure 3.15 panel e. The appearance of the mitochondria of cells treated with JD47, JD49 and staurosporine were more granular when compared to cells treated with JD46 and JD88 (Figure 3.15) indicative of structurally intact mitochondria.

JD46, JD47 and JD88 produced the greatest change in mitochondrial membrane potential in HT-29 cells with the JC-1 dye present in its green monomeric form in 100 % of cells (Figure 3.16), when compared to the untreated control, positive control and JD49.

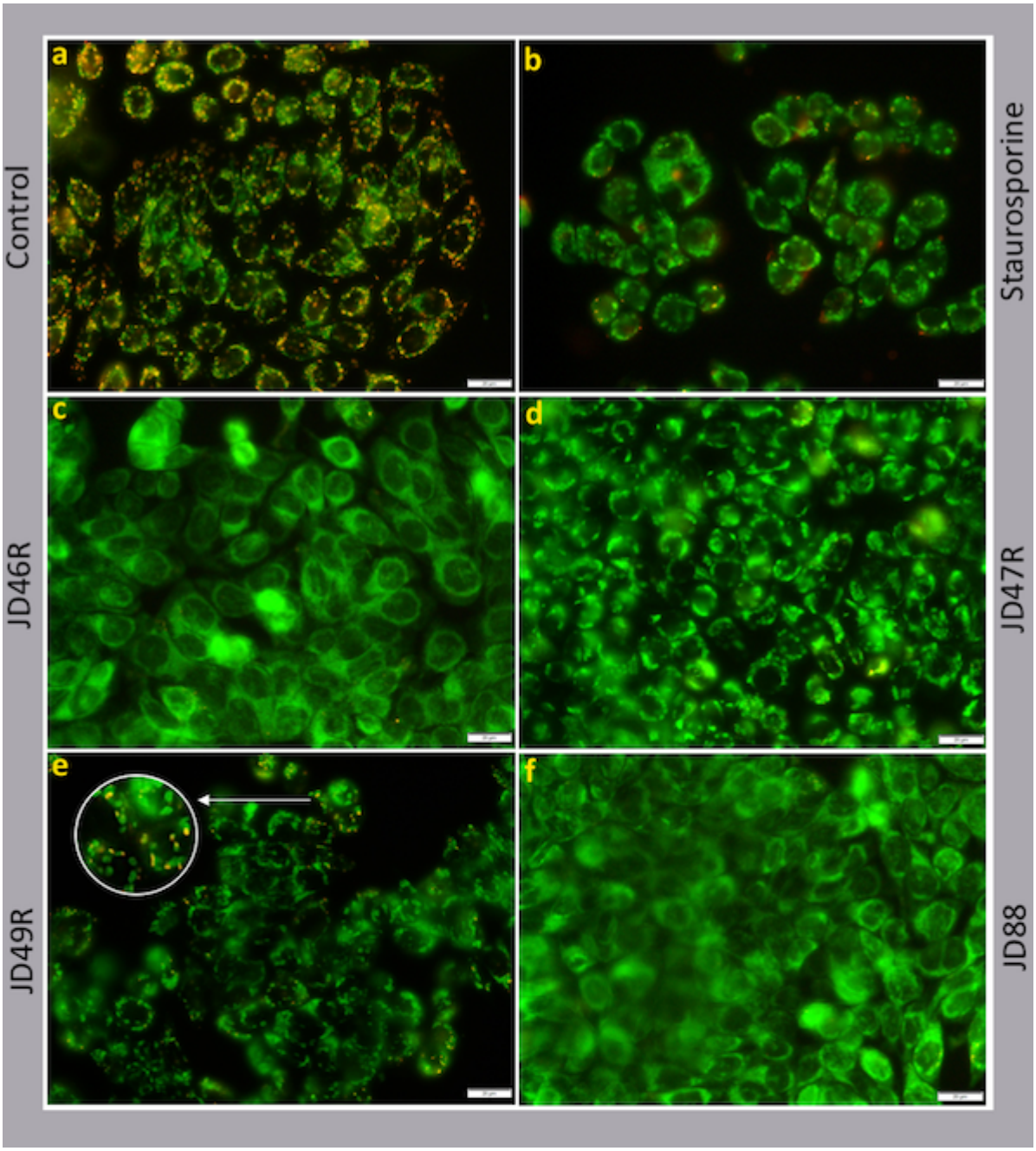


Figure 3.15 Copper-imidazo[1,2-*a*]pyridines cause disruption of the mitochondrial membrane potential in HT-29 cells. HT-29 cells were treated with 10 µM of JD46, JD47, JD49 and JD88 and 200 nM of staurosporine for 12 hours. (Magnification : 400 X, exposure time: 121 ms and ISO: 400) (scalebar: 20 µm).

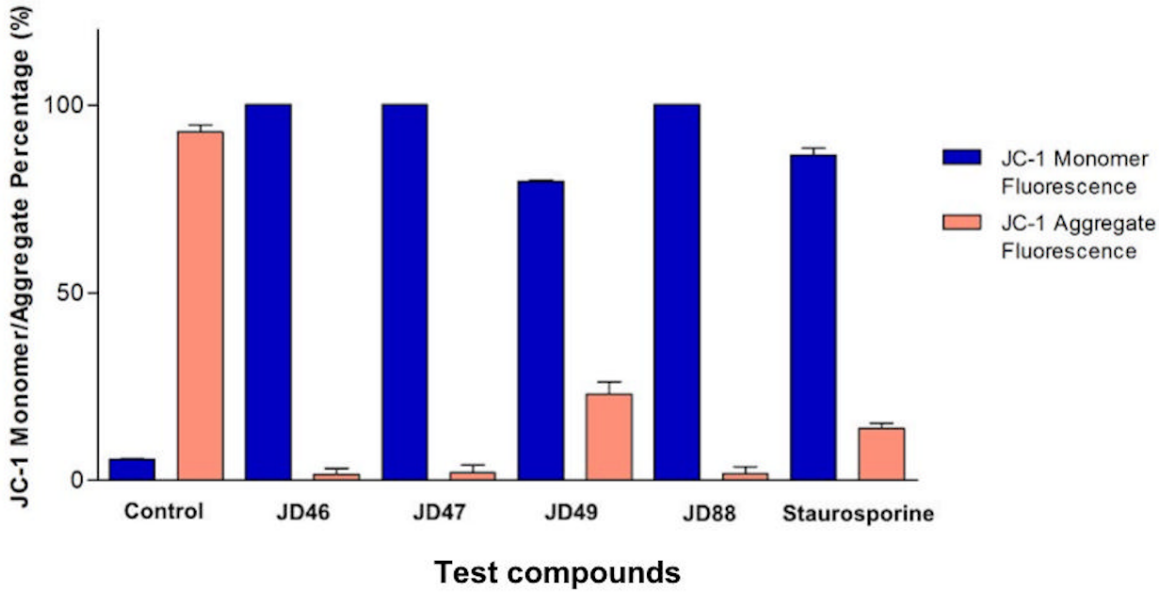


Figure 3.16 Percentage of HT-29 cells showing JC-1-aggregates and JC-1-monomers after treatment with copper-imidazo[1,2-*a*]pyridines and staurosporine. HT-29 cells were treated with 10 µM of JD46, JD47, JD49 and JD88 and 200 nM of staurosporine for 12 hours. Each bar represents the mean ± SEM of values obtained from three independent experiments. The percentage is expressed as the ratio of cells fluorescing positive for JC-1 monomer and JC-1-aggregate.

3.5.2 The effects of copper-imidazo[1,2-*a*]pyridines on the mitochondrial membrane potential of DLD-1 cells

The effects of the copper-imidazo[1,2-*a*]pyridines on DLD-1 cells are shown in Figure 3.17 and Figure 3.18. Untreated DLD-1 control cells showed red-orange fluorescence, indicating JC-1 aggregates and an intact mitochondrial membrane potential (Figure 3.17 panel a). In contrast, staurosporine showed diffuse green fluorescence, indicating a disrupted mitochondrial membrane potential since the JC-1 dye remained in its green monomeric form (Figure 3.17 panel b).

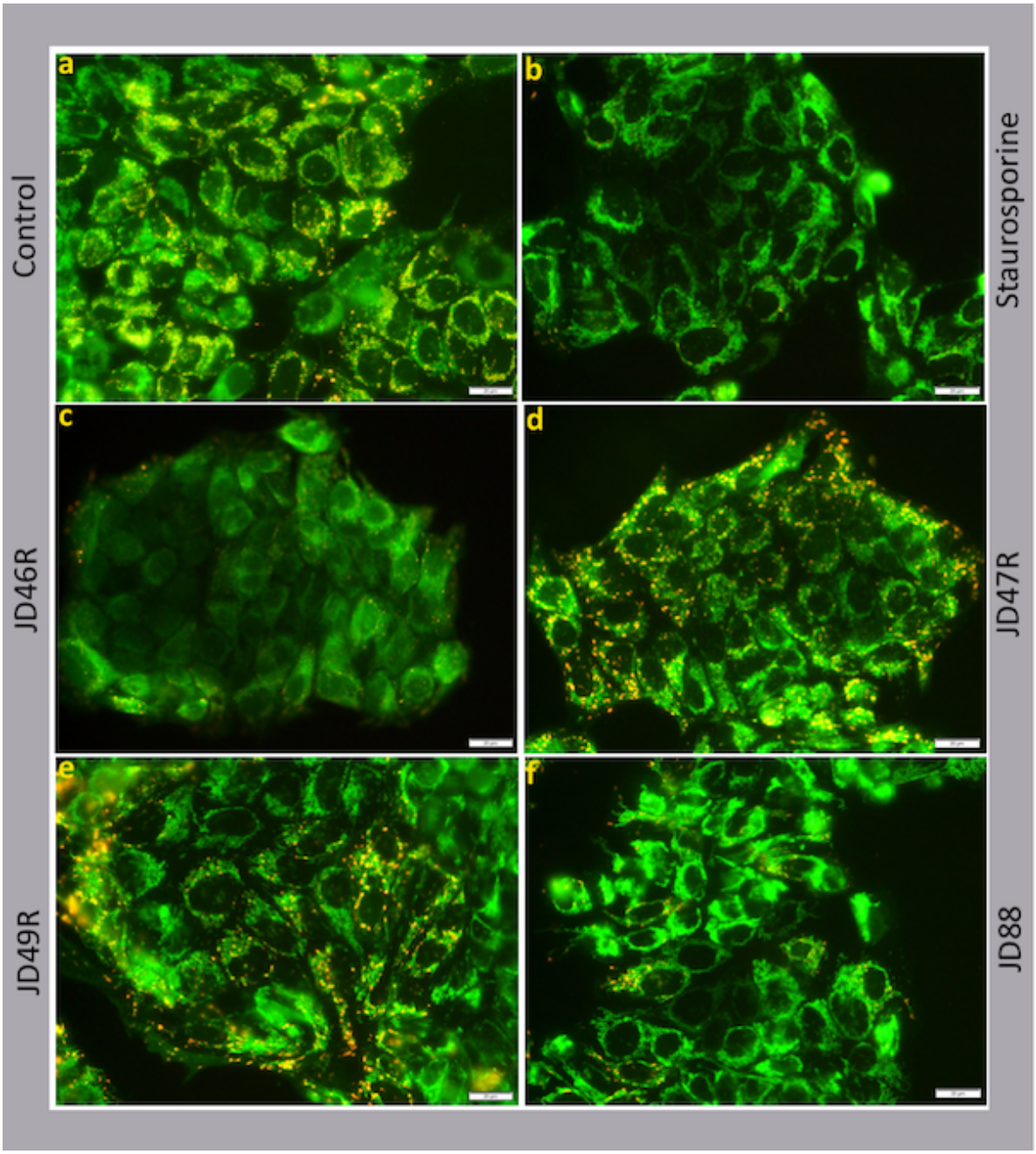


Figure 3.17 Copper-imidazo[1,2-*a*]pyridines cause disruption of the mitochondrial membrane potential in DLD-1 cells. DLD-1 cells were treated with 10 uM of JD46, JD47, JD49 and JD88 and 200 nM of staurosporine for 16 hours. (Magnification: 400 X, exposure time: 121 ms and ISO: 400) (scalebar: 20 µm).

Analysis of the images showed that 93.2 % of JD46 treated cells displayed green monomer fluorescence, indicating an almost complete loss of mitochondrial membrane potential (Figure 3.17 panel c and Figure 3.18). In contrast, 64.5 % of JD47 treated cells fluoresced red-orange showing the presence of mitochondria with an intact membrane potential (Figure 3.17 panel d and Figure 3.18). JD49 was more active than JD47, showing a loss of

mitochondrial membrane potential with 34.2% of cells fluorescing red-orange (Figure 3.17 panel e and Figure 3.18). Similarly to JD46, 88.6 % of JD88 treated cells fluoresced green indicating a loss of mitochondrial membrane potential (Figure 3.17 panel f and Figure 3.18). In addition, the fluorescence displayed by JD46 was more diffuse indicating that the mitochondria may have lost its structural integrity.

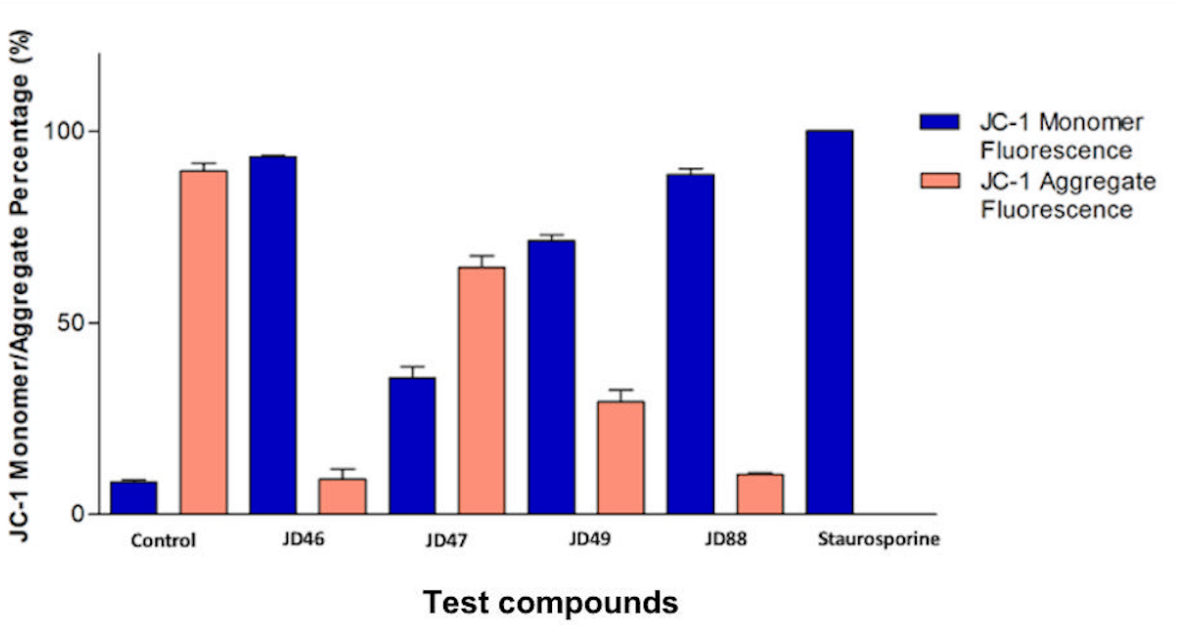


Figure 3.18 Percentage of DLD-1 cells showing JC-1-monomers and JC-1-aggregates after treatment with copper-imidazo[1,2-*a*]pyridines and staurosporine. DLD-1 cells were treated with 10 µM of JD46, JD47, JD49 and JD88 and 200 nM of staurosporine for 16 hours. Each bar represents the mean ± SEM of percentages obtained from three independent experiments. The percentage is expressed as the ratio of cells fluorescing positive for JC-1 monomer and JC-1-aggregate.

When DLD-1 cells were treated with 10 µM of the copper-imidazo[1,2-*a*]pyridines and compared to an untreated control, a change in mitochondrial membrane potential was detected for all compounds. JD46 and JD88 were the most effective in disrupting the mitochondrial membrane potential (Figure 3.18) followed by JD49. Cells treated with JD47 exhibited the lowest JC-1 monomer fluorescence.

After treatment with copper-imidazo[1,2-*a*]pyridines, there was a substantial increase in cells exhibiting JC-1 monomer fluorescence in both cell lines suggesting that the copper-imidazo[1,2-*a*]pyridines cause a loss of $\Delta\psi m$. JD46 caused the greatest loss of mitochondrial membrane potential, with 100 % and 93.2 % of the JC-1 dye remaining in its green monomeric state in HT-29 and DLD-1 cells respectively. Similarly, JD49 exhibited

comparable green fluorescence between HT-29 and DLD-1 cells; 79.7 % and 71.4 % respectively. However, JD47 displayed a dissimilarity in results between the cell lines; in DLD-1 cells, 64.5 % of cells formed red-orange JC-1-aggregates whereas 97.9 % of HT-29 cells exhibited green fluorescence indicative of a loss of mitochondrial membrane potential (Figure 3.18). Copper-imidazo[1,2-*a*]pyridines produced the greatest loss of mitochondrial membrane potential in HT-29 cells compared to DLD-1 cells.

3.6 The determination of the induction of caspase-9 activity in HT-29 and DLD-1 cells

Caspase-9 is an initiator caspase which is activated when complexed with the apoptotic protease activating factor (Apaf-1) and cytochrome c, forming an apoptosome (Brentnall *et al.,* 2013). In turn, caspase-9 directly cleaves and activates effector caspases. Activation of caspase-9 is an indicator for apoptosis via the intrinsic pathway.

Caspase-9 activity in HT-29 and DLD-1 cells was detected using the Abcam Active Caspase-9 FITC staining kit (ab65615). The procedure was carried out as described in Materials and Methodology, section 2.5.5 The FITC conjugated caspase-9 inhibitor selectively binds to active caspase-9 but not to inactive caspase-9. Apoptotic cells display a bright green signal and caspase negative cells display a weak signal. Cells were viewed with an Olympus BX41 microscope using the U-MNIBA3 filter cube for FITC detection. Images were captured using an Olympus DP72 camera with constant exposure times and ISO settings. Results are representative of at least three independent experiments and are shown below from Figure 3.19 to Figure 3.21. The Olympus CellSens software was used to calculate the percentage of cells showing caspase-9 activity in each experiment and is presented Figure 3.21.

3.6.1 Induction of caspase-9 activity by copper-imidazo[1,2-*a*]pyridines in HT-29 cells

The ability of copper-imidazo[1,2-*a*]pyridines to induce caspase-9 activity in HT-29 cells was assessed 18 hours after treatment with 10 μM of test compounds and 200 nM of staurosporine and are shown in Figure 3.19 and Figure 3.21.

Untreated HT-29 cells showed no fluorescent signal indicating the absence of activated caspase-9 (Figure 3.19 panel a and b). In HT-29 cells, 89.8 % of staurosporine treated cells were caspase-9 positive and fluoresced bright green (Figure 3.19 panel k-l). HT-29 cells treated with JD46 and JD88 caused the greatest percentage of cells showing caspase-9 activation; JD46 with 100 % and JD88 with 99 % positive cells (Figure 3.19 panel c-d and panel i-j). JD47 treated cells showed low caspase-9 activation with 15.2 % staining positive for activated caspase-9 (Figure 3.19 panel e-f). The phase contrast image of JD47 treated cells (Figure 3.19 panel f) shows extensive membrane blebbing in caspase-9 negative cells, indicated by white arrows. Sixty-one percent of JD49 treated cells were caspase-9 positive (Figure 3.19 panel g-h.)

These results indicate that each test compound is able to activate caspase-9 in HT-29 cells under these treatment conditions, albeit not to the same extent. At 10 μM, JD46 and JD88 were more effective than staurosporine, JD47 and JD49. JD47 was the least effective caspase-9 inducer in HT-29 cells.

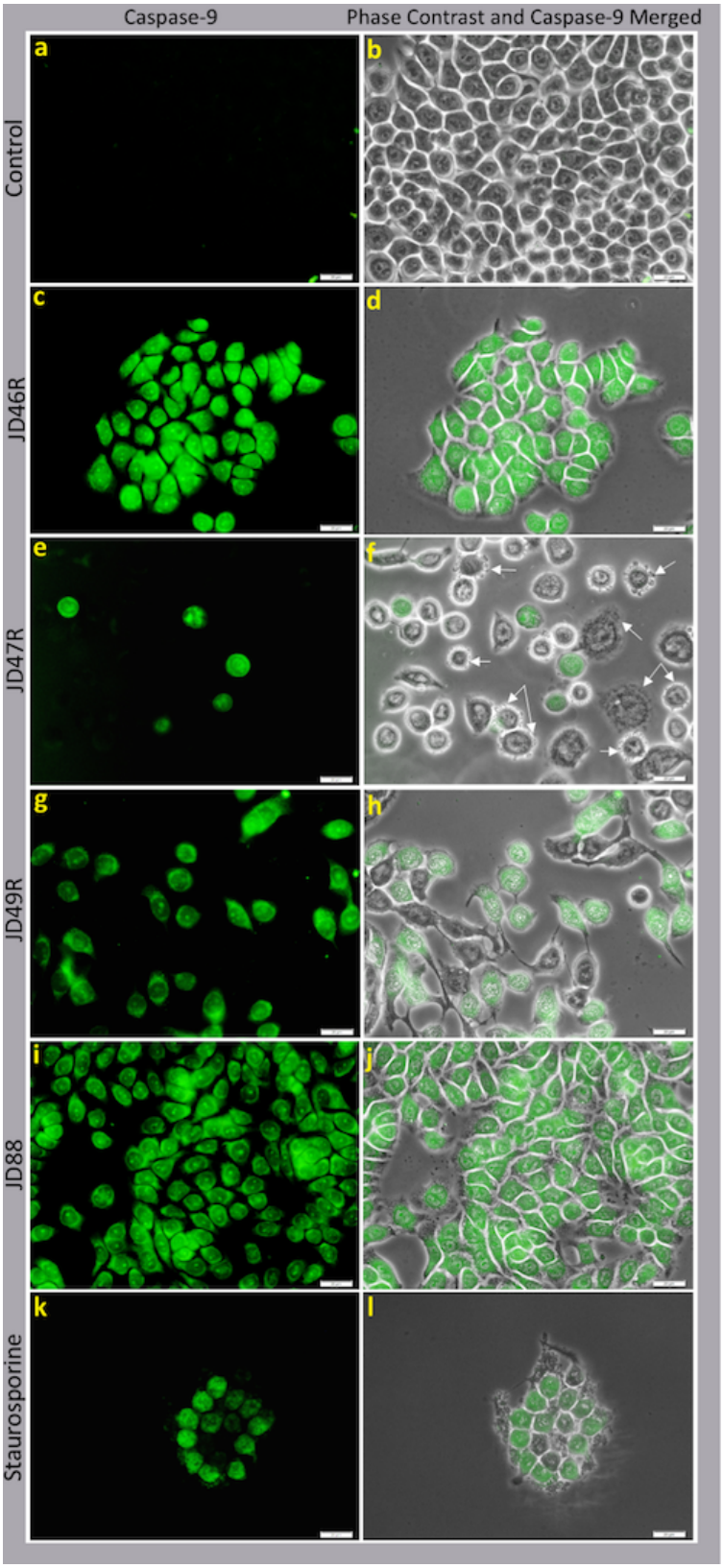


Figure 3.19 Copper-imidazo[1,2-*a*]pyridines stimulate caspase-9 activity in HT-29 cells.
Cells were treated with 10 µM of JD46, JD47, JD49 and JD88 and 200 nM of positive control staurosporine for 18 hours. (Magnification: 400 X, exposure time: 340 ms and ISO: 400) (scalebar: 20 µm).

3.6.2 Induction of caspase-9 activity by copper-imidazo[1,2-*a*]pyridines in DLD-1 cells

After 18 hours, untreated DLD-1 control cells showed no caspase-9 activity. Background fluorescence was attributed to non-specific binding (Figure 3.20 panel a-b). Ninety-two percent of DLD-1 cells treated with the positive control, staurosporine were positive for caspase-9 activity (Figure 3.20 panel k-l and Figure 3.21).

As in HT-29 cells, JD46 treated cells showed the highest percentage, (91 %) of cells staining positive for caspase-9 (Figure 3.20 panel c-d). JD88 treated cells however, displayed the lowest caspase-9 activity with 11.2 % showing indistinct non-specific green fluorescence (Figure 3.20 panel i-j and Figure 3.21). This is in contrast to the effects of JD88 on HT-29 cells. JD47 and JD49 were similar with a low intensity green fluorescent signal in 21.5 % and 22.8 % of DLD-1 cells, respectively (Figure 3.20, panel d, f, h and j and Figure 3.21). The low intensity of the signal indicates that this fluorescence is most likely not related to caspase-9 activation.

The results indicate that JD46 is the most efficient activator of caspase-9 activity in both HT-29 and DLD-1 cells with 100 % and 91 % of the cells displaying bright green fluorescence, respectively (Figure 3.21). In comparison to HT-29 cells, DLD-1 cells treated with JD47, JD49 and JD88 showed weaker green signals, suggesting non-specific binding. The HT-29 cells were more sensitive to copper-imidazo[1,2-*a*]pyridines in inducing caspase-9 activity than DLD-1 cells.

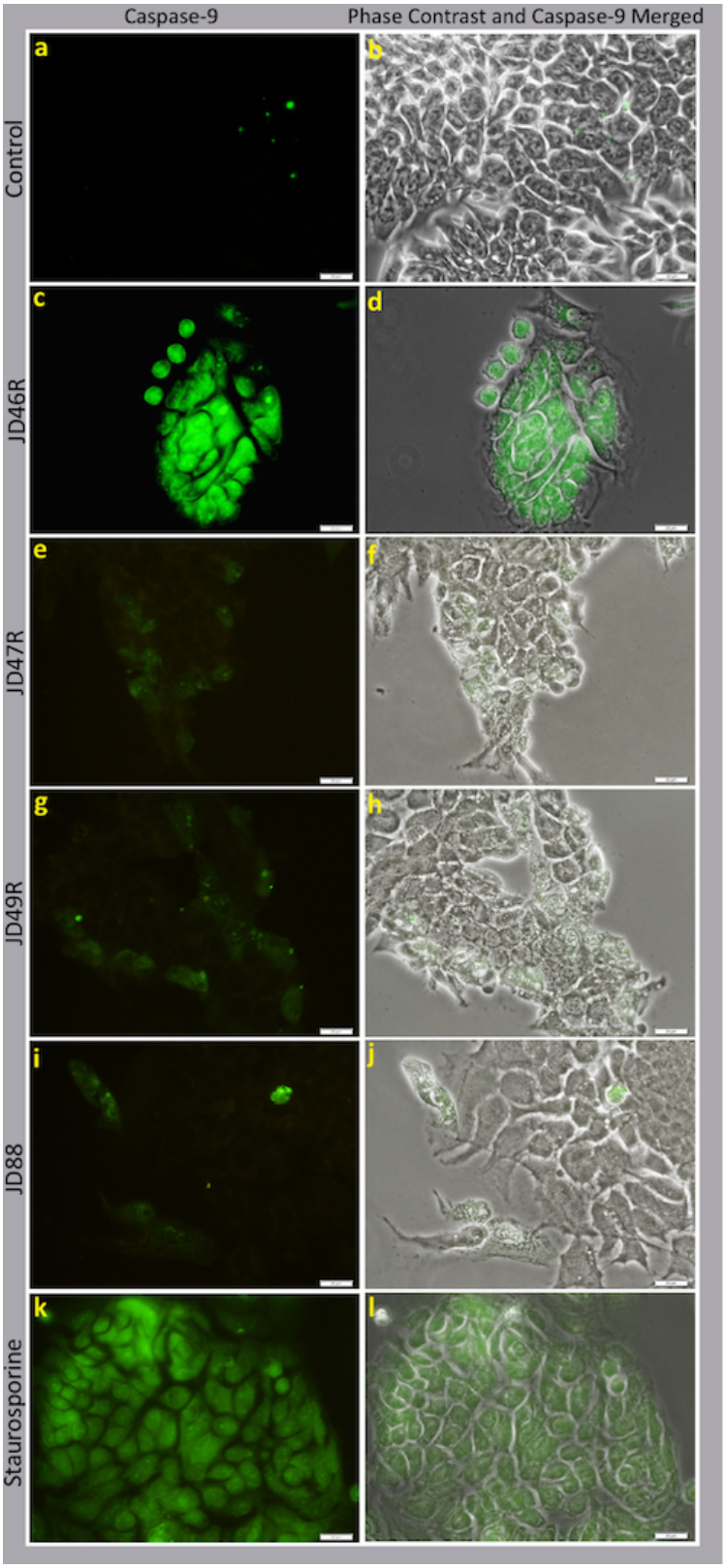


Figure 3.20 JD46 stimulates caspase-9 activity in DLD-1 cells. Cells were treated with 10 µM of JD46, JD47, JD49 and JD88 and 200 nM of positive control staurosporine for 18 hours. (Magnification: 400 X, exposure time: 340 ms and ISO: 400) (scalebar: 20 µm).

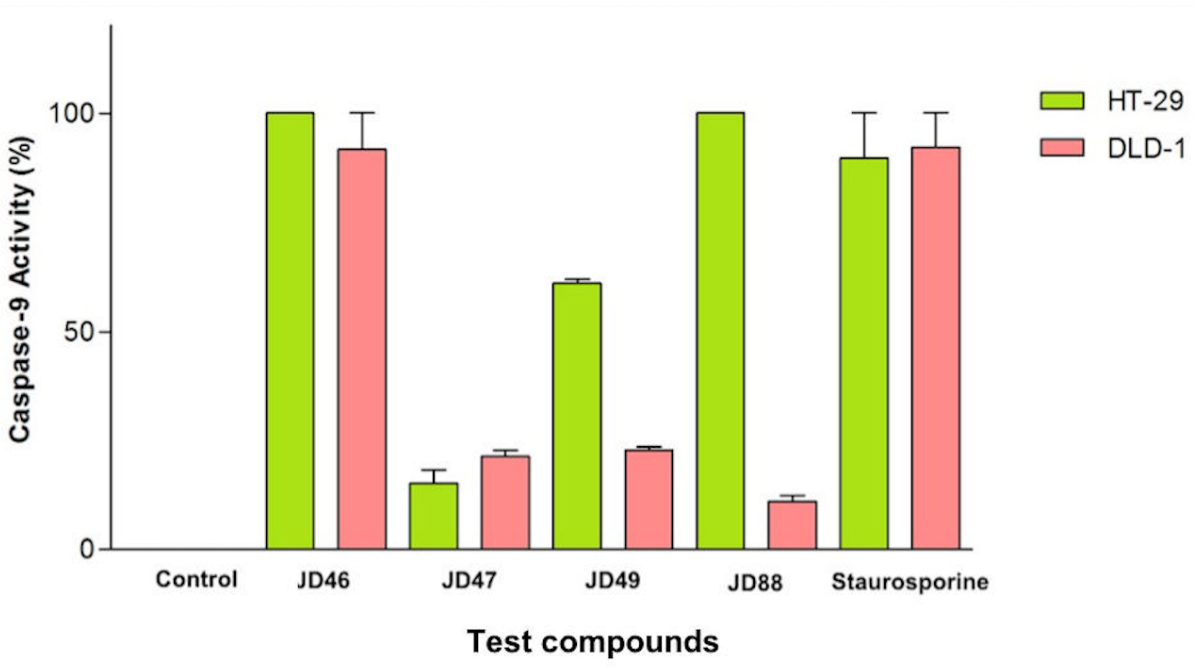


Figure 3.21 Percentage of caspase-9 apoptotic cells in HT-29 and DLD-1 cells treated with copper-imidazo[1,2-*a*]pyridines and staurosporine. HT-29 and DLD-1 cells were treated with 10 µM of JD46, JD47, JD49 and JD88 and 200 nM of staurosporine for 18 hours. Each bar represents the mean ± SEM of values obtained from three independent experiments. The percentage is expressed as the ratio of cells fluorescing positive for Caspase-9 against the total number of cells in the field of view.

3.7 The effect of copper-imidazo[1,2-*a*]pyridines on the apoptotic protein profile of HT-29 cells

The availability of protein arrays makes it possible to simultaneously evaluate the effect of test compounds on the expression levels of multiple proteins involved in apoptosis and its regulation. Since HT-29 cells were most sensitive to three of the copper-imidazo[1,2-*a*]pyridines (JD46, JD47, JD88), their effect was evaluated on HT-29 cells alone and not DLD-1 cells. The expression levels of 35 apoptosis-related proteins were detected using the Proteome Profiler ™ Human Apoptosis Array Kit (R&D Systems) as described in section 2.6 of materials and methodology. The experiments were repeated twice and the positive control was excluded due to cost constraints. HT-29 cells (10.0×10^6) were treated with 5.0 µM of JD46, JD47 and JD88 for 18 hours. A lower concentration of copper-imidazo[1,2-*a*]pyridines was chosen to avoid rapid cell death. For each treatment, the appropriate amount of lysate containing 400 µg of total protein was incubated with a prepared membrane, overnight. Chemiluminescence was detected and images captured using a BIO-RAD ChemiDoc ™ MP

Imager in the single accumulation mode. Images were analyzed with the BIO-RAD Image Lab Software Version 6 to obtain relative expression levels. Changes of expression levels greater than 20 % were considered to be meaningful and are included in the analysis. Results are shown in Table 3.5 and Figure 3.22 to Figure 3.25. Changes below 20 % are shown in Appendix F, Figure F2.

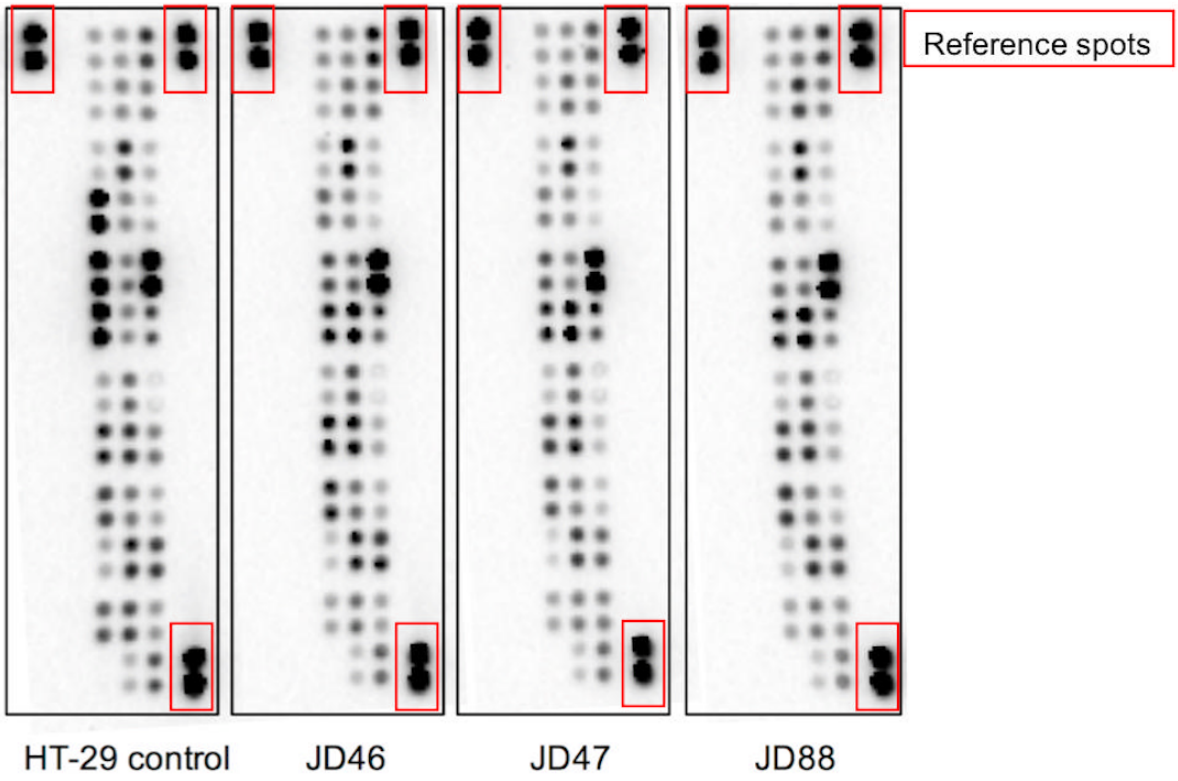


Figure 3.22 Chemiluminescent signals of apoptosis-related proteins captured on nitrocellulose membranes. HT-29 cells were treated for 18 hours with 5.0 µM of JD46, JD47 and JD88. Chemiluminescent images were captured using BIO-RAD ChemiDoc ™ MP Imager.

3.7.1 Copper-imidazo[1,2-*a*]pyridines decrease the levels of apoptotic inhibitory proteins

Cellular inhibitors of apoptosis (cIAPs) inhibit death-receptor mediated apoptosis (Guicciardi *et al*., 2011), such as apoptosis initiated by TRAIL R1/DR4 and TRAIL R2/DR5 receptors. Analysis of proteomic data shows that the expression of cIAP-1 and cIAP-2 were decreased when cells were treated with the copper-imidazo[1,2-*a*]pyridines (Table 3.5 and Figure 3.23). In comparison, there was an overall increase in TRAIL death receptor expression with the exception of TRAIL R2/DR5 in JD46 treated cells (Figure 3.23). These results indicate that the HT-29 cells treated with copper-imidazo[1,2-*a*]pyridines were able to overcome the

inhibitory effects of cIAP mediated inhibition of the TRAIL receptors in(Figure 3.23). Other inhibitors of apoptosis, livin and XIAP act by inhibiting caspase activity and are expressed in CRC cancer cells (Lee *et al*., 2011). Table 3.5 and Figure 3.23 shows that both livin and XIAP expression were decreased after treatment with copper test compounds. Compared to the untreated control, all IAP proteins (cIAP-1, cIAP-2, livin and XIAP) were decreased. These results indicate that the copper compounds caused inhibition of IAPs and were therefore able to overcome their inhibitory effect of apoptosis.

Table 3.5 Expression levels of proteins displaying a greater than 20 % change in HT-29 cells. Proteins are included where at least one of the compounds caused a greater than 20 % increase or decrease of the protein. Expression was calculated in HT-29 cells relative to an untreated control. Cells were treated with 5 µM of JD46, JD47 and JD88 for 18 hours.

	% Increase relative to the control		
Proteins	**JD46**	**JD47**	**JD88**
Bad	24.40	*Decreased by 10.46**	*Decreased by 3.71**
HO1/HMOX1/HSP32	136.00	138.60	164.67
TRAIL R1/DR4	33.71	33.12	42.60
TRAIL R2/DR5	*12.28**	37.48	70.08
PON2	27.76	*Decreased by 7.08**	*12.49**
Pro-Caspase-3	*Decreased by 10.32**	*Decreased by 20.00**	65.52
	% Decrease relative to the control		
Bcl-2	*16.93**	*17.94**	24.04
Bcl-x	39.38	50.60	21.59
Catalase	42.23	23.85	34.14
cIAP-1	46.64	63.49	49.63
cIAP-2	22.25	32.39	26.10
Claspin	*1.12**	26.69	*6.97*
Clusterin	30.97	*5.74**	15.69
Cytochrome c	22.59	42.00	35.32
HIF-1a	*7.10**	28.86	*15.42**
HtrA2/Omi	43.93	48.39	46.65
Livin	35.90	37.23	42.81
Phospho-p53 (S15)	67.37	73.31	72.18
Phospho-p53 (S46)	53.29	57.36	60.36
Phospho-p53 (S392)	34.67	43.10	33.40
TNF R1/TNFRSF1A	40.95	28.95	36.47
XIAP	53.81	43.70	52.69
*indicate that % increase/decrease were not consistent for all three test compounds			

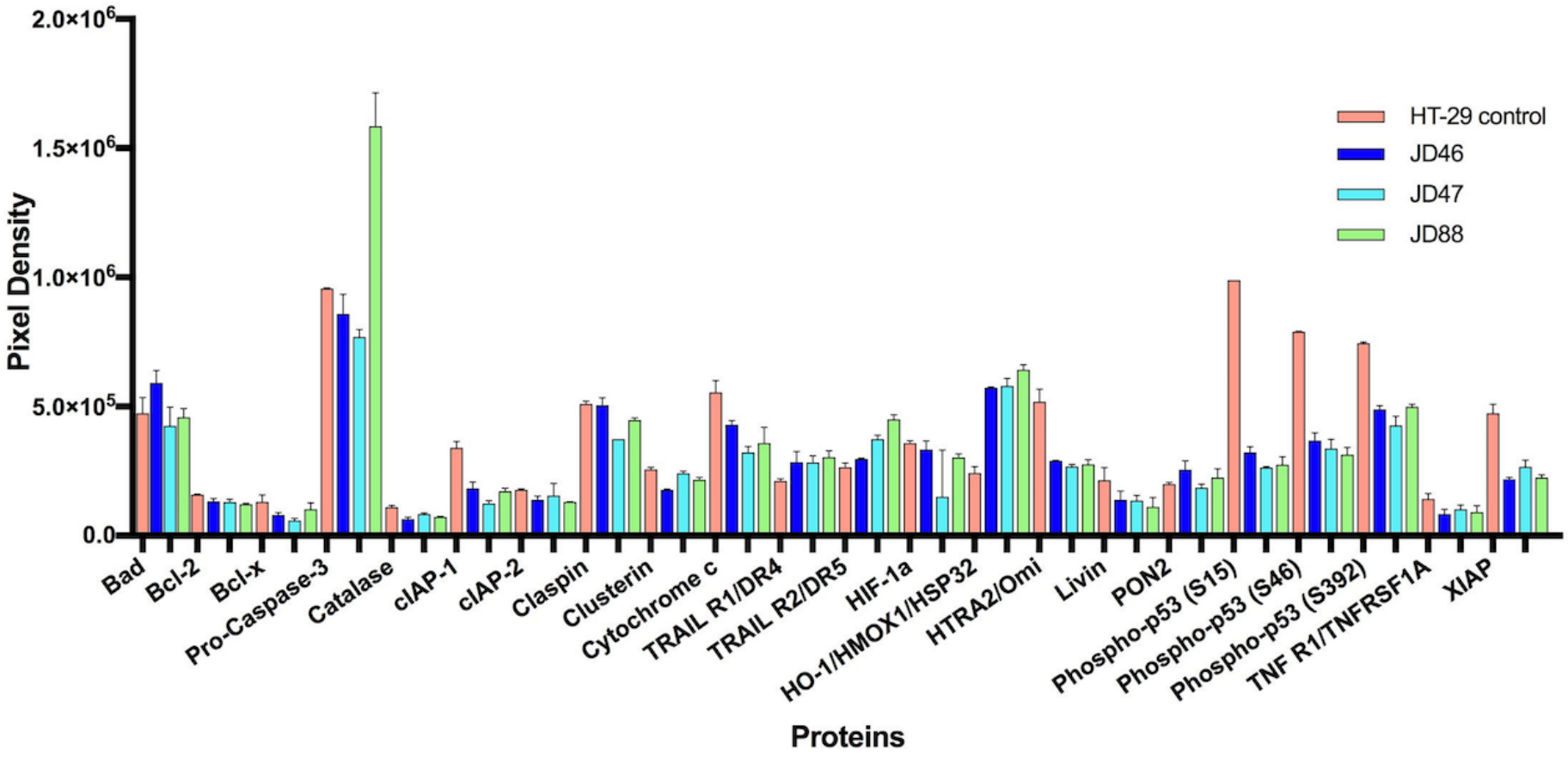


Figure 3.23 Expression of apoptosis-related proteins in HT-29 cells which showed a greater than 20 % change when treated with copper-imidazo[1,2*α*] pyridines. HT-29 cells were treated with 5.0 µM of JD46, JD47 and J88 for 18 hours. The intensity of the chemiluminescent signals was quantified using the Image Lab Software Version 6. Proteins displaying changes of expression levels greater than 20 % are included in this graph.

3.7.2 Copper-imidazo[1,2-*a*]pyridines decreases the levels of TNFR1

Tumor necrosis factor receptor 1 (TNFR1) is a death receptor which results in the activation of apoptosis via the extrinsic pathway. The Fas-associated death domain (FADD) adaptor protein and procaspase-8 bind to TNFR1 resulting in the death-inducing signaling complex (DISC) formation which ultimately leads to apoptotic cell death (Fischer *et al.*, 2015). TNFR1, in addition mediates activation of the NFκB pathway which in turn prevents TRAIL mediated apoptosis (Kim *et al.*, 2002). Figure 3.23 and Table 3.5 show that TNF R1/TNFRSF1A were decreased in all copper compounds relative to the untreated control. JD46 displayed the greatest decrease of 40.95 % followed by JD88 (36.47 %) and JD47 (28.95 %).

3.7.3 Copper-imidazo[1,2-*a*]pyridines increases the levels of HO-1/HMOX-1/HSP32

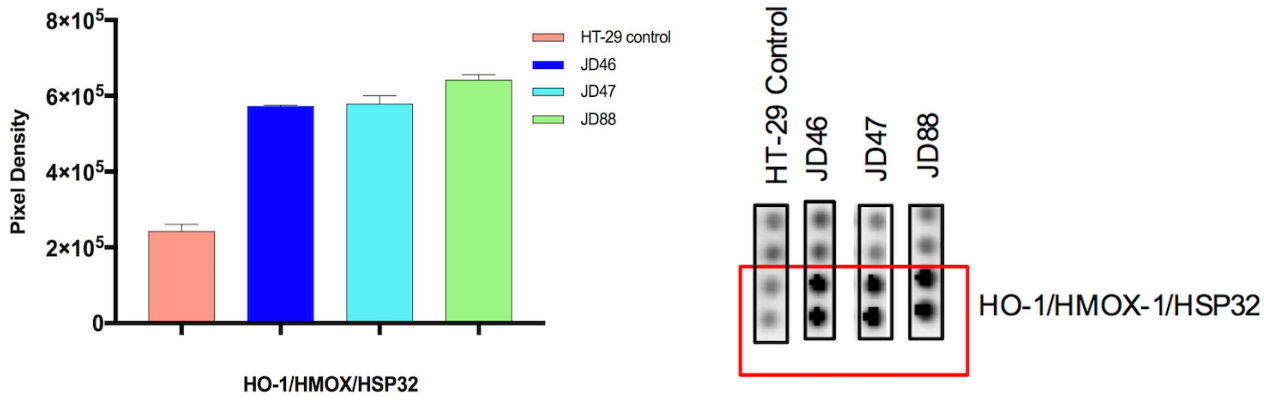


Figure 3.24 Copper-imidazo[1,2-*a*]pyridines increased HO-1/HMOX1/HSP-32 expression in HT-29 cells. HT-29 cells were treated with 5 µM of JD46, JD47 and JD88 for 18 hours and a change of protein expression was compared to an untreated control. Arrays were incubated with 400 µg of each cell lysate.

Heme oxygenase-1 (HO-1/HMOX-1) also known as heat shock protein 32 (HSP32) has cytoprotective properties when cells are exposed to oxidative stress, hypoxia and high temperatures and lowers the rate of apoptosis (Chatterjee and Burns, 2017; Zhu *et al.*, 2015). Of all the expressed proteins, Figure 3.22, Figure 3.23, Figure 3.24 and Table 3.5 shows that the HO-1/HMOX1/HSP32 protein had the highest percentage increase of protein expression relative to the HT-29 control. JD46 increased by 136.00 %, JD47 increased by 138.60 % and JD88 increased by 164.67 %. HSP27 had a marginal increase of 7.19 % in JD46 treated cells but a decrease between 3-4 % in JD47 and JD88 (Appendix F, Figure F2). HSP60 was

decreased by 16.76 % in JD47 treated cells and by 8.80 % and 3.28 % in JD88 and JD47, respectively (Appendix F, Figure F2). HSP70 had marginal increase below 2.00 % in JD46 and JD88 treated cells and a decrease of 2.60 % in JD47 treated cells (Appendix F, Figure F2).

3.7.4 Copper-imidazo[1,2-*a*]pyridines decreases the levels of p53 in HT-29 cells

Phosphorylation of p53 protects the protein from MDM2 degradation, allowing p53 to accumulate within the cell (Weinberg, 2014). According to Figure 3.23, Figure 3.25 and Table 3.5, the various phosphorylated forms of p53 was prominently present in the untreated HT-29 cells. The high p53 levels in the control is not unexpected since mutated p53 is known to accumulate in the cytoplasm of HT-29 cell lines (Ahmed *et al*., 2013). The copper-imidazo[1,2-*a*]pyridines caused a decrease in the expression levels of all three p53 proteins as shown in Figure 3.23, Figure 3.25 and Table 3.5. When treated with JD46, JD47 and JD88, p53 phosphorylated at serine sites 15, 46 and 392 displayed a meaningful decrease in p53 ranging between 30 – 74 % (Figure 3.23, Figure 3.24 and Table 3.5).

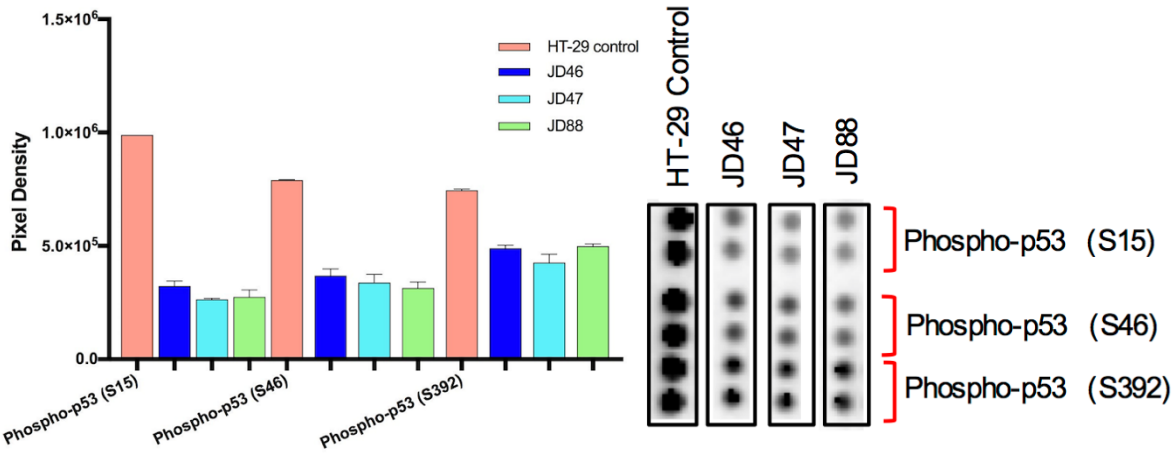


Figure 3.25 Copper-imidazo[1,2-*a*]pyridines decreased phosphorylated p53 expression in HT-29 cells. HT-29 cells were treated with 5 µM of JD46, JD47 and JD88 for 18 hours and protein expression levels decreased compared to the untreated control. Arrays were incubated with 400 µg of each cell lysate.

3.7.5 Changes in other apoptotic proteins

3.7.5.1 The Bcl-2 family

The Bcl-2 family of proteins regulate the intrinsic apoptotic pathway and is subdivided into pro-apoptotic and anti-apoptotic proteins. According to the results obtained from proteomic profiling, the expression of the pro-apoptotic protein, Bad was increased by 24.40 % in JD46 treated cells yet decreased in JD47 and JD88 treated cells (Table 3.5 and Figure 3.23). Copper-imidazo[1,2-*a*]pyridines decreased the expression of the anti-apoptotic proteins, Bcl-2 and Bcl-x. JD88 was the only compound to decrease Bcl-2 by more than 20 % (Table 3.5). However, Bcl-x was decreased by all three copper-imidazo[1,2-*a*]pyridines;JD46 by 39.38 %, JD47 by 50.60 % and JD88 by 21.59 % (Table 3.5).

3.7.5.2 Pro-caspase-3 and cleaved caspase-3

Pro-caspase-3 activates caspase-3, a central executioner caspase in the caspase cascade. Table 3.5 and Figure 3.23 shows a 65.52 % increase in the pro-caspase-3 protein in JD88 treated cells. In comparison, JD46 and JD47 caused a decrease in pro-caspase-3 of 10 and 20 % respectively (Table 3.5). Cleaved caspase-3 decreased by 16.52 % in JD46 treated cells and by 15.95 % in JD88 cells (Appendix F, Figure F2). An 8.87 % cleaved caspase-3 increase was observed in JD47 treated cells (Appendix F, Figure F2).

3.7.5.3 Cytochrome c

The cytochrome c protein is found between the inner and outer mitochondrial membranes. During induction of the intrinsic apoptotic pathway, cytochrome c is released from the mitochondria into the cytosol where it forms the apoptosome with Apaf-1 resulting in the activation of the caspase cascade via caspase-9 (Weinburg, 2014). According to Table 3.5 and Figure 3.23, cytochrome c expression decreased in all test compounds compared to the untreated control. JD47 exhibited the highest decrease of 42.00 % followed by JD88 (35.32 %) and lastly, JD46 (22.59 %).

3.7.5.4 Catalase

Catalase is an enzyme that converts hydrogen peroxide (a reactive oxygen species) to water and oxygen (Jeong and Joo, 2016). In the absence of catalase, there is an increase in ROS resulting in oxidative damage (Jeong and Joo, 2016). Compared to the untreated HT-29 control, copper-imidazo[1,2-*a*]pyridines decreased the expression of catalase (Table 3.5). JD46 decreased catalase expression by 43.23 %, followed by JD88 (34.14 %) and lastly, JD47 (23.85 %).

3.7.5.5 Claspin

During DNA damage, claspin is phosphorylated and mediates the activation of checkpoint kinase 1 (Chk1) thus activating checkpoint arrest. Proteosome-dependent claspin degradation was shown by Semple et al (2007) resulting in decreased levels of claspin (Semple *et al*., 2007). Compared to the untreated control, Figure 3.23 and Table 3.5 shows that claspin expression was decreased in JD47 treated cells by 26.60 %. JD46 and JD88 showed smaller decreases in protein expression of 1.12 % and 6.97 %, respectively (Appendix F, Figure F2).

3.7.5.6 Clusterin

Clusterin is a glycoprotein with a cytoprotective role activated in response to cell stress, resembling HSPs (Chene *et al*., 2004; Koltai, 2014). The clusterin isoform protects the cell from apoptosis by inhibiting the action of the pro-apoptotic protein, Bax. Clusterin also promotes angiogenesis (Koltai, 2014). According to Figure 3.23 and Table 3.5, clusterin was decreased by 30.97 % in JD46 treated HT-29 cells compared to the untreated control. JD47 and JD88 showed a lower decrease of less than 20 % (5.74 % in JD47 and 15.69 % in JD88 treated cells) (Table 3.5). Bax had less meaningful increases between 8.00 % and 14.00 % in JD46 and JD88 treated cells and a marginal decrease of 2.56 % in JD47 treated cells (Appendix F, Figure F2).

3.7.5.7 HIF-1*α*

In response to hypoxic stress, the hypoxia inducible factor (HIF-1α) protein induces apoptosis by binding to the MDM2 protein, thereby stabilizing p53. Additionally, HIF-1α can inhibit

the anti-apoptotic effect of Bcl-2 by increasing the expression of the Bcl-2 binding protein, BNIP3 (Masoud and Li, 2015; Greijer and van der Wall, 2004). Cells with increased amounts of HIF are resistant to hypoxia induced apoptosis indicating that HIF-1α can also inhibit apoptosis (Masoud and Li, 2015; Greijer and van der Wall, 2004). Increased levels of hypoxia inducible factor (HIF-1α) are associated with tumor progression and metastasis. Table 3.5 and Figure 3.23 shows that HIF-1α was increased in JD47 treated cells by 28.86 % whereas JD46 and JD88 displayed a decrease of 7.10 % and 15.42 %, respectively.

3.7.5.8 HtrA2/Omi and Smac/Diablo

HtrA2/Omi and Smac/Diablo are mitochondrial direct IAP-binding proteins that are released into the cytosol from the mitochondria during apoptosis initiation. The proteins induce apoptosis through the intrinsic pathway in a caspase-dependent manner (Hegde et al., 2001). Compared to the untreated HT-29 control, the expression of the HtrA2/Omi protein was decreased when cells were exposed to JD46, JD47 and JD88 (Table 3.5 and Figure 3.23). The Smac/Diablo protein was increased in JD47 and JD88 by 19.33 % and 18.08 %, respectively and by 5.36 % in JD46 treated cells (Appendix F, Figure F2).

Chapter IV. Discussion

In this study, the cytotoxic effects of synthetic test compounds on the cell viability of HT-29 and DLD-1 colorectal cancer cells were determined. A total of 25 compounds belonging to three different classes; nucleoside analogues (JLPs), epidermal growth factor receptor kinase inhibitors (EKIs) and copper-imidazo[1,2-*a*]pyridines were screened against both cell lines. The IC_{50} values were obtained for compounds displaying more than an 80 % inhibition of cell growth at a concentration of 50 μM. Four copper-imidazo[1,2-*a*]pyridines were selected for further investigation due to their high potency against both cell lines. Copper-complexes show promising anticancer activity and are currently under various phases of preclinical evaluation (McGivern *et al*., 2018). An evaluation of the mechanism of cell death is required for further preclinical development of potential anticancer agents. Therefore, the mechanism of cell death and a set of specific apoptotic marker assays were investigated after exposing cells to the copper-imidazo[1,2-*a*]pyridines. In addition, the effect of the three most potent copper-imidazo[1,2-*a*]pyridines on an apoptotic protein array was determined.

4.1 The cytotoxicity of nucleoside analogues, EKI inhibitors and copper-imidazo[1,2-*a*] pyridines on HT-29 and DLD-1 cells

A comparison of the three classes of compounds screened at the start of this study showed that the EKIs had poor cytotoxic activity compared to the nucleoside analogues and copper-imidazo[1,2-*a*]pyridines. No further work was performed on the EKIs. IC_{50} values were determined for the six active nucleoside analogues and the four copper-imidazo[1,2-*a*]pyridines (Table 4.1a and table 4.1b).

As reported in Chapter III. Section 3.1, DLD-1 cells were more sensitive than HT-29 cells to nucleoside analogues with IC_{50} values ranging between 11.0 and 20.0 μM and between 16.0 and 26.0 μM, respectively (Table 4.1a). All further investigations were focused on the copper-imidazo[1,2-*a*]pyridines.

Comparatively, four copper-imidazo[1,2-*a*]pyridines at a concentration of 50 μM caused more than an 80 % reduction in cell viability in both HT-29 cells and DLD-1 cells. Dose response curves of the copper-imidazo[1,2-*a*]pyridines are shown in Appendix C, Figure C3 and C4 and indicate that when HT-29 and DLD-1 cells were treated with increasing

concentrations of test compounds for 48 hours, the percentage of viable cells decreased in a dose-dependent manner. JD46 was the most toxic to both cell lines with IC_{50} values of 0.85 ± 0.03 µM in HT-29 cells and 9.25 ± 0.41 µM in DLD-1 cells respectively (Table 4.1b). Due to their low IC_{50} values in both cell lines, the copper-imidazo[1,2-*a*]pyridines were selected for further investigation.

Table 4.1 (A) IC_{50} values of nucleoside analogues in HT-29 and DLD-1 cell lines.

Compounds	Cell lines	
Nucleoside Analogues	**IC_{50} value (µM) HT-29**	**IC_{50} value (µM) DLD-1**
JLP065	23.13	19.89
JLP089	18.16	15.65
JLP093	20.05	11.16
JLP090.3	22.79	21.14
JLP117.1	16.14	13.21
JLP118.1	25.89	12.06

Table 4.1 (B) IC_{50} values of copper-imidazo[1,2-*a*]pyridines in HT-29 and DLD-1 cell lines.

Compounds	Cell lines	
Copper-imidazo[1,2-*a*]pyridines	**IC_{50} value (µM) HT-29**	**IC_{50} value (µM) DLD-1**
JD46	0.85	9.25
JD47	1.74	11.57
JD49	8.33	11.28
JD88	0.88	9.50

The copper-imidazo[1,2-*a*]pyridines showed some selectivity towards HT-29 cells with IC_{50} values of JD46, JD47 and JD88 between 0.8 and 1.8 µM, whereas JD49 had an IC_{50} value of 8.33 µM. The IC_{50} values of DLD-1 cells ranged between 9.0 and 12.0 µM for JD46, JD47, JD49 and JD88. Both cell lines are categorized as Dukes' C colorectal adenocarcinomas (Ahmed *et al.*, 2013 and American Type Culture Collection, 2016). However, different genetic mutations (Table 4.2) are present in the two cell lines (Ahmed *et al.*, 2013) that may account for the differences in sensitivity of each cell line to the copper-imidazo[1,2-

a]pyridine test compounds. The results presented in this study were published in as part of a larger study where other cancers were investigated (Dam *et al*., 2017).

A study by Gandin et al (2012) found that the phosphine copper (I) complex $[Cu(thp)_4][PF_6]$ was several-fold more active that cisplatin and oxaliplatin (a key drug in the FOLFOX regimen) in colorectal cancer cell lines. In particular, MTT assays showed that in the DLD-1 cell line, $[Cu(thp)_4][PF_6]$ had an IC_{50} value of 0.37 μM, whereas cisplatin and oxaliplatin had IC_{50} values of 8.01 μM and 5.81 μM, respectively after a 72 hour incubation. In addition, $[Cu(thp)_4][PF_6]$ was able to overcome acquired resistance to oxaliplatin (Gandin *et al*., 2012). In a study by Uyar et al (2017), manganese and copper complexes were analysed for their cytotoxicity against DLD-1 cells using the MTT assay after a 24 hour incubation. Copper complexes displayed the highest cytotoxicity with an IC_{50} value of 142.9 μM compared to the IC_{50} value of 193.8 μM in manganese complexes (Uyar *et al*., 2017). Compared to the IC_{50} values obtained in this dissertation, IC_{50} values obtained from the study by Gandin *et al* (2012) may not be therapeutically significant.

Studies carried out by Konarikova *et al* (2016) and Hajrezaie *et al* (2014) investigated the effects of copper (II) complexes on HT-29 cells. Konarikova *et al* (2016) found that four Schiff base copper (II) complexes were cytotoxic against HT-29 cells. more info here. Two of the four complexes displayed increased efficacy against HT-29 cells. The most active copper (II) complex, had an imidazole ligand in its structure and had an IC_{50} value of 0.17 μM followed by complex 3 which had an IC_{50} value of 0.57 μM after a 24 hour incubation using the MTT assay. Complex 1 and 2 had IC_{50} values of 10.00 μM and 31.00 μM, respectively (Konarikova *et al*., 2016). Similarly, Hajrezaie *et al* (2014) found that the copper (II) complex, $Cu(BrHAP)_2$ had potent cytotoxic effects against HT-29 cells with an IC_{50} value of 2.87 μM after a 24 hour treatment (Hajrezaie *et al*., 2014). A study by Tardito *et al* (2011) found that when HT1080 and HeLa cells were treated with equal amounts of $CuCl_2$ and disulfiram, an inhibitor of aldehyde dehydrogenase, $CuCl_2$ shifted the IC_{50} value of disulfiram from 5.2 μM to 0.4 μM and from 15.7 μM to 0.4 μM in HT1080 and HeLa cells, respectively (Tardito *et al*., 2011). In conjunction with the cytotoxic results presented in this study, copper complexes show promising potential as anti-cancer agents and are currently under investigation.

Table 4.2 Mutations in key cancer genes in the HT-29 and DLD-1 colorectal cancer cell lines. Table adapted from Ahmed *et al* (2013).

Cell lines	Mutations in colorectal cancer genes				
	KRAS	**BRAF**	**PIK3CA**	**PTEN**	**p53**
HT-29	G13D	wildtype	E545K D549N	wildtype	S241F
DLD-1	wildtype	V600E	E545K	wildtype	R273H

The effects of test compounds were compared to the positive controls camptothecin and staurosporine in all experiments. Camptothecin, a topoisomerase I inhibitor (Chu *et al*., 2014) and staurosporine, a non-selective protein kinase inhibitor, are both known for their ability to induce apoptosis (Ding *et al*., 2017). Camptothecin had an IC_{50} value of 8.5 μM and 9.84 μM in HT-29 and DLD-1 cells, respectively. Staurosporine exhibited greater toxicity with IC_{50} values of 0.20 μM in HT-29 cells and 0.15 μM in DLD-1 cells. Camptothecin was omitted as a control from the apoptosis assays due to its unpredictable solubility and variation in potency between different batch numbers and suppliers. Due to these inconsistencies, staurosporine was selected to use as a positive control following completion of the morphological investigations.

4.1.1 Structure activity relationships of copper-imidazo[1,2-*a*]pyridines

The four active compounds showed differences in potencies on HT-29 cells. These differences may be due to the presence of different substitutions on the imidazole ring. The increased potency of JD46 may be due to the absence of a substituent at position 4 and 5 of the imidazole ring. Interestingly, the addition of a chlorine group in position 5 (JD49), causes notable loss of potency while the addition of a bromine group on position 5 (JD88) seemed not to have any effect on the potency. The addition of bromine at position 4 in JD47 caused a small decrease in the cytotoxic potency JD47 (IC_{50} = 1.74 μM) when compared to the JD46 and JD88 (IC_{50}= 0.85 μM and 0.88 μM, respectively). In addition, statistical analysis comparing JD46 and JD47 showed a significant difference between these compounds ($p < 0.05$, $p = 0.03$), indicative of increased JD46 cytotoxicity. JD88 and JD47 also had a significant difference of $p < 0.05$, $p = 0.03$, showing that the difference between the two compounds were significant. The addition of chlorine to position 5 of the imidazo[1,2-*a*]pyridine ring decreased the activity of JD49 (IC_{50} = 8.33 μM).

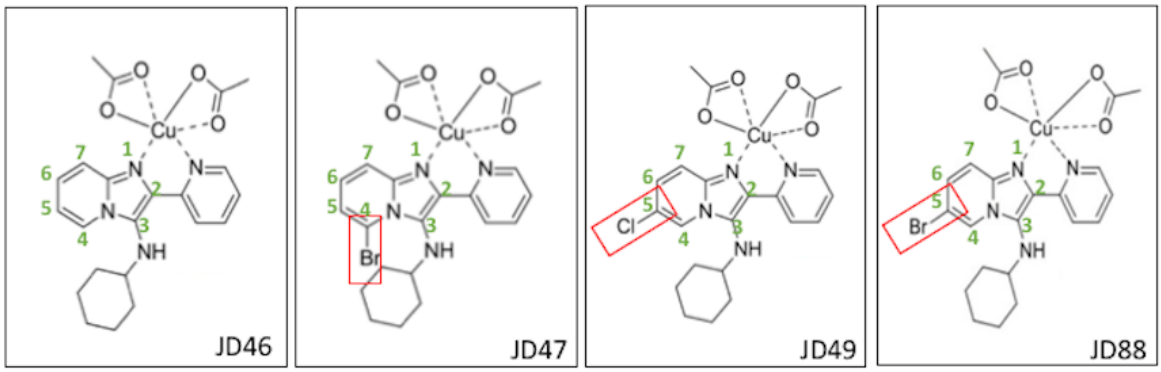


Figure 4.1 Substituent additions to C5 and C4 of the imidazo[1,2-*a*]pyridine ring of copper-imidazo[1,2-*a*]pyridine test compounds impacts their potency.

4.2 The effect of copper-imidazo[1,2-*a*]pyridines on the morphology of the HT-29 and DLD-1 cells

Apoptotic cells display distinct morphological features such as cell shrinkage, chromatin condensation, membrane blebbing and nuclear fragmentation, (Wong, 2011). In this study, morphological changes induced by copper-imidazo[1,2-*a*]pyridines in HT-29 and DLD-1 cells were observed in culture from 12 - 48 hours using phase contrast microscopy. This guided the selection of treatment periods for the investigation of specific apoptotic assays such as annexin-V binding, caspase-3/7 activity, mitochondrial membrane potential and caspase-9 activity.

At a concentration of 10 µM, changes in the shape of a cell and membrane blebbing was evident in both HT-29 and DLD-1 cells treated with all four copper-imidazo[1,2-*a*]pyridines starting at 12 hours, as reported in Chapter III, Section 3.2. DLD-1 cells tend to grow in tight clusters as seen in untreated controls however, after treatment with test compounds, a decrease in growth density was observed. Treatment of cells for 48 hours with JD46, JD47, and JD88, but not JD49, caused the majority of cells to detach from the growth surface. This correlates with the IC_{50} values obtained for each copper-imidazo[1,2-*a*]pyridines with JD49 being the lowest.

Membrane blebbing is a characteristic feature associated with the execution phase of apoptosis (Andrade *et al*., 2010). They are protrusions of the cell membrane that form as a result of actin-myosin contractions (Charras, 2008). All the copper-imidazo[1,2-*a*]pyridines

caused membrane blebbing in both HT-29 and DLD-1 cells as reported in Chapter III, Section 3.2.1 providing support for the induction of apoptosis.

The fluorescent stains, acridine orange (AO), ethidium bromide (EtBr) and Hoechst 33342 (HO) were used to distinguish between viable, apoptotic and necrotic cells (Monga *et al*, 2013). At a test compound concentration of 10 μM, there was no evidence of necrotic cell death in both cell lines for any of the compounds, indicating that cell membranes were intact. Necrosis is characterized by an uncontrolled release of inflammatory cellular contents whereas, inflammation is evaded in apoptosis (Fink and Cookson, 2005), This is of great importance to cancer patients when they are treated with chemotherapy agents since apoptotic cell death does not cause the severe tumor lysis syndrome that accompanies necrotic cell death.

Apoptotic cells show an increase in HO fluorescence intensity and the formation of globular structures in the nucleus. Chromatin condensation is an additional morphological feature of early apoptotic cells and is seen in HT-29 and DLD-1 cell lines in Figure 3.7 and Figure 3.8, respectively. As reported in Chapter III. Section 3.2, Figure 3.7, nuclear fragmentation was observed in HT-29 cells treated with JD46, JD47 and JD88 when stained with HO. In HT-29 cells, JD49, the least potent copper-imidazo[1,2-*a*]pyridine, showed no profound nuclear fragmentation, but there was evidence of chromatin condensation (Figure 3.7, panel k). This observation is not unexpected and is consistent with its lower potency compared to the other copper-imidazo[1,2-*a*]pyridines, as described above. Morphological analysis of the DLD-1 cells showed similar changes to that of HT-29 cells when treated with the imidazo[1,2-*a*]pyridines. Staurosporine treated cells showed distinct nuclear fragmentation of the cells that remained attached to the growth surface, this being more obvious in HT-29 cells since a greater percentage of cells remained attached to the growth surface.

4.3 Annexin-V binding to phosphatidylserine and induction of caspase-3/7 activity indicate that copper-imidazo[1,2-*a*]pyridines cause apoptosis

The exposure of phosphatidylserine on the external surface of the cell membrane is a characteristic feature of early apoptosis. Caspase-3/7 activity provides further evidence for the induction of apoptosis as a mechanism of cell death. In this study, analysis of annexin-V

and caspase-3/7 activity provides further evidence for the induction of apoptosis by copper-imidazo[1,2-*a*]pyridines in HT-29 and DLD-1 colorectal cancer cells. Caspase-3/7 execution caspases, cleaves structural proteins such as the inhibitor of caspase activated DNase (ICAD), which activates caspase activated DNase (CAD) resulting in cell disassembly, DNA fragmentation and apoptosis (Flanagan *et al*., 2016 and Larsen *et al*., 2010). *In vivo*, caspase-3/7 also triggers the release of anti-inflammatory cytokines thereby suppressing the inflammatory response (Flanagan *et al*., 2016). Copper-imidazo[1,2-*a*]pyridines were able to induce caspase-3/7 activity and the exposure of PS on the external surface of the cell membranes in both HT-29 and DLD-1 cells, albeit to varying degrees, providing further evidence for cell death via apoptosis.

At a concentration of 10 μM, copper-imidazo[1,2-*a*]pyridines were able to induce PS translocation in HT-29 and DLD-1 cells. Annexin-V binding was more prevalent in HT-29 cells compared to DLD-1 cells indicating that PS exposure on cell surface was greater in the HT-29 cell line. After a 12 hour treatment, HT-29 cells treated with JD47 showed the highest percentage binding of annexin-V (71.5 %) and JD46 showed the least annexin-V percentage binding (39.4 %). In HT-29 cells, JD46 and JD88 showed a higher percentage of late apoptotic/necrotic cells than JD47 treated cells (Table 3.2 and Figure 3.9 and 3.10). In HT-29 cells, JD49 caused a higher percentage of early apoptotic cells than JD46 but no cells were positive for PI. This indicates that induction of apoptosis is time-dependent and JD49 most likely induced apoptosis at a slower rate due to its lower potency. In contrast, JD49 caused the most annexin-V binding in DLD-1 cells (Table 3.3 and Figure 3.11 and 3.12). Despite these differences, all the copper-imidazo[1,2-*a*]pyridine compounds induced apoptosis after a longer exposure time in DLD-1 cells. At a 200 nM concentration, staurosporine caused 97.0 % of HT-29 cells to undergo late apoptosis/early necrosis whereas only 4.9 % of DLD-1 cells showed late apoptosis/early necrosis, indicating that there are differences in the responses of the two cell lines to apoptotic stimuli.

The induction of caspase-3/7 activity is a late apoptotic event and was therefore measured after a 20 hour treatment with test compounds. All test compounds were able to induce caspase-3/7 activity in both cells lines. However, the increase in caspase-3/7 activity was higher in HT-29 cells than in DLD-1 cells which is consistent with their increased potency. (Chapter III. Section 3.4). In HT-29 cells, at a concentration of 10 μM, JD88 caused the greatest fold increase in caspase-3/7 whereas it caused the lowest increase in DLD-1 cells.

JD46 caused the highest fold increase in DLD-1 cells and followed JD88 in HT-29 cells. Staurosporine caused the lowest increase in HT-29 cells yet a high increase in DLD-1 cells. These discrepancies may be attributed to the molecular characteristics of each cell line as described in Table 4.2. The increase in activity of caspase-3/7 indicates that copper-imidazo[1,2-*a*]pyridines induced apoptosis in both cells. In a study by Konarikova *et al* (2016), caspase-3 activity was measured in HT-29 cells to evaluate apoptosis. It was found that the copper (II) complexes induced an increase in caspase-3 activity. Furthermore, a study by Hajrezaie *et al* (2014) identified the increased caspase-3/7 activity in HT-29 cells when treated with the copper (II) complex, $Cu(BrHAP)_2$.

4.4 Copper-imidazo[1,2-a]pyridines cause a loss of mitochondrial membrane potential and increase the activity of caspase-9 in HT-29 and DLD-1 cells

Mitochondria play an integral role in the regulation of apoptosis through the release of pro-apoptotic proteins, such as cytochrome c from the intermembrane mitochondrial space into the cytosol where it interacts with Apaf-1 to activate pro-caspase-9 and subsequently, caspase-9 (Gogvadze *et al*., 2006). Mitochondria produce reactive oxygen species (ROS) and in metal-induced apoptosis, it mediates apoptosis through metal-induced ROS production (Hajrezaie *et al*., 2014). An electrochemical gradient formed across the outer and inner mitochondrial membranes can be used to measure mitochondrial function (Sakamuru *et al*., 2016). A loss of the mitochondrial membrane potential facilitates the release of the pro-apoptotic protein cytochrome c and the apoptotic factors, Smac/DIABLO and HTRA2/Omi (Gottlieb *et al*., 2003; Wong, 2011). Once released into the cytosol, cytochrome c interacts with Apaf-1, resulting in the activation of pro-caspase-9, a characteristic of the intrinsic apoptotic pathway, which in turn proteolytically cleaves and activates effector caspase-3, 6 and 7, resulting in apoptosis (Eleftheriadis *et al*., 2016). The ability of copper-imidazo[1,2-a]pyridines to cause apoptosis through activation of the intrinsic pathway was confirmed by evaluating the effect of copper-imidazo[1,2-*a*]pyridine test compounds on the mitochondrial membrane potential and on caspase-9 activity.

In this study, at a concentration of 10 μM, the copper-imidazo[1,2-*a*]pyridines caused a decrease in mitochondrial membrane potential ($\Delta\psi m$) in HT-29 and DLD-1 cells, albeit not

to the same extent. Copper-imidazo[1,2-*a*]pyridines induced a greater disruption of Δψm in HT-29 cells. Figure 3.16 shows that JD46, JD47 and JD88 caused a total loss of mitochondrial membrane potential in HT-29 cells. Figure 3.17 and Figure 3.18 shows JD46 caused the greatest decrease of Δψm in DLD-1 cells and JD47 caused the least with more cells forming JC-1 aggregates that fluoresces red, indicative of an intact membrane potential. The positive control, staurosporine, showed complete disruption in mitochondrial membrane potential in both cell lines. In DLD-1 cells, copper-imidazo[1,2-*a*]pyridines caused less of an effect compared to staurosporine.

Increased ROS production may result in the failure to suppress anti-apoptotic factors thus initiating apoptosis (Hajrezaie *et al*., 2014). A study by Hajrezaie *et al* (2014) used mitochondrial membrane potential fluorescent probes to assess the effect of increased ROS production on the mitochondria of HT-29 cells. The copper (II) complex, $Cu(BrHAP)_2$ increased ROS and caused Δψm depolarization indicating apoptosis was induced via the intrinsic (mitochondrial) pathway (Hajrezaie *et al*., 2014). Further investigation of the ability of copper-imidazo[1,2-*a*]pyridines to induce ROS production is required.

After an 18 hour treatment with 10 μM of copper-imidazo[1,2-*a*]pyridines, HT-29 and DLD-1 cells showed varying degrees of caspase-9 activation. All test compounds induced caspase-9 activation in HT-29 cells; JD46 caused the highest and JD47, the lowest (Chapter III. Section 3.6). JD46 was the only test compound to cause caspase-9 activation in DLD-1 cells with JD47, JD49 and JD88 displaying indistinct fluorescence. This is consistent with the lower potency of the copper-imidazo[1,2-*a*]pyridines in DLD-1 cells. Staurosporine activated caspase-9 in both cells. Data from this study showed that all the test compounds induced caspase-9 in HT-29 cells providing evidence for the activation of the intrinsic apoptotic pathway in this cell line. In the study by Konarikova *et al* (2016) mentioned in section 4.1, three copper (II) complexes activated caspase-9 in HT-29 cells. Those results, taken together with results from this study indicates that copper complexes have the ability to induce apoptosis via the intrinsic pathway. In DLD-1 cells, only JD46 stimulated caspase-9 activation, indicative of this compound causing apoptosis through the intrinsic pathway. These results correlate with the observations made with the JC-1 assay. Compounds that caused a loss of mitochondrial membrane potential induced caspase-9 activation in both HT-29 and DLD-1 cells confirming activation of the intrinsic apoptotic pathway.

4.5 The apoptotic protein profile of test compounds on HT-29 cells

The morphological changes, translocation of PS, activation of caspase-3/7, disruption of the mitochondrial membrane potential and the activation of caspase-9 in HT-29 cells provides evidence for cell death by apoptosis. In order to obtain greater insight into the apoptotic effects, an apoptotic protein array was employed to determine the effects of the copper-imidazo[1,2-*a*]pyridines on the expression of other apoptotic regulatory proteins. Since HT-29 cells were most sensitive and due to cost constraints, this was performed on HT-29 cells with the three most active copper-imidazo[1,2-*a*]pyridines: JD46, JD47 and JD88.

4.5.1 Copper-imidazo[1,2-*a*]pyridines decrease the expression of cIAP-1 and cIAP-2 and increases the expression of TRAIL R1/DR4 and TRAIL R2/DR5 in HT-29 cells

Apoptosis occurs via two pathways; the extrinsic (death receptor) or the intrinsic (mitochondrial) pathway. The extrinsic pathway is mediated by death receptors from the tumor necrosis factor receptor (TNFR) family, such as TNFR1, Fas and TRAIL (Portt *et al*., 2011). This activation leads to the formation of the DISC that activates caspase-8. The intrinsic pathway is facilitated by internal metabolic stress which releases pro-apoptotic proteins into the cytosol, forming the apoptosome, resulting in the activation of caspase-9 (Barreiro-Iglesias *et al*., 2017). The release of cytochrome c into the cytosol is mediated by pro-apoptotic proteins such as the Bcl-2 family members and HtrA2/Omi (Portt *et al*., 2011). The Bcl-2 family of proteins is divided into pro-apoptotic proteins (Bax, Bak) and anti-apoptotic proteins (Bcl-2, Bcl-X) based on their function and structure (Dai *et al*., 2016). Typically in cancer, pro-apoptotic proteins are suppressed and anti-apoptotic proteins are upregulated contributing to uncontrolled cell division (Rathore *et al*., 2017). Upregulation of inhibitor of apoptosis proteins (IAPs) such as cIAP-1, cIAP-2, Livin and XIAP inhibit TRAIL-induced apoptosis (Finlay *et al*., 2014). In this study, the copper-imidazo[1,2-*a*]pyridines caused a decrease in the IAPs and an increase in the death receptors TRAIL R1/DR4 and TRAIL R2/DR5 (Table 4.3).

4.5.1.1 Copper-imidazo[1,2-*a*]pyridines decreases the expression of inhibitors of apoptosis proteins in HT-29 cells

The inhibitors of apoptosis proteins; cIAP-1, cIAP-2, XIAP and livin, prevents the activation of caspase-3 (Rathore *et al*., 2017). The expression levels of cIAP-1, cIAP-2, Livin and XIAP were decreased by more than 20 % when HT-29 cells were treated with copper-imidazo[1,2-*a*]pyridines (Table 4.3). These results indicate that the decrease in IAPs may sway the cells from an anti-apoptotic to an apoptotic state. The XIAP protein is a potent inhibitor of caspase-3, 7 and 9 followed by the cIAPs, which are considerably weaker. Copper-imidazo[1,2-*a*]pyridines were able to induce caspase-3/7 and caspase-9 activity as mentioned earlier. These results collectively indicate that JD46, JD47 and JD88 copper-imidazo[1,2-*a*]pyridines have decreased the IAPs in HT-29 cells, thereby overcoming their anti-apoptotic effects.

Table 4.3 The percentage expression of inhibitors of apoptosis proteins and death receptor proteins in HT-29 cells.

	% Decrease relative to the control		
Protein	**JD46**	**JD47**	**JD88**
cIAP-1	46.64	63.49	49.63
cIAP-2	22.25	32.39	26.10
Livin	35.90	37.23	42.81
XIAP	53.81	43.70	52.69
	% Increase relative to the control		
TRAIL R1/DR4	33.71	33.12	42.60
TRAIL R2/DR5	*12.28**	37.48	70.08

* Proteins with expression levels below the 20 % cut-off.

4.5.1.2 Copper-imidazo[1,2-*a*]pyridines increases the expression of TRAIL R1/DR4 and TRAIL R2/DR5 in HT-29 cells

There was a meaningful increase in expression levels of TRAIL R1/DR4 and TRAIL R2/DR5 when cells were treated with the copper-imidazo[1,2-*a*]pyridines at a 5 µM concentration for 18 hours (Table 4.3). According to Huang *et al* (2016), HT-29 is a TRAIL-

resistant cell line and when treated with an IAP antagonist, HT-29 cells were more sensitive to TRAIL (Huang *et al*., 2016). The cIAPs inhibit death-receptor mediated apoptosis (Guicciardi *et al*., 2011). The copper-imidazo[1,2-*a*]pyridines may act as an IAP inhibitor and the decrease in cIAPs may have caused the HT-29 cells to shift towards an apoptotic ready state.

4.5.2 Copper-imidazo[1,2-*a*]pyridines decreases TNFR1 in HT-29 cells

TNFR1 induces the activation of various signalling pathways, including the activation of the transcription factor NFκB (nuclear factor kappa-in activated B cells) (Hayden and Ghosh, 2014). NFκB is a family of transcription factors involved in inflammation, cell survival and proliferation. TNFR1 recruits the TRADD adaptor protein which in turn, induces the activation of anti-apoptotic mediators such as NFκB. NFκB promotes the transcription of the anti-apoptotic IAP proteins which is able to prevent TNFR1- mediated apoptosis (Redza-Dutordoir and Averill-Bates, 2016). Results from Chapter III. Section 3.7 show that TNFR1 was decreased in HT-29 cells treated with the active copper-imidazo[1,2-*a*]pyridines (Table 4.4). The cIAP-1 and cIAP-2 proteins facilitate TNFR1-induced activation of NFκB (Varfolomeev *et al*., 2008). However, since these IAP proteins were decreased by JD46, JD47 and JD88 (Table 4.3), it follows that TNFR1-induced activation of NFκB may have been inhibited. The decreased NFκB decreases NFκB-driven cell proliferation. It is likely that the additional decrease in the TNFR expression further enhanced the pro-apoptotic status of the HT-29 cells. These results are consistent with the apoptotic effects observed using direct apoptotic activity assays.

Table 4.4 The percentage expression of TNFR1 in HT-29 cells.

	% Decrease relative to the control		
Protein	**JD46**	**JD47**	**JD88**
TNF R1/TNFRSF1A	40.95	28.95	36.47

4.5.3 Copper-imidazo[1,2-*a*]pyridines decreases Bcl-2 and Bcl-x expression in HT-29 cells

Bcl-2 and Bcl-x are anti-apoptotic proteins belonging to the Bcl-2 family that along with pro-apoptotic proteins belonging to the Bcl-2 family (Bad, Bid, Bax), mediate apoptosis via the intrinsic (mitochondrial) pathway (Wong, 2011). The decreased expression of the anti-apoptotic Bcl-2 and Bcl-x proteins by copper-imidazo[1,2-*a*]pyridines and the increase of the Bad pro-apoptotic protein expression by JD46 indicate that these compounds were able to sway the cells to a pro-apoptotic state and activate the intrinsic pathway. Data obtained from apoptotic marker assays showed that this is consistent with the disruption of the mitochondrial membrane potential and activation of caspase-9 in HT-29 cells. Results from Table 4.5 provides additional support of apoptosis mediated through the intrinsic pathway in HT-29 cells.

Table 4.5 The percentage expression of Bcl-2, Bcl-x and Bad in HT-29 cells.

	% Decrease relative to the control		
Protein	**JD46**	**JD47**	**JD88**
Bcl-2	*16.93**	*17.94**	24.04
Bcl-x	39.38	50.60	21.59
Bad	24.40 (Increased)	*Decreased by 10.46**	*Decreased by 3.71**

* Proteins with expression levels less than the 20 % cut-off were not deemed to be significant.

4.5.4 Copper-imidazo[1,2-*a*]pyridines decreases the expression of HtrA2/Omi in HT-29 cells

The serine protease HTRA2/Omi is released from the mitochondria to the cytosol under DNA stress where it stimulates cell death (Goo *et al*., 2013). HtrA2/Omi cleaves the IAPs and through the intrinsic pathway, facilitating caspase-dependent apoptosis (Merski *et al*., 2017; Hegde *et al*., 2001). In this study, copper-imidazo[1,2-*a*]pyridines decreases HtrA2/Omi levels (Table 4.6). While this is contradictory to expectations, it is possible that HtrA2/Omi is consumed while exerting its effect on the cIAPs or activation of the cIAPs may lead to its

own degradation via proteasomes. Further investigation into the role, enzymatic status and protein dynamics of HtrA2/Omi in the HT-29 cell line is required.

Table 4.6 The percentage expression of HtrA2/Omi in HT-29 cells.

	% Decrease relative to the control		
Protein	**JD46**	**JD47**	**JD88**
HtrA2/Omi	43.93	48.39	46.65

4.5.5 Copper-imidazo[1,2-*a*]pyridines increases HO-1/HMOX/HSP32 expression

HO-1/HMOX1/HSP32 is an endoplasmic reticulum (ER) heme group containing protein that has cytoprotective properties in response to oxidative and chemical stress (Bansal *et al*., 2014). For the purposes of clarity, HO-1/HMOX1/HSP32 will be referred to as HSP32. HSP32 exerts its effects by degrading heme to biliverdin and bilirubin (Bansal *et al*., 2014). The accumulation of reactive oxygen species (ROS) such as hydrogen peroxide, hydroxyl radicals and superoxide in a cell causes oxidative stress that facilitates apoptosis and triggers the HSP32 defence system to prevent cellular damage (Kalo *et al*., 2012; Tan *et al*., 2016).

In this study, HT-29 cells treated with JD46, JD47 and JD88 had the most noteworthy increase in the HSP32 protein expression (Chapter III. Table 3.5, Figure 3.23, Chapter IV. Table 4.7). ROS are produced in the mitochondria as a result of normal metabolism. They are able to target mitochondrial DNA (mtDNA) prone to oxidative damage. This in turn, disrupts the function of the respiratory chain, further increasing ROS production thereby activating the intrinsic (mitochondrial) pathway (Redza-Dutordoir and Averill-Bates, 2016). The reactive oxygen species hyperpolarizes the mitochondrial membrane, resulting in a loss of mitochondrial membrane potential, facilitating the release of mitochondrial cytochrome c. The loss of cytochrome c in the mitochondria in turn, increases ROS production (Redza-Dutordoir and Averill-Bates, 2016). In this study, cytochrome c expression decreased in HT-29 cells treated with copper-imidazo[1,2-*a*]pyridines (Chapter III. Table 3.5). The increase in the HSP32 protein may be due to its protective response against the oxidative stress induced by the copper-imidazo[1,2-*a*]pyridine test compounds. According to McGivern *et al* (2018), copper complexes have been shown to generate reactive oxygen species that are able to induce DNA damage and alter structural proteins. The change in the mitochondrial

membrane potential induces the release of apoptotic proteins from the mitochondria to the cytosol, as mentioned above in Section 4.4. The decrease in the mitochondrial membrane potential in HT-29 cells supports the theory that, ROS have been generated upon treatment with the copper-imidazo[1,2-*a*]pyridines, thereby increasing HSP32. In summary, there is strong evidence that the copper-imidazo[1,2-*a*]pyridines cause oxidative stress which increases HSP32.

Table 4.7 The percentage expression of HSP32 in HT-29 cells.

	% Increase relative to the control		
Protein	**JD46**	**JD47**	**JD88**
HO-1/HMOX1/HSP32	136.00	138.60	164.67

4.5.6 Copper-imidazo[1,2-*a*]pyridines decreases catalase expression

According to Jeong and Joo (2016), catalase converts the formation of the ROS, hydrogen peroxide to water and oxygen. If catalase is inhibited, there is an accumulation of hydrogen peroxide augmenting oxidative damage. The decrease in catalase caused by the copper-imidazo[1,2-*a*]pyridines (Table 4.8) may have resulted in an accumulation of reactive oxygen species. This is supported indirectly by the observation that HSP32 is increased in section 4.5.5.

Table 4.8 The percentage expression of catalase in HT-29 cells.

	% decrease relative to the control		
Protein	**JD46**	**JD47**	**JD88**
Catalase	42.23	23.85	34.14

4.5.7 Copper-imidazo[1,2-*a*]pyridines decreases expression levels of phosphorylated p53

Three different phosphorylated forms of p53 protein were markedly suppressed when treated with all three the copper-imidazo[1,2-*a*]pyridines (Table 4.9). In normal cells the tetrameric p53 complex binds to four MDM2 molecules which are in turn ubiquinated targeting it for proteosomal degradation. In normal cells p53 has very short half-life in the cell cytoplasm. In abnormal cells, the p53 protein is phosphorylated in order to protect itself from MDM2-

induced degradation (Weinburg, 2014). Phosphorylation of p53 alters the domain recognized by MDM2 thereby preventing the p53-MDM2 interaction. MDM2 is unable to initiate ubiquitinylation of p53, p53 thus manages to escape the rapid proteasomal degradation resulting in increased concentrations within the cell (Weinburg, 2014). High expression levels of the phosphorylated forms of the p53 protein in the HT-29 cells was therefore not unexpected since mutated p53 accumulates within the cytoplasm of HT-29 cells (Ahmed *et al*., 2013).

All three copper-imidazo[1,2-*a*]pyridine test compounds caused a notable decrease in the expression of all the phosphorylated forms of the p53 protein as shown in Chapter III. Section 3.7 and below in Table 4.9. The decrease in p53 at serine sites 15, 46 and 392 may be due to loss of p53 phosphorylation. In response to stress, p53 is phosphorylated at serine sites by various kinases. Serine 15 is phosphorylated by the ATM (ataxia-telangiectasia mutated) kinases. Serine 46 is phosphorylated by multiple kinases such as ATM, HIPK2 (homeodomain interacting protein kinase 2) and DYRK2 (dual-specificity tyrosine-phosphorylation-regulated kinase 2), amongst others (Smeenk *et al*., 2011). Serine 392 is phosphorylated by Cdk9 (cyclin dependent kinase 9) (Bagashev *et al*., 2013). If p53 is no longer phosphorylated, MDM2 can bind to p53 and target it for proteasomal degradation. A study by Schumacher *et al* (2001) found that MDM2 was expressed in untreated HT-29 cells in *scid* (severe combined immunodeficiency) mice *in vivo*. In addition, mutant p53, as found in HT-29 cells can be degraded via the p53-MDM2 pathway (Schumacher *et al*., 2001). The copper-imidazo[1,2-*a*]pyridines may inhibit kinases responsible for p53 phosphorylation, enabling MDM2 degradation, a hypothesis that will require further investigation. The imidazo group of the molecules is similar in structure to ATP and may selectively bind to the active site of the kinases.

In addition, as previously mentioned, high doses of reactive oxygen species induce apoptosis and low doses induce cell survival. Low doses of ROS activates p53. According to Redza-Dutordoir and Averill-Bates (2016), apoptosis induced by ROS increased the expression of p53 and p53 phosphorylation at serine sites 15 and 46 in colon cancer cells. In Section 4.5.5, it is postulated that the accumulation of ROS elicited the observed increased HSP32 expression. The potential formation of high levels of ROS may have decreased the p53 phosphorylation at ser15 and ser46. Further investigation of this proposed hypothesis is required.

Table 4.9 The percentage expression of phosphorylated p53 at serine sites 15, 46 and 392 in HT-29 cells.

	% Decrease relative to the control		
Protein	**JD46**	**JD47**	**JD88**
Phospho-p53 (S15)	67.37	73.31	72.18
Phospho-p53 (S46)	53.29	57.36	60.36
Phospho-p53 (S392)	34.67	43.10	33.40

4.5.8 JD88 increases pro-caspase-3 expression

Pro-caspase-3 activates the effector caspase-3, a central executioner caspase in the caspase cascade. JD88 was the only copper-imidazo[1,2-*a*]pyridine to increase the expression of pro-caspase-3 in HT-29 cells (Table 4.10). Despite changes to the protein levels obtained from proteome profiling, HT-29 cells showed an increase in caspase-3/7 enzymatic activity as measured by the caspase-3/7 assay when treated with all the copper-imidazo[1,2-*a*]pyridines. JD88 caused the highest fold-increase in caspase-3/7 activity (Chapter III. Figure 3.13 and Table 3.4). For JD46 and JD47, the effect of active caspase-3 is contradictory to caspase 3 activity assays. Since the caspase-3/7 assay cannot distinguish between the caspase-3 or caspase-7 activity it may mean that the small structural differences between the two compounds caused the activation of caspase-7 rather than caspase-3 The relationship between pro-caspase-3, activated capase-3 and caspase-7 in HT-29 is worthy of further investigation.

Table 4.10 The percentage expression of pro-caspase-3 and cytochrome c in HT-29 cells.

	% Increase relative to the control		
Protein	**JD46**	**JD47**	**JD88**
Pro-caspase-3	*Decreased by 10.32**	*Decreased by 20.00**	65.52

* Proteins with expression levels less than the 20 % cut-off.

4.5.9 Copper-imidazo[1,2-*a*]pyridines decreases expression levels of cytochrome c

Cytochrome c is an essential pro-apoptotic protein released from the mitochondria into the cytosol during the intrinsic apoptotic pathway. It forms the apoptosome with Apaf-1 where it

activates caspase-9. JD46, JD47 and JD88 decreased the levels of the cytochrome c protein in HT-29 cells (Table 4.11). However results obtained in Chapter III. Section 3.6, show that all copper-imidazo[1,2-*a*]pyridines activated caspase-9 in HT-29 cells. The degradation of cytochrome c may be enhanced when present in the cytoplasm. Alternatively, according to Redza-Dutordoir and Averill-Bates (2016), in response to endoplasmic reticulum stress, caspase-9 can be activated in a cytochrome-c independent manner through caspase-12. Further investigation of this pathway is required.

Table 4.11 The percentage expression of cytochrome c in HT-29 cells.

	% decrease relative to the control		
Cytochrome c	22.59	42.00	35.32

4.6 Future investigations

Collectively, the data collected in this study supports the hypothesis that the copper-imidazo[1,2-*a*]pyridines are able to cause apoptotic cell death via activation of the intrinsic pathway in HT-29 cells. It is well known that there is cross-over between the intrinsic and extrinsic pathways and that they are not necessarily mutually exclusive (Westphal *et al*., 2011). As mentioned in Chapter I. Section 3.1, caspase-8 engages the intrinsic pathway through the pro-apoptotic protein, Bid. Caspase-8 cleaves Bid to tBid which initiates the oligomerization of Bax/Bak causing the mitochondria to release cytochrome c (Westphal *et al*., 2011). The Bid protein is not included in the apoptotic protein profile and could be further investigated to understand whether convergence occurs in HT-29 cells treated with the copper-imidazo[1,2-*a*]pyridines test compounds. An evaluation of caspase-8 activity will provide additional information regarding the activation of the death receptor pathway. Based on previous work on the imidazo[1,2-*a*]pyridines (Dahan-Farkas *et al*., 2011), this study focused on the intrinsic pathway. Results obtained from the proteomics indicate that it would be beneficial to explore the effects of the copper-imidazo[1,2-*a*]pyridines on the extrinsic pathway. Furthermore, additional research is required since literature on the ability of copper complexes to induce apoptosis in HT-29 and DLD-1 colorectal cancer cells is limited.

The study identified three copper-imidazo[1,2-*a*]pyridine test compounds showing promising activity as lead compounds against colorectal cancer cells. The evaluation of these

compounds on an *in vivo* colorectal cancer model is the next logical step in the development of these compounds. Further investigations arising from this study is the *in vivo* evaluation of the efficacy of the active compounds on a nude mice model using HT-29 cells as a xenograft.

Chapter V. Conclusion

The purpose of this study was to identify new compounds that may be beneficial in the treatment of colorectal cancer. In this study, we evaluated three different classes of compounds, novel epidermal growth factor receptor kinase inhibitors, nucleoside analogues and copper-imidazo[1,2-*a*]pyridines. The copper-imidazo[1,2-*a*]pyridines showed a cytotoxic effect and prevented cell growth in HT-29 and DLD-1 colorectal adenocarcinoma cells with IC_{50} values in the low micromolar range. Copper-imidazo[1,2-*a*]pyridines were further investigated to determine their mode of cell death and were found to induce apoptotic cell death.

5.1 Copper-imidazo[1,2-*a*]pyridines are cytotoxic towards HT-29 and DLD-1 cell lines

Copper-imidazo[1,2-*a*]pyridines were most active against HT-29 cells. JD46 and JD88 had IC_{50} values below 1.0 μM, JD47 had an IC_{50} value below 2.0 μM and JD49, an IC_{50} value below 9.0 μM. In contrast, DLD-1 cells were also inhibited by the same set of compounds but with higher IC_{50} values. JD46 and JD88 had IC_{50} values of 9.25 μM and 9.50 μM respectively and JD47 and JD49 were less active with IC_{50} values of 11.57 μM and 11.28 μM, respectively. The copper-imidazo[1,2-*a*]pyridines displayed selective toxicity towards the HT-29 cells. This is most likely associated with specific molecular characteristics of the HT-29 cells. A dissection of the differences between the two cell lines and the selective toxicity of the copper-imidazo[1,2-*a*]pyridines may provide insight into the molecular features of CRC.

Substitutions on the imidazole ring of the compounds affects the cytotoxic potency of the copper-imidazo[1,2-*a*]pyridines. JD46 was the most active copper-imidazo[1,2-*a*]pyridine (IC_{50} value 0.85 μM) and it has no substitutions on the imidazole ring, whereas a chorine substitution on position 5 of the imidazole ring in JD49, increased the IC_{50} value to 8.33 μM. Following the same trend, the inclusion of a bromine molecule on position 4 and 5 of the imidazole ring (JD47 and JD88) caused a marginal change in the cytostatic activity (0.88 μM and 1.74 μM, respectively).

5.2 Copper-imidazo[1,2-*a*]pyridines cause cell death by apoptosis

Copper-imidazo[1,2-*a*]pyridines induced apoptosis in both CRC cell lines. At a concentration of 10 μM, no EtBr binding to nuclei was observed for any of the compounds in HT-29 and DLD-1 cells, indicating that necrosis was not a mode of cell death. Morphological studies indicated that all compounds were able to cause changes to HT-29 and DLD-1 cells that are consistent with apoptosis, such as membrane blebbing, nuclear fragmentation and chromatin condensation. The four most active compounds, JD46, JD47, JD49 and JD88 all caused nuclear fragmentation in HT-29 cells.

All copper-imidazo[1,2-*a*]pyridines induced the translocation of PS to the outer surface of the plasma membrane in both cell lines, as measured by annexin-V binding. JD47 caused the most annexin-V binding in HT-29 cells and JD49 caused the most annexin-V binding in DLD-1 cells. Differences between the ability of the compounds to induce PS exposure on the outer cell membrane to increase annexin-V binding can most likely be attributed to the variation in the time it takes to induce apoptosis.

All copper-imidazo[1,2-*a*]pyridines caused an increase in caspase-3/7 activity, providing further evidence of cell death by apoptosis. Induction of caspase-3/7 activity was the highest in HT-29 cells. For each compound, the fold increase in activity was higher in HT-29 cells compared to DLD-1 cells. Taken together, the translocation of PS and the increase of caspase-3/7 activity provides evidence for apoptotic cell death.

5.3 Copper-imidazo[1,2-*a*]pyridines activates the intrinsic apoptotic pathway

The loss of mitochondrial membrane potential and the activation of caspase-9 are both indicators for apoptosis via the intrinsic (mitochondrial) apoptotic pathway. All the copper-imidazo[1,2-*a*]pyridines disrupted the mitochondrial membrane potential in HT-29 and DLD-1 cells. Moreover, the effect was more pronounced in HT-29 cells where all the compounds, JD46, JD47 and JD88 caused a complete loss of mitochondrial membrane potential. In HT-29 cells, the activity of caspase-9, an executioner caspase was increased by all the copper-

imidazo[1,2-*a*]pyridines. This is in contrast to DLD-1 cells where only JD46 induced caspase-9 activity.

5.4 Apoptosis array proteome profiling in HT-29 cells

The apoptosis proteomic array provides additional evidence indicating that the copper-imidazo[1,2-*a*]pyridines may also act via the extrinsic (death receptor) pathway in HT-29 cells. The copper-imidazo[1,2-*a*]pyridines caused an increase in death receptor expression (TRAIL R1/DR4 and TRAIL R1/DR5) expression but conversely caused a decrease in TNFR1 expression. Furthermore, the copper-imidazo[1,2-*a*]pyridines caused a decrease in the inhibitors of apoptosis proteins (IAPs) (cIAP-1, cIAP-2, Livin and XIAP). This indicates that HT-29 cells treated with JD46, JD47 and JD88 were able to overcome the inhibitory effects of IAPs on apoptosis, thereby shifting the cells towards apoptosis.

Copper-imidazo[1,2-*a*]pyridines increased the expression of HO-1/HMOX-1/HSP32. It can be postulated that the increase in HSP32 is a result of copper-mediated ROS production which is known to stimulate apoptosis. The ability of copper-imidazo[1,2-*a*]pyridines to cause ROS formation requires further investigation.

The phosphorylation of p53 at various serine sites protects it against proteosomal degradation and modulates its functions. Copper-imidazo[1,2-*a*]pyridines decreased the ser15, ser46 and ser392 phosphorylated forms of the p53 protein in HT-29 cells. The test compounds may inhibit the kinases responsible for p53 phosphorylation, a hypothesis that will require further investigation.

5.5 In summary:

This study has identified the copper-imidazo[1,2-*a*]pyridines, JD46, JD47 and JD88 as new lead compounds in the search for novel colorectal cancer chemotherapeutic agents. The molecules now require further verification of their anti-cancer activity in an *in vivo* animal model. Further pre-clinical development should also include acute and chronic toxicity evaluation and the determination of pharmacokinetic properties.

References

Abraha, A. M., and Ketema, E.B. (2016). Apoptotic pathways as a therapeutic target for colorectal cancer treatment. *World Journal of Gastrointestinal Oncology, 8*(8), 583-591.

Ahmed, D., Eide, P.W., Eilertsen, I.A., Danielsen, S.A., Eknaes, M., Hektoen, M., Lind, G.E., Lothe, R.A., (2013). Epigenetic and genetic features of 24 colon cancer cell lines. *Oncogenesis, 2*(e71). Doi:10.1038/oncsis.2013.35

Alberts, B., Johnson, A., Lewis, J., Raff, M., Roberts, K., and Walter, P. (2002). Chapter 23: Cancer. In: *Molecular Biology of The Cell,* 4th Edition. New York: Garland Science. pp 1313-1362.

American Type Culture Collection (2016): https://atcc.org/Products/All/CCL221.aspx#generalinformation [Accessed: 21 February 2018]

Andrade, R., Cristol, L., Prado, R., Boyano, M.D., Arluzea, J., and Arechaga, J. (2010). Plasma membrane and nuclear envelope integrity during the blebbing stage of apoptosis: a time-lapse study. *Biology of the Cell, 102*, 25-35. Doi:10.1042/BC20090077

Avelar-Freitas, B.A., Almeida, V.G., Pinto, M.C., Mourao, F.A., Massensini, A.R., Martins-Filho, O.A., Rocha-Vieira, E., and Brito-Melo, G.E. (2014). Trypan blue exclusion assay by flow cytometry. *Brazilian Journal of Medical and Biological Research, 47*(4), 307-315.

Bagashev, A., Fan, S., Mukerjee, R., Claudio, P.P., Chabrashvili, T., Leng, R.P., Benchimol, S., and Sawaya, B.E. (2013). Cdk9 phosphorylates Pirh2 protein and prevents degradation of p53 protein. *Cell Cycle, 12*(10), 1569-1577.

Bansal, S., Biswas, G., and Avadhani, N.G. (2014). Mitochondria-targeted heme oxygenase-1 induces oxidative stress and mitochondrial dysfunction in macrophages, kidney fibroblasts and in chronic alcohol hepatotoxicity. *Redox Biology ,2*, 273-283. Doi:https://doi.org/10.1016/j.redox.2013.07.004

Barreiro-Iglesias, A., Sobrido-Camean, D., and Shifman, M.I. (2017). Retrograde activation of the extrinsic apoptotic pathway in spinal-projecting neurons after a complete spinal cord injury in Lampreys. *BioMed Research International*. Doi:https://doi.org/10.1155/2017/5953674

Bhattacharya, P., and McHugh, T.W. (2017). Lynch Syndrome. In: *StatPearls [internet]*. Treasure Island, (Florida): StatPearls Publishing. https://www.ncbi.nlm.nih.gov/books/NBK431096/ [Accessed 11 October 2017].

Bradford, M.M. (1976). A rapid and sensitive method for the quantitation of microgram quantities of protein utilizing the principle of protein-dye binding. *Analytical Biochemistry, 72*(1-2), 248-254.

Brenner, H., Kloor, M., and Pox, C.P. (2014). Colorectal Cancer. *The Lancet, 383*(9927), 1490-1502.

Brentnall, M., Rodriguez-Menocal, L., De Guevara, R., Cepero, E., and Boise, L. (2013). Caspase-9, caspase-3 and caspase-7 have distinct roles during intrinsic apoptosis. *BMC Cell Biology , 14*(32). https://doi.org/10.1186/1471-2121-14-32

Brunner, D., Frank, J., Appl, H., Schoffl, H., Pfaller, W., and Gstraunthaler, G. (2010). Serum-free Cell Culture: The Serum-free Media Interactive Online Database. *Alternatives to Animal Experimentation, 27*(1), 53-62.

Bullard Dunn, K.M, and Rothenberger, D.A. (2015). Chapter 29: Colon, Rectum, and Anus. In: Brunicardi, F., Andersen, D.K., Billiar, T.R., Dunn, D.L., Hunter, J.G., Matthews, J.B., and Pollock, R.E. (Eds.), *Schwartz's Principles of Surgery,* 10th Edition. New York: McGraw-Hill. https://0-accessmedicine-mhmedical-com.innopac.wits.ac.za/content.aspx?bookid=980&sectionid=59610871 [Accessed 3 October 2017].

Carroll, M.R.R, Seaman, H.E., and Halloran, S.P. (2014). Tests and investigations for colorectal cancer screening. *Clinical Biochemistry, 47*(10-11), 921-939.

Chabner, B., Bertino, J., Clearly, J., Ortiz, T., Lane, A., Supko, J., and Ryan, D. (2011). Chapter 61: Cytotoxic Agents. In: Brunton, L.L., Chabner, B.A., and Knollmann, B.C. (Eds.), *Goodman & Gilman's The Pharmacological Basis of Therapeutics,* 12th Edition. New York: McGraw-Hill. pp 1695-1698.

Chan, A.T., and Giovannucci, E.L. (2010). Primary prevention of colorectal cancer. *Gastroenterology, 138*(6), 2029-2043.

Charras, G.T. (2008). A short history of blebbing. *Journal of Microscopy, 231*(3), 466-478.

Chatterjee, S., and Burns, T.F. (2017). Targeting Heat Shock Proteins in Cancer: A Promising Therapeutic Approach. *International Journal of Molecular Sciences, 18*(9), 1978. Doi: 10.3390/ijms18091978

Chen, J. (2016). The Cell-Cycle Arrest and Apoptotic Functions of p53 in Tumor Initiation and Progression. *Cold Spring Harbor Perspectives in Medicine, 6*(3). Doi: 10.1101/cshperspect.a026104

Chene, P. (2004). Inhibition of the p53-MDM2 Interaction: targeting a protein-protein interface. *Molecular Cancer Research, 2*(1), 20-28.

Choi, Y., Sateia, H.F., Peairs, K.S, and Stewart, R.W. (2017). Screening for colorectal cancer. *Seminars in Oncology, 44*(1), 34-44.

Chu, E. (2017). Chapter 54: Cancer Chemotherapy. In: Katzung, B.G. (Eds.), *Basic and Clinical Pharmacology,* 14th Edition. New York: McGraw-Hill. https://0-accesspharmacy-mhmedical-com.innopac.wits.ac.za/Book.aspx?bookid=2249#175215372 [Accessed 16 November 2017].

Chu, C., Xu, J., Cheng, D., Li, X., Tong, S., Yan, J., and Li, Q. (2014). Anti-Proliferative and Apoptosis-Inducing Effects of Camptothecin-20(s)-O-(2-pyrazolyl-1)acetic Ester in Human Breast Tumor MCF-7 Cells. *Molecules, 19*, 4941-4955. Doi:10.3390/molecules19044941

Clark, J.W., and Longo, D.L. (2014). Chapter 102e: Cancer Cell Biology. In: Kasper, D., Fauci, A., Hauser, S., Longo, D., Jameson, J.L., and Loscalzo, J. (Eds.), *Harrison's*

Principles of Internal Medicine, 19th Edition. New York : McGraw-Hill. https://0-accessmedicine-mhmedical-com.innopac.wits.ac.za/content.aspx?bookid=1130&sectionid=71748230 [Accessed 2 July 2017].

Cohan, J., and Varma, M.G. (2014). Chapter 30: Large Intestine. In: Doherty, G.M. (Eds.), *CURRENT Diagnosis & Treatment: Surgery,* 14th Edition. New York: McGraw-Hill. https://0-accessmedicine-mhmedical-com.innopac.wits.ac.za/content.aspx?bookid=1202&sectionid=71522614 [Accessed 4 August 2017].

Cohen, S.A., Wu, C., Yu, M., Gourgioti, G., Wirtz, R., Raptou, G., Gkakou, C., Kotoula, V., Pentheroudakis, G., Papaxionis, G., Karavasilis, V., Pectasides, D., Kalogeras, K.T., Fountzilas, G., and Grady, W.M. (2016). Evaluation of CpG Island Methylator Phenotype as a Biomarker in Colorectal Cancer Treated With Adjuvant Oxaliplatin. *Clinical Colorectal Cancer, 15*(2), 164-169.

Colussi, D., Brandi, G., Bazzoli, F., and Ricciardiello, L. (2013). Molecular Pathways Involved in Colorectal Cancer: Implications for Disease Behavior and Prevention. *International Journal of Molecular Sciences, 14*(8), 16365-16385.

Comella, P., Casaretti, R., Sandomenico, C., Avallone, A., and Franco, L. (2009). Role of oxaliplatin in the treatment of colorectal cancer. *Therapeutics and Clinical Risk Management, 5*, 229-238. Doi: https://doi.org/10.2147/TCRM.S3583

Cornett, P.A., and O. Dea, T.O. (2018). Chapter 39: Cancer. In: Papadakis, M.A., McPhee, S.J., and Rabow, M.W. (Eds.), *CURRENT Medical Diagnosis and Treatment.* New York: McGraw-Hill. https://0-accessmedicine-mhmedical-com.innopac.wits.ac.za/content.aspx?bookid=2192&sectionid=168004201 [Accessed 2 January 2018].

Dahan-Farkas, N., Langley, C., Rousseau, A., Yadav, D., Davids, H., and de Koning, C. (2011). 6-Substituted imidazo[1,2-a]pyridines: Synthesis and biological activity against colon cancer cell lines HT-29 and Caco-2. *European Journal of Medicinal Chemistry , 46*(9), 4573-

4583.

Dai, H., Meng, X.W., and Kaufmann, S.H. (2016). BCL2 Family, Mitochondrial Apoptosis, and Beyond. *Cancer Translational Medicine, 2*(1), 7-20.

Dam, J., Ismail, Z., Kurebwa, T., Gangat, N., Harmse, L., Marques, H., Lemmerer, A., Bode, M.L. and de Koning, C. (2017). Synthesis of copper and zinc 2-(pyridin-2-yl)imidazo[1,2-a]pyridine complexes and their potential anticancer activity. *European Journal of Medicinal Chemistry, 126*, 353-368. Doi: http://dx.doi.org/10.1016/j.ejmech.2016.10.041

De Marchis, M.L., Tonelli, F., Quaresmini, D., Lovero, D., Della-Morte, D., Silvestris, F., Guadagni, F., and Palmirotta, R. (2017). Desmoid Tumors in Familial Adenomatous Polyposis. *Anticancer Research: International Journal of Cancer Research and Treatment, 37*(7), 3357-3366.

Denoyer, D., Masaldan, S., La Fontaine, S., and Cater, M.A. (2008). Targeting copper in cancer therapy: 'Copper That Cancer'. *Metallomics, 7*(11), 1450-1476.

Ding, Y., Wang, B., Chen, X., Zhou, Y., and Ge, J. (2017). Staurosporine suppresses survival of HepG2 cancer cells through Omi/HtrA2-mediated inhibition of PI3K/Akt signaling pathwa. *Tumor Biology.* Doi: 10.1177/1010428317694317

Duff, J., and Markham, M.J. (2012). Chapter 175: Overview of Cancer and Treatment. In: McKean, S.C., Ross, J., Dressler, D., and Scheurer, D. (Eds.), *Principles and Practice of Hospital Medicine,* 2nd Edition. New York: McGraw-Hill.https://0-accessmedicine-mhmedical-com.innopac.wits.ac.za/content.aspx?bookid=1872&sectionid=146984063 [Accessed 9 January 2017].

Eleftheriadis, T., Pissas, G., Liakopoulos, V., and Stefanidis, I. (2016). Cytochrome c as a Potentially Clinical Useful Marker of Mitochondrial and Cellular Damage. *Frontiers in Immunology, 7*(279). Doi: 10.3389/fimmu.2016.00279

Ewald, B., Sampath, D., and Plunkett, W. (2008). Nucleoside analogs: molecular mechanisms signaling cell death. *Oncogene, 27*, 6522–6537. Doi:10.1038/onc.2008.316

Elmore, S. (2007). Apoptosis: A Review of Programmed Cell Death. *Toxicologic Pathology, 35*(4), 495-516.
Fearon, E.R., and Vogelstein, B. (1990). A genetic model for colorectal tumorigenesis. *Cell, 65*(5), 759-767.

Ferlay, J., Soerjomataram, I., Dikshit, R., Eser, S., Mathers, C., Rebelo, M., Parkin, D.M., Forman, D., and Bray, F. (2015). Cancer incidence and mortality worldwide: sources, methods and major patterns in GLOBOCAN 2012. *International Journal of Cancer, 136*(5), E359-E386.

Fink, S.L., and Cookson, B.T. (2005). Apoptosis, Pyroptosis, and Necrosis: Mechanistic Description of Dead and Dying Eukaryotic Cells. *Infection and Immunity, 73*(4), 1907-1916.

Finlay, D., Vamos, M., Gonzalez-Lopez, M., Ardecky, R.J., Ganji, S., Yuan, H., Su, Y., Cooley, T., Hauser, C.T., Welsh, K., Reed, J.C., Cosford, N.D.P., and Vuori, C. (2014). Small-molecule IAP antagonists sensitize cancer cells to TRAIL-induced apoptosis: Roles of XIAP and cIAPs. *Molecular Cancer Therapeutics, 13*(1), 5-15.

Fischer, R., Kontermann, R.E., and Maier, O. (2015). Targeting sTNF/TNFR1 Signaling as a New Therapeutic Strategy. *Antibodies, 4*, 48-70. Doi:10.3390/antib4010048

Flanagan, L., Meyer, M., Fay, J., Curry, S., Bacon, O., Duessmann, H., John, K.C., Boland, K., McNamara, D.A., Kay, E.W., Bantel, H., Schulze-Bergkamen, H., and Prehn, J.H.M. (2016). Low levels of Caspase-3 predict favourable response to 5FU-based chemotherapy in advanced colorectal cancer: Caspase-3 inhibition as a therapeutic approach. *Cell Death & Disease, 7*(2087). Doi:10.1038/cddis.2016.7

Fleming, M., Ravula, S., Tatishchev, S.F., and Wang, H.L. (2012). Colorectal carcinoma: Pathologic aspects. *Journal of Gastrointestinal Oncology, 3*(3), 153-173.

Gandin, V., Pellei, M., Tisato, F., Porchia, M., Santini, C., and Marzano, C. (2012). A novel copper complex induces paraptosis in colon cancer cells via the activation of ER stress signalling. *Journal of Cellular and Molecular Medicine, 16*(1), 142-151.

Ghanipour, L., Jirstrom, K., Sundstrom, M., Glimelius, B., and Birgisson, H. (2017). Associations of defect mismatch repair genes with prognosis and heredity in sporadic colorectal cancer. *European Journal of Surgical Oncology, 43*(2), 311-321.

Gillet, J.-P., Varma, S., and Gottesman, M.M. (2013). The Clinical Relevance of Cancer Cell Lines. *Journal of the National Cancer Institute, 105*(7), 452-458.

Gogvadze, V., Orrenius, S., and Zhivotovsky, B. (2006). Multiple pathways of cytochrome c release from mitochondria in apoptosis. *Biochima et Biophysica Acta - Bioenergetics, 1757*(5-6), 639-647.

Goldberg, R.M., Sargent, D.J., Morton, R.F., Fuchs, C.H., Ramanathan, R.K., Williamson, S.K., Findlay, B.P., Pitot, H.C.; Alberts, S.R. (2004). A Randomized Controlled Trial of Fluorouracil Plus Leucovorin, Irinotecan, and Oxaliplatin Combinations in Patients With Previously Untreated Metastatic Colorectal Cancer. *Journal of Clinical Oncology, 22*(1), 23-30.

Goo, H.G., Jung, M.K., Han, S.S., Rhim, H., and Kang, S. (2013). HtrA2/Omi deficiency causes damage and mutation of mitochondrial DNA. *Biochima et Biophysica Acta - Molecular Cell Research, 1833*(8), 1866-1875.

Gottlieb, E., Armour, S.M., Harris, M.H., and Thompson, C.B. (2003). Mitochondrial membrane potential regulates matrix configuration and cytochrome c release during apoptosis. *Cell Death & Differentiation, 10*, 709-717.Doi:10.1038/sj.cdd.4401231

Guicciardi, M.E., Mott, J.L., Bronk, S.F., Kurita, S., Fingas, C.D., and Gores, G.J. (2011). Cellular Inhibitor of Apoptosis 1 (cIAP-1) Degradation by Caspase 8 During TNF-related Apoptosis-inducing Ligand (TRAIL)-induced Apoptosis. *Experimental cell research, 317*(1), 107-116.

Greijer, A.E., and van der Wall, E. (2004). The role of hypoxia inducible factor 1 (HIF-1) in hypoxia induced apoptosis. *Journal of Clinical Pathology, 57*(10), 1009-1014.

Gunaldi, M., Kocoglu, H., Okuturlar, Y., Gedikbasi, A., Alis, H., and Hursitoglu, M. (2015). Heat shock protein 70 is a useful marker for predicting colorectal cancer. *Journal of B.U.ON - Official Journal of the Balkan Union of Oncology, 20*(6), 1464-1470.

Gustavsson, B., Carlsson, G., Machover, D., Petrelli, N., Roth, A., Schmoll, H.J., Kveit, K.M., and Gibson, F. (2015). A Review of the Evolution of Systemic Chemotherapy in the Management of Colorectal Cancer. *Clinical Colorectal Cancer and Other Gastrointestinal Malignancies, 14*(1), 1-10.

Hajrezaie, M., Paydar, M., Moghadamtousi, S.Z., Hassandarvish, P., Gwaram, N.S., Zahedifard, M., Rouhollahi, E., Karimian, H., Looi, C.Y., Ali, H.M.,Majid, N. A., and Abdulla, M.A. (2014). A Schiff Base-Derived Copper (II) Complex Is a Potent Inducer of Apoptosis in Colon Cancer Cells by Activating the Intrinsic Pathway. *The Scientific World Journal*. Doi: http://dx.doi.org/10.1155/2014/540463

Hang, J., Cai, B., Xue, P., Wang, L., Hu, H., Zhou, Y., Ren, S., Wu, J., Zhu, M., Chen, D., Yang, H., and Wang, L. (2015). The Joint Effects of Lifestyle Factors and Comorbidities on the Risk of Colorectal Cancer: A Large Chinese Retrospective Case-Control Study. *PLoS One, 10*(12). Doi: https://doi.org/10.1371/journal.pone.0143696

Hassan, M., Watari, H., AbuAlmaaty, A., Ohba, Y., and Sakuragi, S. (2014). Apoptosis and Molecular Targeting Therapy in Cancer. *BioMed Research Internationl, 2014*. Doi:http://dx.doi.org/10.1155/2014/150845

Hatcher, O., and Kumar, A.A. (2014). Chemotherapy and radiotherapy for colorectal cancers. *Surgery (Oxford), 32*(4), 179-184.

Hayden, M., and Ghosh, S. (2014). Regulation of NF-κB by TNF family cytokines. *Seminars in Immunology, 26*(3), 253-266.

Hegde, R., Srinivasula, S.M., Zhang, Z.J., Wassell, R., Mukattash, R., Cilenti, L., DuBois, G., Lazebnik, Y., Zervos, A.S., Fernandes-Alnemri, T., and Alnemri, E.S. (2001). Identification of Omi/HtrA2 as a Mitochondrial Apoptotic Serine Protease That Disrupts Inhibitor of Apoptosis Protein-Caspase Interaction. *Journal of BiologicalapoptChemistry, 277*, 432-438. Doi: 10.1074/jbc.M109721200

Hensley, P., Mishra, M., and Kyprianou, M. (2013). Targeting caspases in cancer therapeutics. *Biological Chemistry, 394*(7), 831-843.

Houston, A., Waldron-Lynch, F.D., Bennett, M.W., Roche, D., O'Sullivan, G.C., Shanahan, F., and O'Connell, J. (2003). Fas Ligand Expressed in Colon Cancer is not Associated with Increased Apoptosis of Tumor Cells *in vivo*. *International Journal of Cancer, 107*(2), 209-214.

Huang, Y., Yang, X., Xu, T., Kong, Q., Zhang, Y., Shen, Y., Wei, Y., Wang, G., and Chen, K-J. (2016). Overcoming resistance to TRAIL-induced apoptosis in solid tumor cells by simultaneously targeting death receptors, c-FLIP and IAPs. *International Journal of Oncology, 49*(1), 153-163.

Jacob, M., Varghese, J., Murray, R.K., and Weil, P.A. (2015). Chapter 56: Cancer: An Overview. In: Rodwell, V., Bender, D., Botham, K., Kennelly, P., and Weil, A. (Eds.), *Harper's Illustrated Biochemistry.* 30th Edition. New York: McGraw-Hill. https://0-accessmedicine-mhmedical-com.innopac.wits.ac.za/content.aspx?bookid=1366&sectionid=73247495 [Accessed 28 July 2017].

Jang, H.J., Kim, B.J., Kim, J.H., and Kim, H.S. (2017). The addition of bevacizumab in the first-line treatment for metastatic colorectal cancer: an updated meta-analysis of randomized trials. *Oncotarget, 8*(42), 73009-73016.

Jasperson, K.W., Tuohy, T.M., Neklason, D.W., and Burt, R.W. (2010). Hereditary and Familial Colon Cancer. *Gastroenterology, 138*(6), 2044-2058.

Jeong, C.H., and Joo, S.H. (2016). Downregulation of Reactive Oxygen Species in Apoptosis. *Journal of Cancer Prevention, 21*(1), 13-20.

Jung, J. (2014). Human Tumor Xenograft Models for Preclinical Assessmentof Anticancer Drug Development. *Toxicological Research, 20*(1), 1-5.

Kalo, E., Kogan-Sakin, I., Solomon, H., Bar-Nathan, E., Shay, M., Shetzer, Y., Dekel, E., Goldfinger, N., Buganim, Y., Stambolsky, P., Goldstein, I., Madar, S., and Rotter, V. (2012). Mutant p53R273H attenuates the expression of phase 2 detoxifying enzymes and promotes the survival of cells with high levels of reactive oxygen species. *Journal of Cell Science, 125*, 5578-5586. Doi: 10.1242/jcs.106815

Kantari, C., and Walczak, H. (2011). Caspase-8 and Bid: Caught in the act between death receptors and mitochondria. *Biochimica et Biophysica Acta - Molecular Cell Research, 1813*(4), 558-563.

Karna, P., Zughaier, S., Pannu, V., Simmons, R., Narayan, S., and Aneja, R. (2014). Induction of Reactive Oxygen Species-mediated Autophagy by a Novel Microtubule-modulating Agent. *Journal of Biological Chemistry, 285*, 18737-18748. Doi: 10.1074/jbc.M109.091694

Katsidzira, L., Chokunonga, E., Gangaidzo, I.T., Rusakaniko, S., Borok, M., Matsena-Zingoni, Z., Thomson, S., Ramesar, R., and Matenga, J.A. (2016). The incidence and histo-pathological characteristics of colorectal cancer in a population based cancer registry in Zimbabwe. *Cancer Epidemiology: The International Journal of Cancer Epidemiology, Detection and Prevention*, *44,* 96-100. Doi: 10.1016/j.canep.2016.08.001

Kim, Y., R.F., S., Qian, T., Lemasters, J., and Brenner, D. (2002). TRAIL-Mediated Apoptosis Requires NF-kB Inhibition and the Mitochondrial Permeability Transition in Human Hepatoma Cells. *Hepatology, 36*(6), 1498-1508.

Knickelbein, K., and Zhang, L. (2015). Mutant KRAS as a critical determinant of the therapeutic response of colorectal cancer. *Genes and Diseases, 2*(1), 4-12.

Koltai, T. (2014). Clusterin: a key player in cancer chemoresistance and its inhibition . *OncoTargets and Therapy, 7*, 447-456. Doi: https://doi.org/10.2147/OTT.S58622

Konarikova, K., Perdikaris, G.A., Gbelcova, H., Andrezalova, L., Sveda, M., Ruml, T., Laubertova, L., and Zitnanova, I. (2016). Effect of Schiff base Cu(II) complexes on signaling pathways in HT-29 cells. *Molecular Medicines Report, 14*(5), 4436-4444.

Krieg, A., Werner, T.A., Verde, P.E., Stoecklein, N.H., and Knoefel, W.T. (2013). Prognostic and Clinicopathological Significance of Survivin in Colorectal Cancer: A Meta-Analysis. *Public Library of Science One, 8*(6), e65338. Doi:https://doi.org/10.1371/journal.pone.0065338

Kroemer, G., Galluzzi, L., Vandenabeele, P., Abrams, J., Alnemri, E., Baehrecke, E., Blagosklonny, M.V., El-Deiry, W.S., Golstein, P.; Green, D.R., Hengartner, M., Knight, R.A., Kumar, S., Lipton, S.A., Malorni, W., Nunez, G., Peter, M.E., Tschopp, J., Yuan, J., Piacentini, M., Zhivotovsky, B., and Melino, G. (2009). Classification of cell death: recommendations of the Nomenclature Committee on Cell Death 2009. *Cell Death and Differentiation, 16*(1), 3-11.

Larsen, B.D., Rampalli, S., Burns, L.E., Brunette, S., Dilworth, F.J., and Megeney, L.A. (2010). Caspase 3/caspase-activated DNase promote cell differentiation by inducing DNA strand breaks. *Proceedings of the National Academy of Sciences of the United States of America , 107*(9), 4230-4235.

Lee, K., Lee, S., Lee, H., Back, S., Cho, S., and Lee, J. (2011). Inhibitors of Apoptosis Proteins Expression and Their Prognostic Significance in Colorectal Carcinoma. *The Korean Journal of Pathology, 45*(4), 397-405.

Li, J., and Yuan, J. (2008). Caspases in apoptosis and beyond. *Oncogene, 27*, 6194-6206. Doi: 10.1038/onc.2008.297

Liu, J., Zhang, C., Hu, W., and Feng, Z. (2015a). Tumor suppressor p53 and its mutants in cancer metabolism. *Cancer Letters, 356*(2), 197-203.

Liu, K., Liu, P.C., Liu, R., and Wu, X. (2015b). Dual AO/EB Staining to Detect Apoptosis in Osteosarcoma Cells Compared with Flow Cytometry. *Medical Science Monitor Basic Research, 21*, 15-20. Doi: 10.12659/MSMBR.893327

Martinez-Macqueda, D., Miralles, B., and Recio, I. (2015). Chapter 11: HT29 Cell Line. In: Verhoeckx, K.; Cotter, P.; Lopez-Exposito, I.; Klieveland, C.; Lea, T.; Mackie, A.; Requena, T.; Swiatecka, D.; and Wichers, H. (Eds.), *The Impact of Food Bioactives on Health.*

Springer, Cham. pp 113-124. Doi: https://doi.org/10.1007/978-3-319-16104-4_11

Marques, R.P., Duarte, G.S., Sterrantino, C., Pais, H.L., Quintela, A., Martins, A.P., and Costa, J. (2017). Triplet (FOLFOXIRI) versus doublet (FOLFOX or FOLFIRI) backbone chemotherapy as first-line treatment of metastatic colorectal cancer: A systematic review and meta-analysis. *Critical Reviews in Oncology/Hematology, 118*, 54-62. Doi:10.1016/j.critrevonc.2017.08.006

Masoud, G.N., and Li, W. (2015). HIF-1α pathway: role, regulation and intervention for cancer therapy. *Acta Pharmaceutica Sinica B, 5*(5), 378-389.

Mathur, A., Hong, Y., Kemp, B.K, Barrientos, A.A., and Erusalimsky, J.D. (2000). Evaluation of fluorescent dyes for the detection of mitochondrial membrane potential changes in cultured cardiomyocytes. *Cardiovascular Research, 46*(1), 126-138.

McGivern, T., Afsharpour, S., and Marmion, C. (2018). Copper complexes as artificial DNA metallonucleases: From Sigman's reagent to next generation anti-cancer agent? *Inorganica Chimica Acta, 472*, 12-39. Doi: https://doi.org/10.1016/j.ica.2017.08.043

Meric-Bernstam, F., and Pollock, R. (2015). Chapter 10: Oncology. In: Brunicardi, F., Andersen, D., Billiar, T., Dunn, D., Hunter, J., Matthews, J., and Pollock, R. (Eds.), *Schwartz's Principles of Surgery.* 10th Edition. New York: McGraw-Hill. http://0-accessmedicine.mhmedical.com.innopac.wits.ac.za/content.aspx?bookid=980&sectionid=59610851. {Accessed 18 July 2017].

Merski, M., Moreira, C., Abreu, R.M.V., Ramos, M.J., Fernandes, P.A., Martins, L.M., Pereira, P.J.B., and Macedo-Ribeiro, S. (2017). Molecular motion regulates the activity of the Mitochondrial Serine Protease HtrA2. *Cell Death & Disease, 8*(e3119). Doi:10.1038/cddis.2017.487

Mohamed, M., and Schofield, J.B. (2014). The pathology of colorectal polyps and cancers (including biopsy). *Surgery (Oxford), 32*(4), 165-171.

Mojarad, E.N., Kuppen, P.J.K., Aghdaei, H.J., and Zali, M.R. (2013). The CpG island

methylator phenotype (CIMP) in colorectal cancer. *Gastroenterology and Hepatology from Bed to Bench, 6*(3), 120-128.

Monga, J., Pandit, S., Chauhan, C.S., and Sharma, M. (2013). Cytotoxicity and apoptosis induction in human breast adenocarcinoma MCF-7 cells by (+)-cyanidan-3-ol. *Experimental and Toxicologic Pathology, 65*(7-8), 1091-1100.

Mpoke, S., and Wolfe, J. (1997). Differential Staining of Apoptotic Nuclei in Living Cells: Application to Macronuclear Elimination in Tetrahymena. *The Journal of Histochemistry & Cytochemistry, 45*(5), 675-683.

Morhason-Bello, I.O., Odedina, F., Rebbeck, T.R., Harford, J, Dangou, J-M., Denny, L., and Adewole, I.F. (2013). Challenges and opportunities in cancer control in Africa: a perspective from the African Organisation for Research and Training in Cancer. *The Lancet: Oncology, 14*(4), e142-e151.

Mosmann, T. (1983). Rapid Colorimetric Assay for Cellular Growth and Survival: Application to Proliferation and Cytotoxicity Assays. *Journal of Immunological Methods, 65*(1-2), 55-63.

Nahacka, Z., Svadlenka, J., Peterka, M., Ksandrova, M., Benesova, S., Neuzil, J., and Andera, L. (2018). TRAIL induces apoptosis but not necroptosis in colorectal and pancreatic cancer cells preferentially via the TRAIL-R2/DR5 receptor. *BBA- Molecular Cell Research, 1865*(3), 522-531.

National Cancer Registry. (2013). National Institute for Communicable Diseases: http://www.nioh.ac.za/assets/files/2013NCR.pdf [Accessed 4 August 2017].

National Cancer Registry. (2014). National Institute for Communicable Diseases: http://www.nicd.ac.za/wp-content/uploads/2017/03/2014-NCR-tables.pdf [Accessed 8 June 2018].

Novellasdemunt, L., Antas, P., and Li, V. S. W. (2015). Targeting Wnt signaling in colorectal

cancer. A Review in the Theme: Cell Signaling: Proteins, Pathways and Mechanisms. *American Journal of Physiology Cell - Cell Physiology, 309*(8), C511-C521.

Olsen, M., and Zhivotovsky, B. (2011). Caspases and cancer. *Cell Death and Differentiation, 18*(9), 1441-1449.

Ouyang, L., Shi, Z., Zhao, S., Wang, F.T., Zhou, T.T., Liu, B., and Bao, J.K. (2012). Programmed cell death pathways in cancer: a review of apoptosis, autophagy and programmed necrosis. *Cell Proliferation in Basic and Clinical Sciences, 45*(6), 487-498.

Papadakis, M.A., and McPhee, S.J. (2017). Colorectal Cancer. In Papadakis, M.A., and McPhee, S.J. (Eds.), *Quick Medical Diagnosis & Treatment* . New York: McGraw-Hill. http://0-accessmedicine.mhmedical.com.innopac.wits.ac.za/content.aspx?bookid=2033&sectionid=152404385 [Accessed 7 January 2018].

Peter, M. H. (2015). The role of CD95 and CD95 ligand in cancer. *Cell Death & Differentiation, 22*, 549-559. Doi: 10.1038/cdd.2015.3

Pino, M.S., and Chung, D.C. (2010). The Chromosomal Instability Pathway in Colon Cancer. *Gastroenterology, 138*(6), 2059-2072.

Pistritto, G., Trisciuoglio, D., Ceci, C., Garufi, A., and D'Orazi, G. (2016). Apoptosis as anticancer mechanism: function and dysgunction if its modulators and targeted therapeutic strategies. *Aging, 8*(4), 603-619.

Portt, L., Norman, G., Clapp, C., Greenwood, M., and Greenwood, M.T. (2011). Anti apoptosis and cell survival: A review. *Biochimica et Biophysica Acta - Molecular Cell Research, 1813*(1), 238-259.

Price, P., and McMillan, T. (1990). Use of Tetrazolium Assay in Measuring the Response of Human Tumor Cells to Ionizing Radiation. *The Journal of Cancer Research*, *50*(5), 1392-1396.

Rabeneck, L., Horton, S., Zauber, A.G., and Earle, C. (2015). Colorectal Cancer. In: Gelband, H., Jha, P., and Sankaranarayanan, R. (Eds.), *Cancer: Disease Control Priorities*, 3rd Edition. Washington (DC): The International Bank for Reconstruction and Development / The World Bank. Doi: 10.1596/978-1-4648-0349-9_ch6

Rahman, H., Qasim, M., Schultze, F., Oellerich, M., and Asif, A. (2011). Fetal calf serum heat inactivation and lipopolysaccharide contamination influence the human T lymphoblast proteome and phosphoproteome. *Proteome Science, 9*(71). Doi: 10.1186/1477-5956-9-71

Ramos, T.V., Mathew, A.J., Thompson, M.L, and Ehrhardt, R.O. (2014). Standardized Cryopreservation of Human Primary Cells. *Current Protocols in Cell Biology*, *64*(1), A.3I.1-A.3I.8

Rathore, R., McCallum, J., Varghese, E., Florea, A., and Busselberg, D. (2017). Overcoming chemotherapy drug resistance by targeting inhibitors of apoptosis proteins (IAPs). *Apoptosis, 22*(7), 898-919.

Redza-Dutordoir, M., and Averill-Bates, D.A. (2016). Activation of apoptosis signalling pathways by reactive oxygen species. *Biochimica et Biophysica Acta - Molecular Cell Research, 1863*(12), 2977-2992.

Ribble, D., Goldstein, N., Norris, D., and Shellman, Y. G. (2005). A simple technique for quantifying apoptosis in 96-well plates. *BMC Biotechnology, 5*(12). Doi: 10.1186/1472-6750-5-12

Rieger, A., Nelson, K., Konowalchuk, J., and Barreda, D. (2011). Modified Annexin V/Propidium Iodide Apoptosis Assay For Accurate Assessment of Cell Death. *Journal of Visualized Experiments, 50*(2597). Doi: 10.3791/2597

Riihimaki, M., Hemminki, A., Sundquist, J., and Hemminki, K. (2016). Patterns of metastasis in colon and rectal cancer. *Scientific Reports, 6.* Doi: 10.1038/srep29765

Rodriguez-Bigas, M.A., Lin, E.H., and Crane, C.H. (2003). Chapter 106: Genetic Pathways in Colorectal Cancer. In: Kufe, D.W., Pollock, R.E., Weichselbaum, R.R., Bast, R.C.,

Gansler, T.S., Holland, J.F., and Frei, E. (Eds.), *Holland-Frei Cancer Medicine,* 6th edition. Hamilton (ON):B.C. Decker. https://www.ncbi.nlm.nih.gov/books/NBK12839/ [Accessed: 18 September 2017].

Rodriguez-Salas, N., Dominguez, G., Barderas, R., Mendiola, M., García-Albéniz, X., Maurel, J., and Batlle, J.F. (2017). Clinical relevance of colorectal cancer molecular subtypes. *Clinical Reviews in Oncology/Hematolog, 109*, 9-19. Doi:https://doi.org/10.1016/j.critrevonc.2016.11.007

Roseweir, A.K., McMillan, D.C., Horgan, P.G., and Edwards, J. (2017). Colorectal cancer subtypes: Translation to routine clinical pathology. *Cancer Treatment Reviews, 57*, 1-7. Doi:https://doi.org/10.1016/j.ctrv.2017.04.006

Sabel, M.S. (2014). Chapter 44: Oncology. In: Doherty, G. (Eds.), *Current Diagnosis and Treatment: Surgery,* 14th Edition. New York: McGraw-Hill. https://0-accessmedicine-mhmedical-com.innopac.wits.ac.za/content.aspx?bookid=1202&sectionid=71529861 [Accessed 16 July 2017].

Safa, A. (2012). c-FLIP, a master anti-apoptotic regulator. *Experimental Oncology, 34*(3), 176-184.

Sakamuru, S., Attene-Ramos, M.S., and Xia, M. (2016). Mitochondrial Membrane Potential Assay. *Methods in Molecular Biology, 1473*, 17-22. Doi: 10.1007/978-1-4939-6346-1_2

Saletti, P., Molinari, F., De Dosso, S., and Frattini, M. (2015). eGFR signaling in colorectal cancer: a clinical perspective. *Gastrointestinal Cancer: Targets and Therapy, 5*, 21-38. Doi:http://dx.doi.org/10.2147/GICTT.S49002

Schumacher, U., Adam, E., Feldhaus, S., Katoh, M., and Lane, D.P. (2001). Cell differentiation and chemotherapy influence p53 and Mdm2 immunoreactivity in human HT29 colon cancer cells grown in scid mice. *Cancer Letters, 166*(2), 215-221.

Semple, J.I., Smits, V.A.J., Fernaud, J.R., Mamely, I., and Freire, R. (2007). Cleavage and degradation of Claspin during apoptosis by caspases and the proteasome. *Cell Death &*

Differentiation, 14, 1433-1442. Doi:10.1038/sj.cdd.4402134

Shi, Y. (2002). Mechanisms of caspase activation and inhibition during apoptosis. *Molecular Cell , 9*(3), 459-470.

Singh, M.P., Rai, S., Suyal, S., Singh, S.K., Singh, N.K., Agarwal, A., and Srivastava, S. (2017). Genetic and epigenetic markers in colorectal cancer screening: recent advances. *Expert Review of Molecular Diagnostics, 17*(7), 665-685.

Slee, E. A., Adrian, C., and Martin, S.J. (2001). Executioner caspase-3, -6, and -7 perform distinct, non-redundant roles during the demolition phase of apoptosis. *Journal of Biological Chemistry, 276*(10), 7320-7326.

Smeenk, L., van Heeringen, S., Koeppel, M., Gilbert, B., Janssen-Megens, E., and Stunnenberg, H. (2011). Role of p53 Serine 46 in p53 Target Gene Regulation. *Public Library of Science One*. Doi: https://doi.org/10.1371/journal.pone.0017574

Smiley, S.T., Reers, M., Mottola-Hartshorn, C., Lin, M., Chen, A., Smith, T.W., Steele, G.D., and Chen, L.B.(1991). Intracellular heterogeneity in mitochondrial membrane potentials revealed by a J-aggregate-forming lipophilic cation JC-1. *Proceedings of the National Academy of Sciences, USA, 88*(9), 3671-3675.

Stepanenko, A.A., and Dmitrenko, V.V. (2015). Pitfalls of the MTT assay: Direct and off-target effects of inhibitors can results in over/underestimation of cell viability. *Gene, 574*(2), 193-203.

Tan, S.-N., Sim, S.-P., and Koo, A. (2016). Potential role of oxidative stress-induced apoptosis in mediating chromosomal rearrangements in nasopharyngeal carcinoma. *Cell & Bioscience, 6*(35). Doi: https://doi.org/10.1186/s13578-016-0103-9

Tardito, S., Bassanetti, I., Bignardi, C., Elviri, M., Mucchino, C., Bussolati, O., Franch-Gazzola, R., and Marchio, L.(2011). Copper Binding Agents Acting as Copper Ionophores Lead to Caspase Inhibition and Paraptotic Cell Death in Human Cancer Cells. *Journal of the American Chemical Society, 133*(16), 6235-6242.

Tardito, S., and Marchio, L. (2009). Copper Compounds in Anticancer Strategies. *Current*

Medicinal Chemistry, 16(11), 1325-1348.

Tisato, F., Marzano, C., Porchia, M., Pellei, M., and Santini, C. (2010) Copper in Diseases and Treatments, and Copper-Based Anticancer Strategies. *Medicinal Research Reviews, 30*(4), 708-749.

Tosi, F., Magni, E., Amatu, A., Mauri, G., Bencardino, K., Truini, M., Veronese, S., De Carlis, L., Ferrari, G., Nichelatti, M., Sartore-Bianchi, A., and Siena, S. (2017). Effect of KRAS and BRAF Mutations on Survival of Metastatic Colorectal Cancer After Liver Resection: A Systematic Review and Meta-Analysis. *Clinical Colorectal Cancer, 16*(3), e153-e163.

Tsai, Y.J, Lin, J-K., Chen, W-S., Jiang, J-K., Teng, H-W., Yen, C-C., Lin, T-C., and Yang, S-H. (2016). Adjuvant FOLFOX treatment for stage III colon cancer: how many cycles are enough? *Springerplus, 5*(1), 1318. Doi: 10.1186/s40064-016-2976-9

Turnpenny, P., and Ellard, S. (2005) Chapter 14: Cancer genetics. In: Turnpenny, P., and Ellard, S. (Eds.), *Emery's Elements of Medical Genetics,* 12th Edition. Elselvier Churchill Livingstone. pp 203-244.

Uyar, Z., Erdener, D., Koyuncu, I., and Arslan, U. (2017). Synthesis, Characterization, and Cytotoxic Activities of a Schiff Base Ligand and Its Binuclear Copper(II) and Manganese(III) Complexes. *Journal of the Turkish Chemical Society , 4*(3), 963-980.

Valle, L. (2017). Recent Discoveries in the Genetics of Familial Colorectal Cancer and Polyposis. *Clinical Gastroenterology and Hepatology, 15*(6), 809-819.

Varfolomeev, E., Goncharov, T., Fedorova, A.V., Dynek, J.N., Zobel, K., Deshayes, K., Fairbrother, and W.J.,Vucic, D. (2008). c-IAP1 and c-IAP2 are critical mediators of tumor necrosis factor alpha (TNFalpha)-induced NF-kappaB activation. *The Journal of Biologic Chemistry, 283*(36), 24295-24299.

Vento, S. (2013). Cancer control in Africa: which priorities? *The Lancet, 14*(4), 277-279.

Vermes, I., Haanen, C., Steffens-Nakken, H., and Reutelingsperger, C. (1995). A novel assay for apoptosis Flow cytometric detection of phosphatidylserine expression on early apoptotic cells using fluorescein labelled Annexin V. *Journal of Immunological Methods*, *184*(1), 39-51.

Wang, S., Wang, L., Zhou, Z., Deng, Q., Li, L., Zhang, M., Liu, L., and Li, Y. (2017). Leucovorin Enhances the Anti-cancer Effect of Bortezomib in Colorectal Cancer Cells. *Scientific Reports, 7*. Doi: 10.1038/s41598-017-00839-9

Wee, P., and Wang, X. (2017). Epidermal Growth Factor Receptor Cell Proliferation Signaling Pathways. *Cancers, 9*(5), 52. Doi: 10.3390/cancers9050052

Weinburg, R. (2014). Chapter 9: p53 and Apoptosis: Master Guardian and Executioner. In: R. Weinberg. (Eds.), *The Biology of Cancer.* 2nd Edition. New York and London: Garland Science. pp 331-390.

Wells, B.,G. Schwinghammer, T.L., DiPiro, J.T., and DiPiro, C.V. (2017). Chapter 61: Colorectal Cancer. In: Wells, B.G., Schwinghammer, T., DiPiro, J., DiPiro, C., (Eds.), *Pharmacotherapy Quick Guide*, 10th Edition. New York: McGraw-Hill.http://0-accesspharmacy.mhmedical.com.innopac.wits.ac.za/content.aspx?bookid=2177&sectionid=165473914. [Accessed 5 November 2017].

Westphal, D., Dewson, G., Czabotar, P.E., and Kluck, R.M. (2011). Caspase-8 cleaves Bid to tBid which initiates the oligomerization of Bax/Bak causing the mitochondria to release cytochrome c . *Biochimica et Biophysica Acta - Molecular Cell Research, 1813*(4), 521-531.

Williet, N., Petcu, C.A., Rinaldi, L., Cottier, M., Del Tedesco, E., Clavel, L., Dumas, O., Jarlot, C., Bouarioua, N., Roblin, X., Peoc'h, M., and Phelip, J-M. (2017). The level of epidermal growth factor receptors expression is correlated with the advancement of colorectal adenoma: validation of a surface biomarker. *Oncotarget, 8*(10), 16507-16517.

Wolpin, B.M., and Mayer, R.J. (2008). Systemic Treatment of Colorectal Cancer. *Gastroenterology, 134*(5), 1296-1310.

Wong, R.S.Y. (2011). Apoptosis in cancer: from pathogenesis to treatment. *Journal of Experimental and Clinical Cancer Research, 30*(1). Doi: https://doi.org/10.1186/1756-9966-30-87

Wu, J., Liu, T., Rios, Z., Mei, Q., Lin, X., and Cao, S. (2017a). Heat Shock Proteins and Cancer. *Trends in Pharmacological Sciences, 38*(3), 226-256.

Yokoyama, W.M., Thompson, M.L., and Ehrhardt, R.O. (2012). Cryopreservation and Thawing of Cells. *Current Protocols in Immunology*, *99*(1), A.3G.1-A.3G.5

Yue, X., Zhao, Y., Xu, Y., Zheng, M., Feng, Z., and Hu, W. (2017). Mutant p53 in Cancer: Accumulation, Gain-of-Function, and Therapy . *Journal of Molecular Biology, 429*(11), 1595-1606.

Zeestraten, E.C.M., Benard, A., Reimers, M.S., Schouten, P.C., Liefers, G.J., van de Velde, C.J.H., and Kuppen, P.J.K. (2013). The Prognostic Value of the Apoptosis Pathway in Colorectal Cancer: A Review of the Literature on Biomarkers Identified by Immunohistochemistry. *Biomarkers in Cancer, 5*, 13-29. Doi:https://doi.org/10.4137/BIC.S11475

Zhang, Y., and Lozano, G. (2017). p53: Multiple Facets of a Rubik's Cube. *Annual Review of Cancer Biology, 1*, 185-201. Doi: https://doi.org/10.1146/annurev-cancerbio-050216-121926
Zhu, X.F., Li, W., Ma, J.Y., Shao, N., Zhang, Y.J., Liu, R.M., Wu, W.B., Lin, Y., and Wang, S.M. (2015). Knockdown of heme oxygenase-1 promotes apoptosis and autophagy and enhances the cytotoxicity of doxorubicin in breast cancer cells. *Oncology Letters, 10*(5), 2970-2980

Appendix

Appendix A Structures of the 'non-active' test compounds

Table A1 The effect of the 'non-active' epidermal growth factor receptor kinase inhibitors on HT-29 and DLD-1 cells

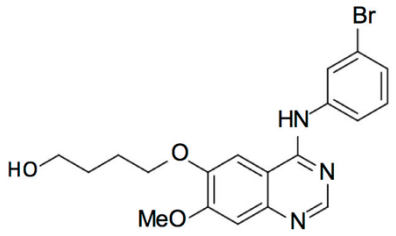
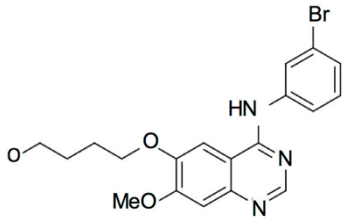
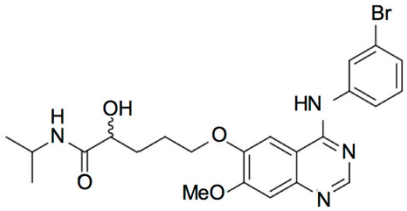
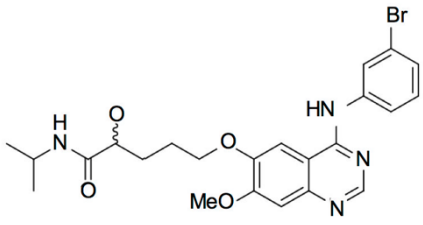
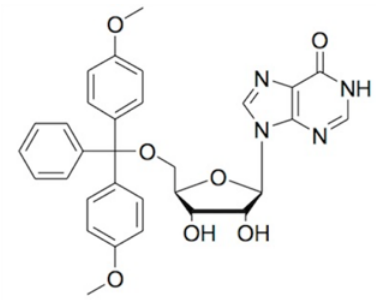
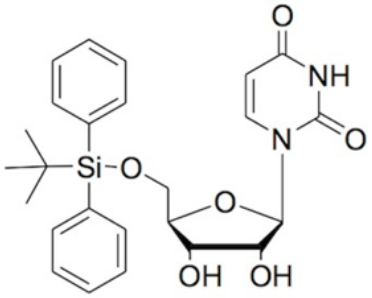
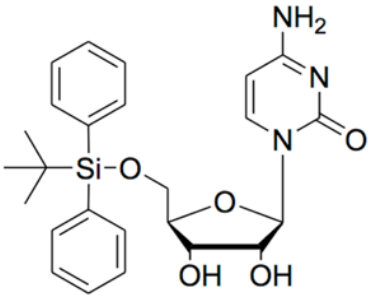
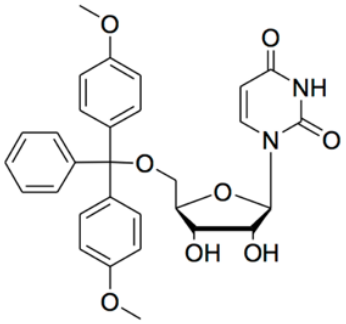
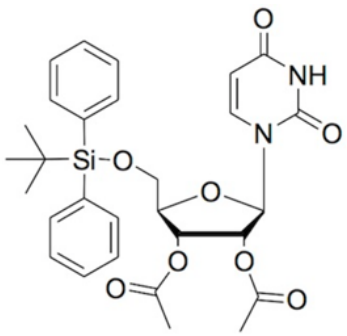
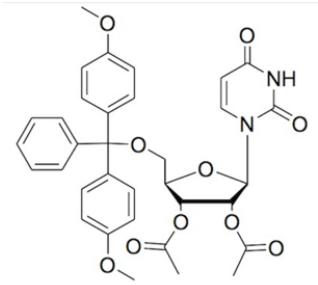
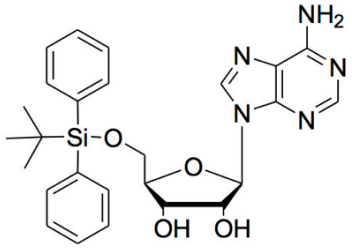
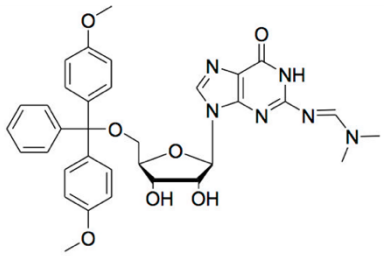
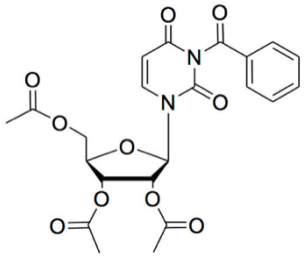
Compound name	Compound structure	HT-29	DLD-1
EKI100	 Molecular weight: 418.28 g/mol	% growth at 50 µM = 89.92 ± 9.14 IC_{50} value = Not determined	% growth at 50 µM = 42.71 ± 0.82 IC_{50} value = Not determined
EKI101	 Molecular weight: 416.27	% growth at 50 µM = 58.49 ± 9.98 IC_{50} value = Not determined	% growth at 50 µM = 52.95 ± 0.25 IC_{50} value = Not determined
EKI102	 Molecular weight: 503.39	% growth at 50 µM = 54.18 ± 1.72 IC_{50} value = Not determined	% growth at 50 µM = 44.78 ± 0.60 IC_{50} value = Not determined
EKI103	 Molecular weight: 501.37	% growth at 50 µM = 67.28 ± 3.29 IC_{50} value = Not determined	% growth at 50 µM = 63.60 ± 0.65 IC_{50} value = Not determined

Table A2 The effect of the 'non-active' nucleoside analogues on HT-29 and DLD-1 cells

Compound name	Compound structure	HT-29	DLD-1
JLP065	 Molecular weight: 570.59 g/mol	% growth at 50 µM = 20.44 ± 0.49 IC50 values = 23.13 ± 0.33	% growth at 50 µM = 16.20 ± 0.63 IC_{50} value =19.89 ± 2.19
JLP089	 Molecular weight: 482.60 g/mol	% growth at 50 µM = 20.39 ± 0.47 IC_{50} value = 18.16 ± 0.46	% growth at 50 µM = 17.19 ± 1.13 IC_{50} value =15.65 ± 0.79
JLP093	 Molecular weight: 481.61 g/mol	% growth at 50 µM = 20.37 ± 0.82 IC_{50} value = 20.05 ± 0.86	% growth at 50 µM = 17.70 ± 1.11 IC_{50} value = 11.16 ± 0.12
JLP090.3	 Molecular weight: 546.57 g/mol	% growth at 50 µM = 18.33 ± 0.44 IC_{50} value = 22.79 ± 0.25	% growth at 50 µM = 19.94 ± 0.47 IC_{50} value = 21.14 ± 1.06

JLP117.1	 Molecular weight: 566.67 g/mol	% growth at 50 µM = 17.40 ± 0.94 IC_{50} value = 16.14 ± 0.33	% growth at 50 µM = 20.11 ± 0.39 IC_{50} value = 13.21 ± 0.18
JLP118.1	 Molecular weight: 630.64 g/mol	% growth at 50 µM = 20.38 ± 0.81 IC_{50} value = 25.89 ± 0.36	% growth at 50 µM = 19.72 ± 0.17 IC_{50} value = 12.08 ± 0.09
JLP095.2	 Molecular weight: 505.64 g/mol	% growth at 50 µM = 76.99 ± 1.98 IC_{50} value = Not determined	% growth at 50 µM = 75.75 ± 2.18 IC_{50} value = Not determined
JLP0.771	 Molecular weight: 640.69 g/mol	% growth at 50 µM = 96.36 ± 7.42 IC_{50} value = Not determined	15.65 ± 0.79 % growth at 50 µM = 54.86 ± 0.89
JLP087	 Molecular weight: 474.42 g/mol	% growth at 50 µM = 103.71 ± 2.37 IC_{50} value = Not determined	% growth at 50 µM = 90.52 ± 2.40 IC_{50} value = Not determined

Appendix B MTT calibration curves

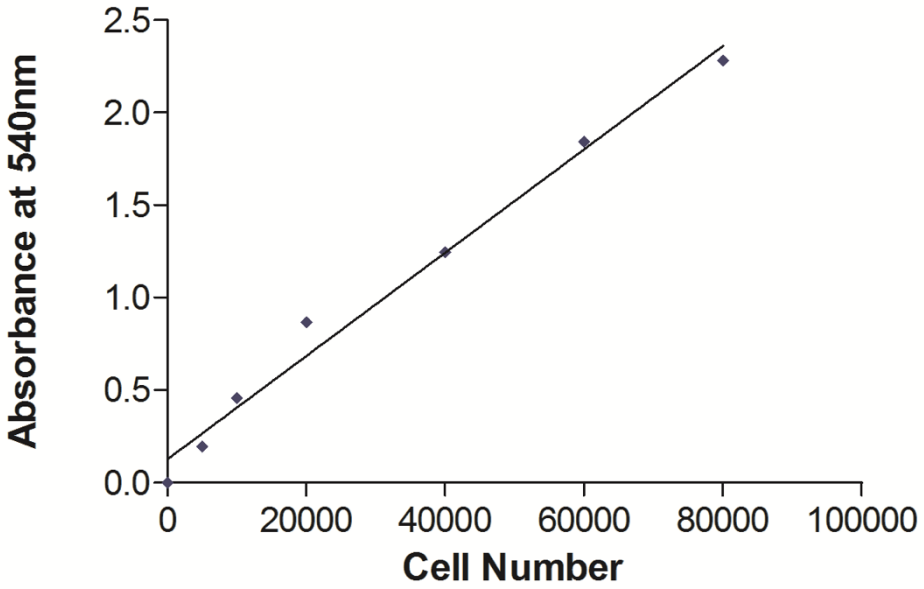


Figure B1 Calibration Curves obtained from the MTT assay for HT-29 cells

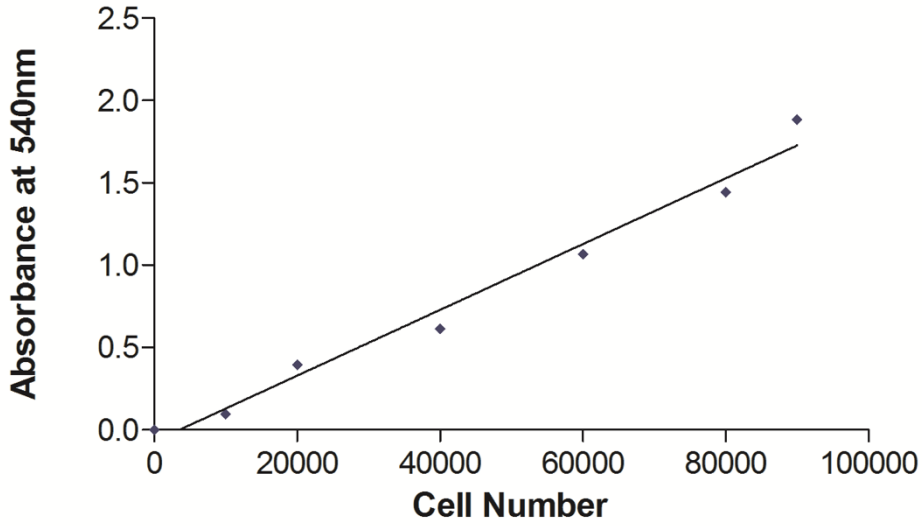


Figure B2 Calibration Curves obtained from the MTT assay for DLD-1 cells

Appendix C Dose response curves

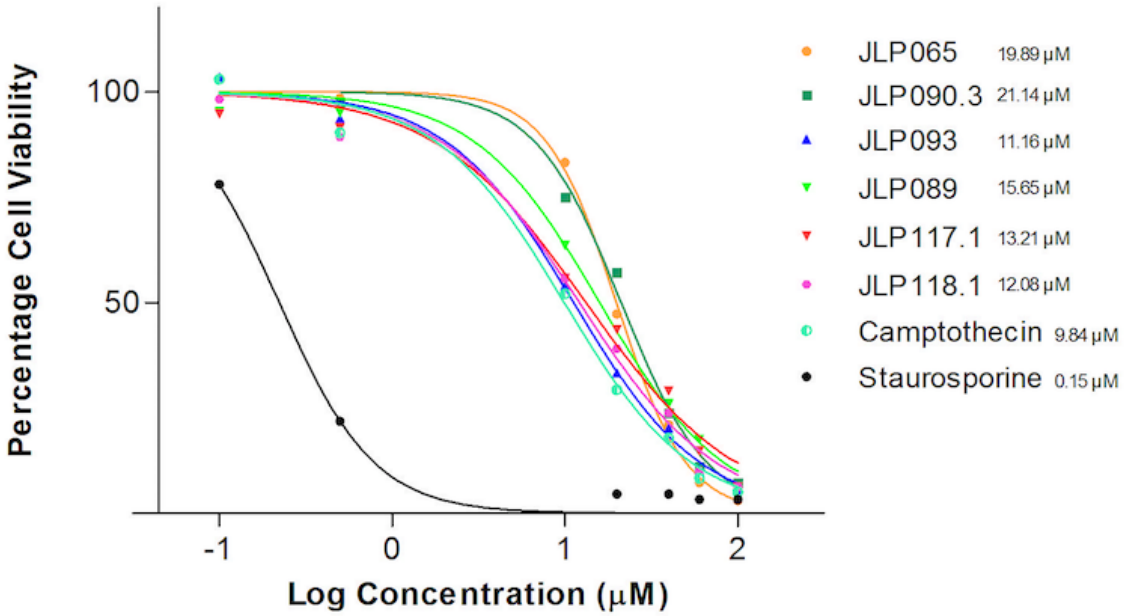


Figure C1 Dose response curve of nucleoside analogues, camptothecin and staurosporine in DLD-1 cells. DLD-1 cell lines were exposed to concentrations of test compounds ranging from 0.05 μM to 100 μM for 48 hours. Each point represents the mean cell viability and standard error of five experiments performed on HT-29 cells.

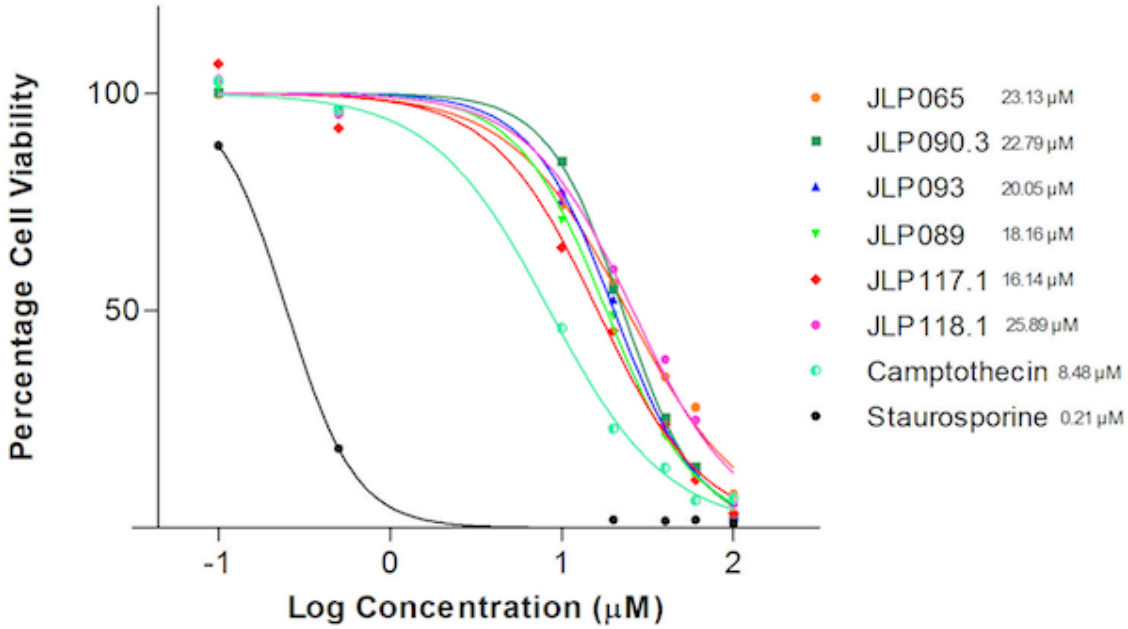


Figure C2 Dose response curve of nucleoside analogues, camptothecin and staurosporine in HT-29 cells. HT-29 cell lines were exposed to concentrations of test compounds ranging from 0.05 μM to 100 μM for 48 hours. Each point represents the mean cell viability and standard error of five experiments performed on HT-29 cells.

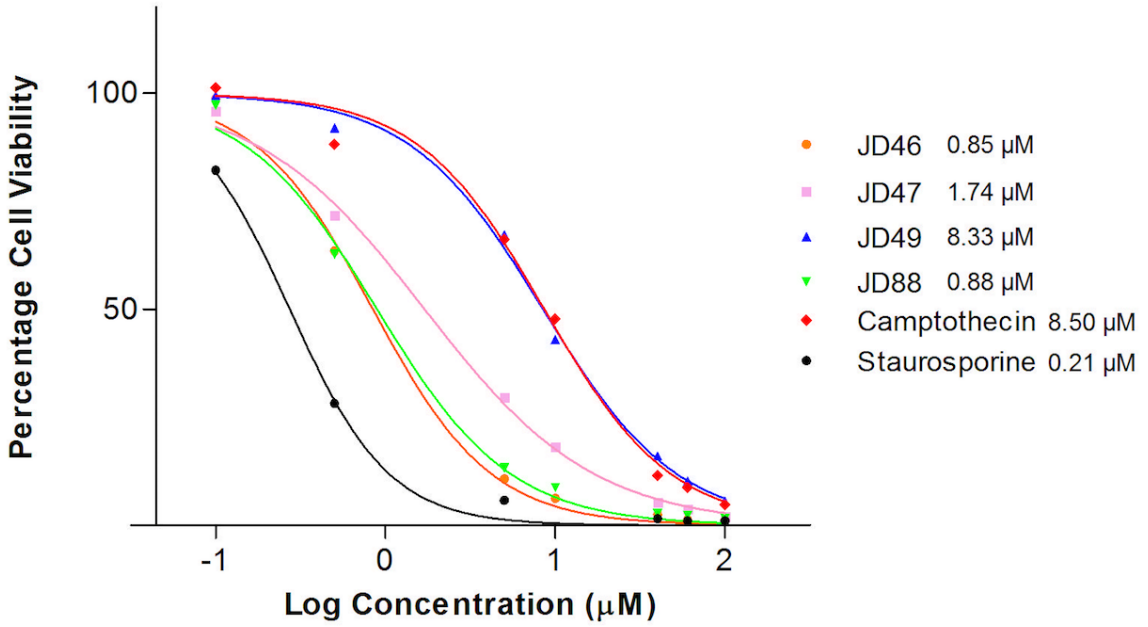


Figure C3 Dose response curves of copper-imidazo[1,2-*a*]pyridines, camptothecin and staurosporine in HT-29 cells. HT-29 cell lines were exposed to concentrations of test compounds ranging from 0.05 μM to 100 μM for 48 hours. **E**ach point represents the mean cell viability and standard error of five experiments performed on HT-29 cells.

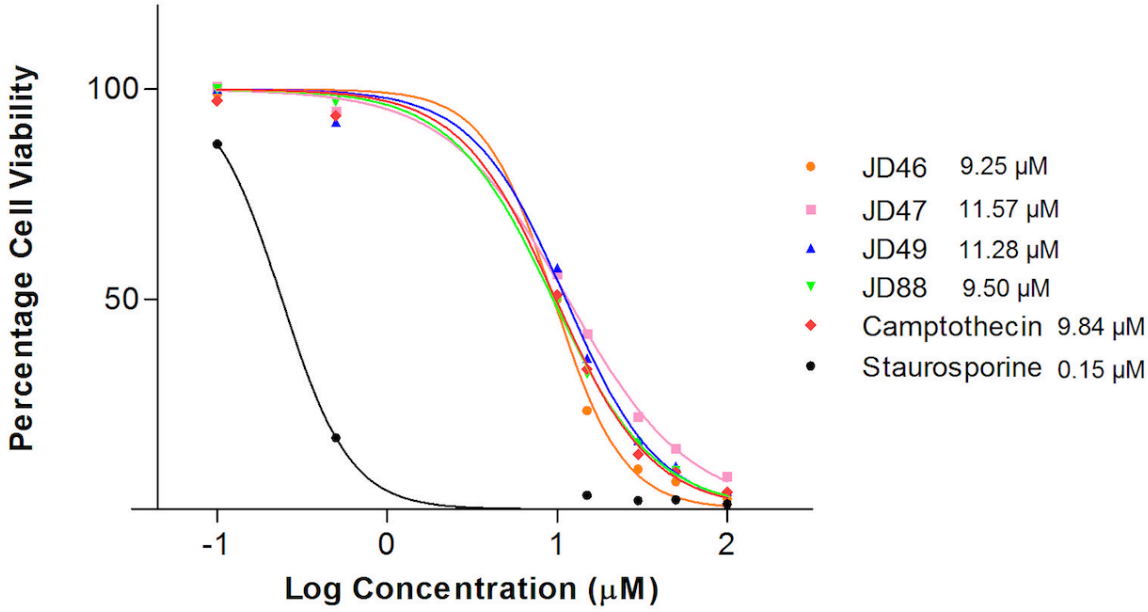
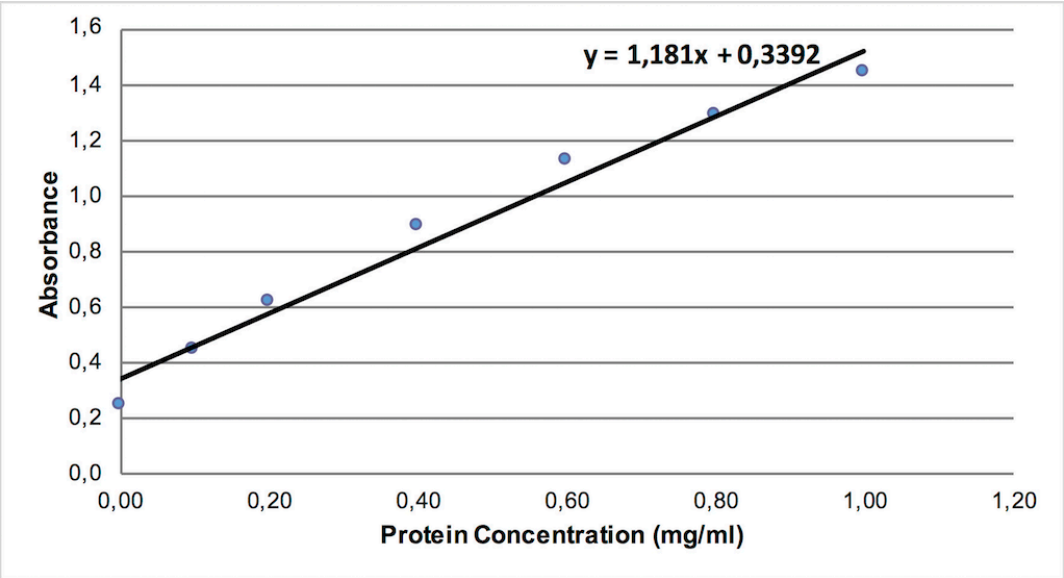


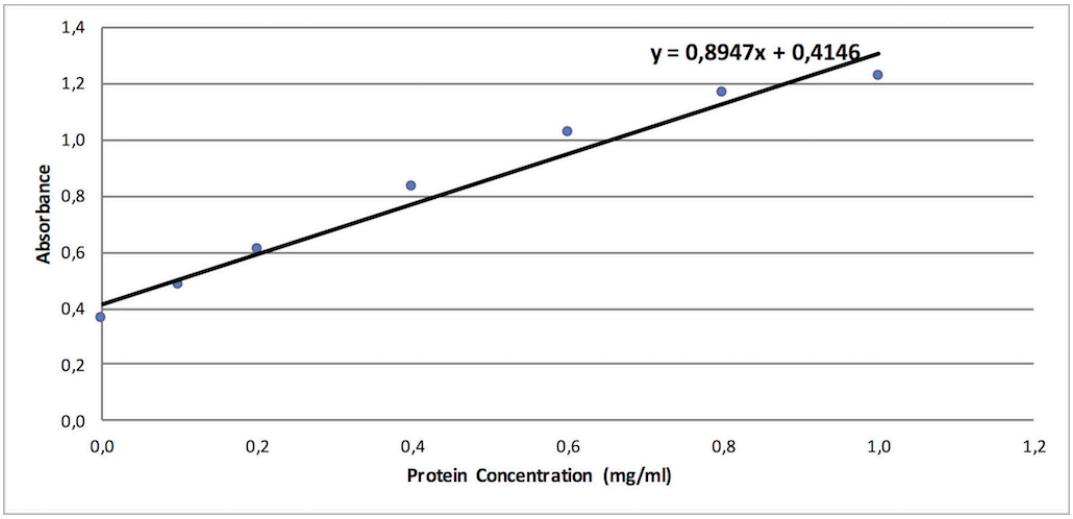
Figure C4 Dose response curve of copper-imidazo[1,2-*a*]pyridines, camptothecin and staurosporine in DLD-1 cells. DLD-1 cell lines were exposed to concentrations of test compounds ranging from 0.05 μM to 100 μM for 48 hours, Each point represents the mean cell viability and standard error of five experiments performed on DLD-1 cells

Appendix D Standard curves

1.



2.



3.

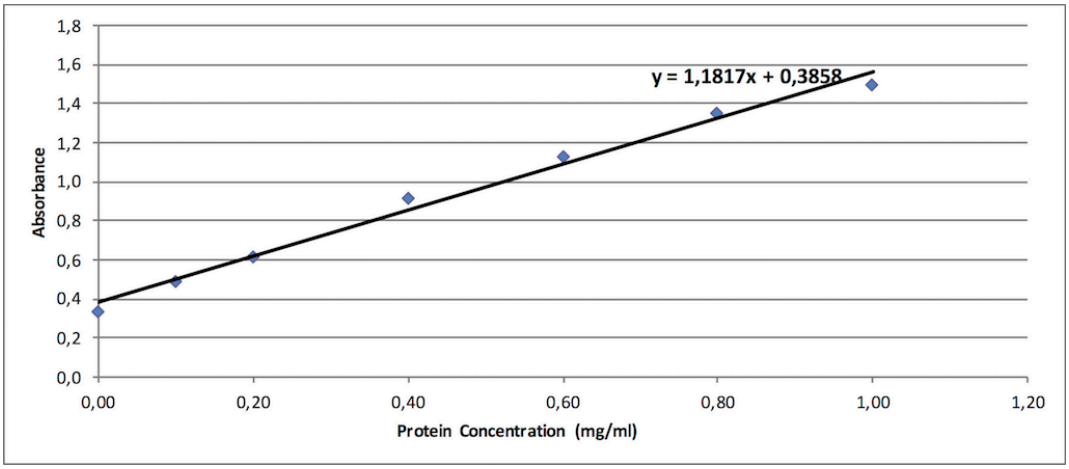


Figure D1-3 Standard curves for protein determination in the caspase-3 assay

4.

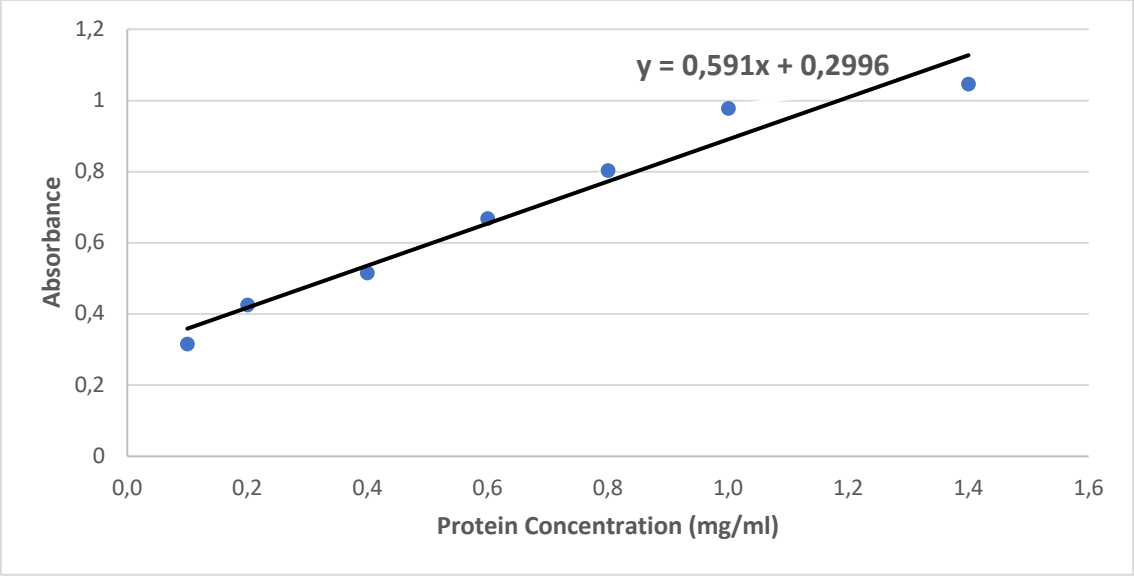


Figure D4 Standard curve for protein determination in the human apoptosis array

Appendix E Caspase-3/7 calculations for specific activity

Table E1 Caspase-3/7 activity in HT-29 cells after exposure to 10 µM copper imidazo[1,2-*a*]pyridines and 200 nM staurosporine. Raw data is representative of three independent experiments.

	Control	Staurosporine	JD46	JD47	JD49	JD88
Relative fluorescence reading	16255559	27368440	57174640	38323412	37599024	57462924
	15226764	31377818	45818240	29338101	34198409	45933882
	11462353	25676499	56207495	38213996	37291828	62498111
Average protein concentration	1.26	1.34	1.26	1.18	1.28	1.17
	1.55	1.69	1.50	1.19	1.54	1.54
	0.69	0.90	1.04	0.91	098	0.97
Specific Activity caspase/protein	12929824.7	20457515.05	45434432.0	32569870.2	29383484.3	49177243.1
	9850960.4	18529905.79	30600216.0	24675721.7	22143086.2	29828018.7
	16579349.5	28632412.3	54261700.7	42136902.4	37896699.1	64311465.6
Caspase-3/7 increase	1.00	1.58	3.51	2.52	2.27	3.80
	1.00	1.88	3.11	2.50	2.25	3.03
	1.00	1.73	3.27	2.54	2.29	3.88

Table E2 Caspase-3/7 activity in DLD-1 cells after exposure to 10 µM copper imidazo[1,2-*a*]pyridines and 200 nM staurosporine. Raw data is representative of three independent experiments

	Control	Staurosporine	JD46	JD47	JD49	JD88
Relative fluorescence reading	35610796	77715464	75502260	48149860	68984164	43675516
	41459744	59560288	84602128	59065464	54436354	48953176
	1568410	4213956	3493749	2317066	2565379	1882446
Average protein concentration	1.20	1.23	1.23	1.24	1.64	1.23
	1.66	1.54	1.59	1.55	1.52	1.57
	0.89	0.90	0.91	0.87	1.02	0.87
Specific activity caspase/protein	29755190.12	63348529.91	61242420.7	38740852.2	42126291.46	35507108.29
	25040694.61	38768025.66	53369191.2	38197232.1	35705586.98	31233264.33
	1768551.3	4700360.956	3836464.5	2657913.6	2504722.717	2154650.83
Caspase-3/7 increase	1.00	2.13	2.06	1.30	1.42	1.19
	1.00	1.55	2.13	1.53	1.43	1.25
	1.00	2.66	2.17	1.50	1.42	1.22

Appendix F Apoptotic protein profile

Table F1 The human apoptosis array coordinates

Coordinate	Proteins	Coordinate	Proteins
A1, A2	Reference spots	C13, C14	HO-2/HMOX2
A23,A24	Reference spots	C15, C16	HSP27
B1, B2	Bad	C17, C18	HSP60
B3, B4	Bax	C19, C20	HSP70
B5, B6	Bcl-2	C21, C22	HTRA2/Omi
B7, B8	Bcl-x	C23, C24	Livin
B9, B10	Pro-Caspase-3	D1, D2	PON2
B11, B12	Cleaved Caspase-3	D3, D4	p21/CIP1/CDKN1A
B13, B14	Catalase	D5, D6	p27/Kip1
B15, B16	clAP-1	D7, D8	Phospho-p53 (S15)
B17, B18	clAP-2	D9, D10	Phospho-p53 (S46)
B19, B20	Claspin	D11, D12	Phospho-p53 (S392)
B21, B22	Clusterin	D13, D14	Phospho-Rad17 (S635)
B23, B24	Cytochrome C	D15, D16	SMAC/Diablo
C1, C2	TRAIL R1/DR4	D17, D18	Survivin
C3, C4	TRAIL R2/DR5	D19, D20	TNF RI/TNFRSF1A
C5, C6	FADD	D21, D22	XIAP
C7, C8	Fas/TNFRSF6/CD95	D23, D24	PBS (negative control)
C9, C10	HIF-1α	E1, E2	Reference spots
C11, C12	HO-1/HMOX1/HSP32		

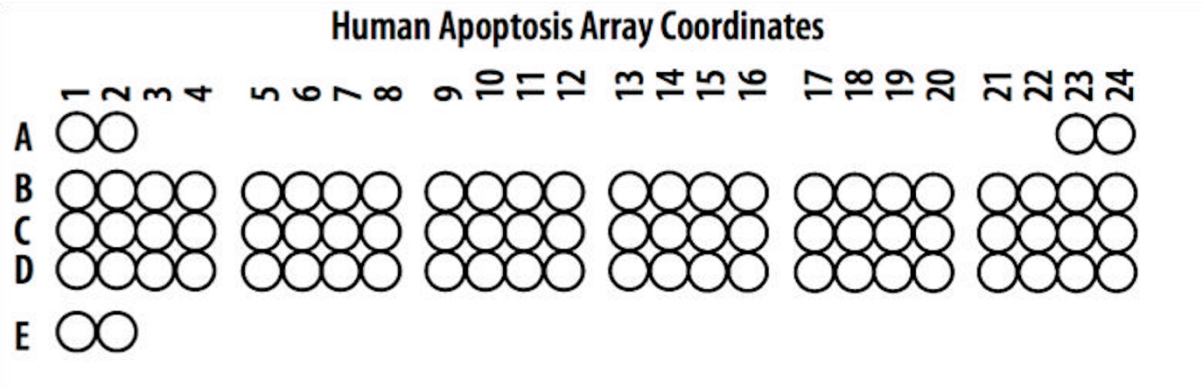


Figure F1 The human apoptosis array coordinates. Image from R&D Systems Protocol Booklet

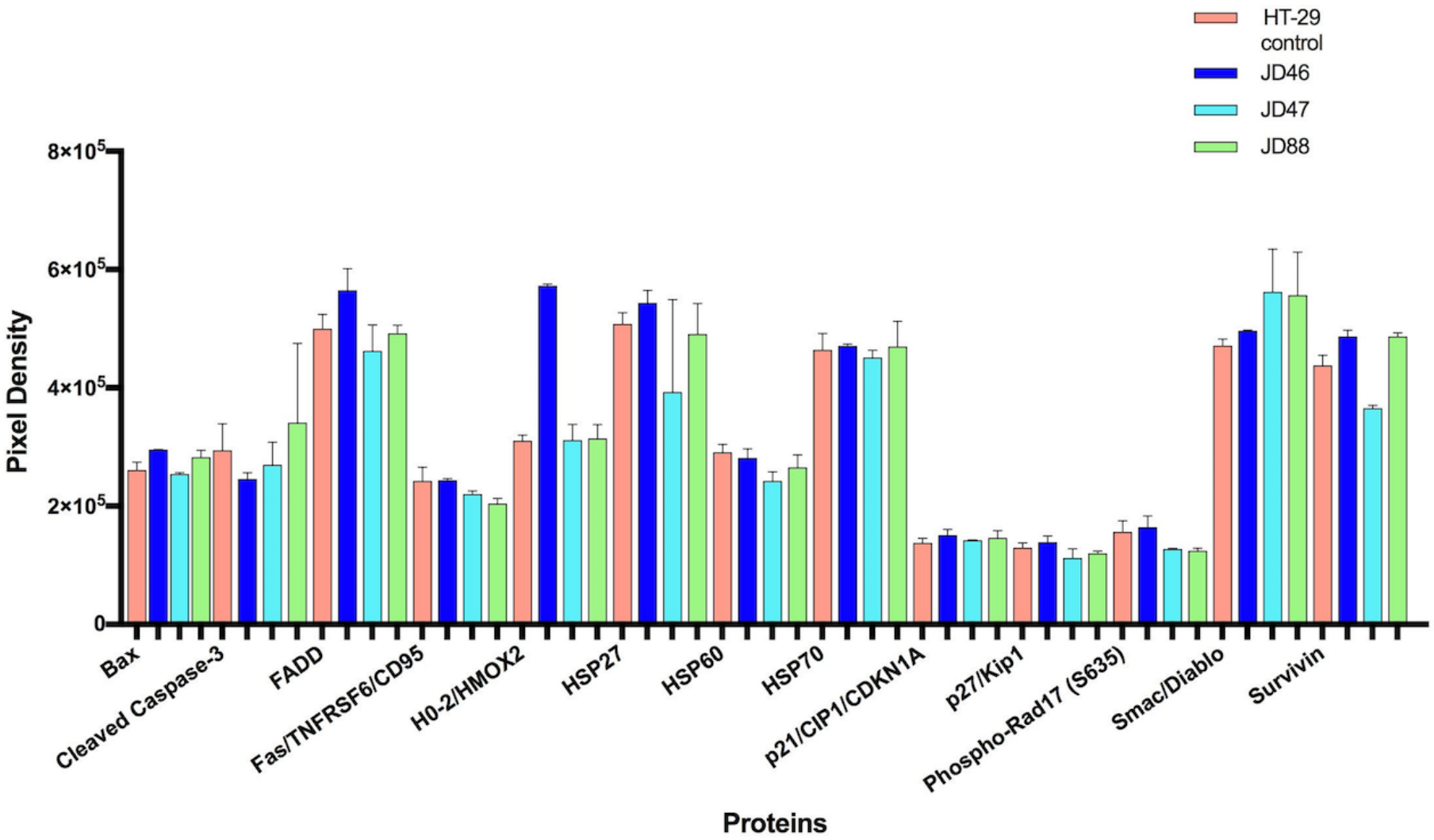


Figure F2 Expression of apoptosis-related proteins in HT-29 cells which showed a less than 20 % change when treated with copper-imidazo[1,2*a*] pyridines. HT-29 cells were treated with 5.0 µM of JD46, JD47 and J88 for 18 hours. The intensity of the chemiluminescent signals were quantified using the Image Lab Software Version 6. Proteins displaying changes of expression levels less than 20 % are included in this graph.

Appendix G Human ethics clearance certificate

Human Research Ethics Committee (Medical)

Research Office Secretariat: Senate House Room SH10005, 10th floor. Tel +27 (0)11-717-1252
Medical School Secretariat: Tobias Health Sciences Building, 2nd floor Tel +27 (0)11-717-2700
Private Bag 3, Wits 2050, www.wits.ac.za. Fax +27 (0)11-717-1265

Ref: W-CJ-150413-2 13/04/2015

TO WHOM IT MAY CONCERN:

Waiver: This certifies that the following research does not require clearance from the Human Research Ethics Committee (Medical).

Investigator: **Dr I Harmse, Ms N Gangat. (Student number 457470)**

Project title: **The effect of novel small molecule inhibitors on lung and colorectal cancer cell lines.**

Reason: This is a laboratory study using two lung cancer cell lines and three colorectal cell lines. There are no human participants

UNIVERSITY OF THE WITWATERSRAND JOHANNESBURG 2015 - 04 - 13

Professor Peter Cleaton-Jones

Chair: Human Research Ethics Committee (Medical)

Copy – HREC (Medical) Secretariat: Zanele Ndlovu, Langutani Masingi.

Appendix H Approval for change of title

UNIVERSITY OF THE WITWATERSRAND, JOHANNESBURG

Private Bag 3 Wits, 2050
Fax: 027117172119
Tel: 02711 7172076

Reference: Mrs Sandra Benn
E-mail: sandra.benn@wits.ac.za

09 March 2018
Person No: 457470
TAA

Miss N Gangat
3 Dorothy Road
Norwood
2192
South Africa

Dear Miss Gangat

Master of Science in Medicine: Change of title of research

I am pleased to inform you that the following change in the title of your Dissertation for the degree of **Master of Science in Medicine** has been approved:

From:	**The effects of novel compounds on colorectal and lung cancer cell lines**
To:	**The effect of Copper Imidazo [1,2 - a] pyridine complexes on HT-29 and DLD -1 colorectal cancer cells**

Yours sincerely

Mrs Sandra Benn
Faculty Registrar
Faculty of Health Sciences